UNIVERSITÉ DE LORRAINE

Ecole doctorale EMMA

THÈSE

Pour l'obtention du titre de :

DOCTEUR de L'UNIVERSITÉ DE LORRAINE

Spécialité: Mécanique des Matériaux

Présentée par :

MOHAMED SAHBI LOUKIL

Étude expérimentale et numérique de la fissuration intralaminaire dans les composites à hautes performances

---

Thèse soutenue publiquement le 04 octobre 2013 à Luleå devant le jury composé de :

M. Constantinos Soutis	**Professeur des universités, Université de Manchester, Manchester, Angleterre**	**Rapporteur**
M. Yves Berthaud	Professeur des universités, Université Pierre et Marie Curie, Cachan, France	Rapporteur
M. Mikael Sjodahl	**Professeur des universités, Université de Technologie de Luleå, Luleå, Suède**	**Examinateur**
M. Andrejs Krasnikovs	Professeur des universités, Université Technique de Riga, Riga, Lettonie	Examinateur
M. Zoubir Ayadi	**Professeur des universités, Université de Lorraine, Nancy, France**	**Directeur de thèse**
M. Janis Varna	Professeur des universités, Université de Technologie de Luleå, Luleå, Suède	Co-directeur de thèse
Mme. Isabelle Royaud	**Professeur des universités, Université de Lorraine, Nancy, France**	**Invitée**
M. Ali Kallel	Professeur des universités, Faculté des Sciences de Sfax, Sfax, Tunisie	Invité
M. Zouhir Fakhfakh	**Professeur des universités, Faculté des Sciences de Sfax, Sfax, Tunisie**	**Invité**

Institut Jean Lamour –UMR 7198- Département SI2M – Equipe 305
Parc de Saurupt - CS 50840- 54011 NANCY Cedex

Université de Lorraine – Pôle M4 : matière, matériaux, métallurgie, mécanique

“The whole of science is nothing more than a refinement of everyday thinking”

Albert Einstein

Dedication

This doctoral thesis is lovingly dedicated to my parents. To my mother, Bahija, for her constant love, unlimited patience, support and encouragement. To my father, Zouhir, his endless support, care and prayers have sustained me throughout my life. Without their sacrifices towards my education, this thesis work would not be possible. Thank you for giving me strength to chase my dreams.

This thesis is dedicated to my brother, Thabet, who has inspired me to believe that all dreams are possible. He taught me to dream big and not accept failure.

This thesis is dedicated to my sister, Amani, for her love, support and constant encouragement. She took care of my family during the years of my studies.

This thesis is dedicated to my wonderful beloved future wife, Salma, for her love, patience, support, inspiration and continuous sharing of every moment. I am grateful, as well, to my family-in-law.

Preface

This doctoral thesis contains the results from my work at the division of materials science in Luleå University of Technology, Sweden and at the division of mechanics of materials in University of Lorraine, France during the period from October 2009 to September 2013.
There are many people who deserve my gratitude since they have been contributing to this work.

First and foremost, I would like to express my sincerest gratitude to my both supervisors Professor Janis Varna from Sweden and Professor Zoubir Ayadi from France for their scientific guidance and HUGE contribution to this thesis. I am also grateful to them for their support, not only in the work, but also in personal level, and for creating such warm atmosphere which makes working in their divisions a great pleasure.

I am very thankful to Professor Roberts Joffe for his remarks, ideas and fruitful suggestions, during this period.
My gratitude also goes to Professor Ali Kallel and Professor Zouhir Fakhfakh from Tunisia for being the persons who gave me the opportunity to come to Europe.

Special thanks also go to all my colleagues at Polymeric Composite Materials Group who have always been friendly and supportive, making the working environment very fun.
I would like to thank in particular all people who work at EEIGM in Nancy for the nice discussions during lunches and coffee breaks.
My list would not be completed if I would not mention my colleagues at Swerea SICOMP AB for the wonderful working atmosphere.

Luleå, August 2013

Loukil Mohamed Sahbi

Abstract

The macroscopic failure of composite laminates subjected to tensile increasing load is preceded by initiation and evolution of several microdamage modes. The most common damage mode and the one examined in this thesis is intralaminar cracking in layers. Due to this kind of microdamage the laminate undergoes stiffness reduction when loaded in tension. For example, the elastic modulus in the loading direction and the corresponding Poisson's ratio will decrease.

The degradation of the elastic properties of these materials is caused by reduced stress in the damaged layer which is mainly due to two parameters: crack opening displacement (COD) and crack sliding displacement (CSD). At fixed applied load these parameters depend on the properties of the damaged and surrounding layers, on layer orientation and on thickness. When the number of cracks per unit length is high (high crack density in the layer) the COD and CSD are reduced because of to crack interaction.

The main objective of the second chapter of this thesis is to investigate the effect of crack interaction on COD using FEM and to describe the identified dependence on crack density in a simple and accurate form by introducing an interaction function dependent on crack density. This interaction function together with COD of non-interactive crack gives accurate predictions of the damaged laminate properties. The application of this function to more complex laminate lay-ups is demonstrated. All these calculations are performed assuming that cracks are equidistant.

However, the crack distribution in the damaged layer is very non-uniform, especially in the initial stage of multiple cracking. In the third chapter, the earlier developed model for general symmetric laminates is generalized to account for non-uniform crack

distribution. This model is used to calculate the axial modulus of cross-ply laminates with cracks in internal and surface layers. In parametric analysis the COD and CSD are calculated using FEM, considering the smallest versus the average crack spacing ratio as non-uniformity parameter. It is shown that assuming uniform distribution we obtain lower bond to elastic modulus. A "double-periodic" approach presented to calculate the COD of a crack in a non-uniform case as the average of two solutions for periodic crack systems is very accurate for cracks in internal layers, whereas for high crack density in surface layers it underestimates the modulus reduction.

In the fourth chapter, the thermo-elastic constants were calculated using shear lag models and variational models in a general calculation approach (GLOB-LOC) for symmetric laminates with transverse cracks in 90° layer. The comparison of these two models with FEM was presented for cross-ply and quasi-isotropic laminates.

Using FEM, we assume linear elastic material with ideal crack geometry. Fiber bridging over the crack surface is possible which can affect COD and CSD. The only correct way to validate these assumptions is through experiments.

The main objective of the fifth and the sixth chapter is to measure these parameters for different laminate lay-ups in this way providing models with valuable information for validation of used assumptions and for defining limits of their application. In particular, the displacement field on the edge of a $[90/0]_s$ and $[90_3/0]_s$ carbon fiber/epoxy laminates specimens with multiple intralaminar cracks in the surface layer is studied. The specimen full-field displacement measurement is carried out using ESPI (Electronic Speckle Pattern Interferometry).

List of relevant publications and presentations

Journal papers

[1] *Loukil M.S*, Varna J and Ayadi Z. Engineering expressions for thermo-elastic constants of laminates with high density of transverse cracks, *Composite Part A: Applied Science and Manufacturing*, 2013, Vol 48(1), pp.37-46

[2] *Loukil M.S*, Varna J and Ayadi Z. Applicability of solutions for periodic intralaminar crack distributions to non-uniformly damaged laminates, *Journal of Composite Materials*, 2013, Vol 47(3), pp.287-301

[3] *Loukil M.S*, Hussain W, Kirti A, Purpus A and Varna J. Thermo-elastic constants of symmetric laminates with cracks in 90-layer: application of simple models, *Plastics, Rubber and Composites*, 2013, Vol42(4), pp157-166

[4] *Loukil M.S*, Varna J and Ayadi Z. Damage characterization in Glass Fiber/Epoxy laminates using Electronic Speckle Pattern Interferometry, *Experimental Techniques*, 2013, In press

[5] *Loukil M.S*, Ayadi Z and Varna J. Experimental and numerical analysis of the Crack Opening Displacement Profile in Damaged Cross-ply Laminates, submitted to *Composite Science and Technology*

Conference papers

[6] *Loukil M.S*, Varna J and Ayadi Z. Characterization of damaged composite laminates by an optical measurement of the displacement field, *IOP Conference Series: Materials Science and Engineering*, 2012, No 012004

[7] Zrida H, *Loukil M.S*, Varna J and Ayadi Z. Crack opening displacement determination in damaged cross-ply laminate using ESPI, *IOP Conference Series: Materials Science and Engineering, 2012, No 012002*

[8] Varna J, *Loukil M.S* and Ayadi Z. Degradation of elastic properties of non-uniformly damaged composite laminates, *IOP Conference Series: Materials Science and Engineering, 2013, Submitted*

List of Conference Presentations

Invited speaker

- ✓ 6th International Conference "Supply on the Wings", Frankfurt/Main (Germany), November 2-4, 2011

Oral communication

- ✓ POLYCHAR 17 : World Forum on Advanced Materials, Rouen (France), April 20-24, 2009
- ✓ 5th EEIGM International Conference, Advanced Materials Research, Nancy (France), November 4-5, 2009
- ✓ Conférence Nationale « Matériaux 2010 », Nantes (France), October 18-22, 2010
- ✓ 5th International Conference on Composites Testing and Model Identification, Lausanne (Switzerland), February 14-16, 2011
- ✓ 6th EEIGM International Conference, Advanced Materials Research, Nancy (France), November 7-8, 2011
- ✓ 3rd International Meeting on Dielectric Materials IMDM'3, Monastir (Tunisia), December 14-18, 2011
- ✓ 17th International Conference on Mechanics of Composite Materials, Riga (Latvia), May 28- Jun 1, 2012
- ✓ Workshop « Composite Damage : Status and future directions-4 », Uppsala (Sweden), September 3-5, 2012
- ✓ 10th International conference on durability of composite systems, Brussels (Belgium), September 17-19, 2012
- ✓ 12th International Conference on Deformation and Fracture of Composite and 6th Structural Integrity, Cambridge (England), April 8-11, 2013
- ✓ 6th International Conference on Composites Testing and Model Identification, Aalborg (Denmark), April 22-24, 2013
- ✓ Workshop « Composite Damage : Status and future directions-5 », Roskilde (Denmark), May 27-29, 2013

Contents

Dedication i

Preface iii

Abstract v

List of relevant publications and presentations vii

Chapter 1. General Introduction 1

Chapter 2 15

2.1. Inroduction 15

2.2. Material model of damaged symmetric laminates with intralaminar cracks 20
2.2.1 Model formulation 20
2.2.2 Thermo-elastic constants of balanced laminates with cracks in 90-layers 22

2.3. Numerical parametric analysis of COD 24
2.3.1 Definitions, interaction mechanisms and FEM model 24
2.3.2 Internal cracks 29
2.3.3 Surface cracks 30

2.4. Stiffness of cross-ply laminates 31
2.4.1 Stiffness of cross-ply laminates with damage in inside layers 32
2.4.2 Stiffness of cross-ply laminates with damage in surface layers 33

2.5. Quasi-isotropic laminates 34
2.5.1 Generalization of the methodology 34
2.5.2 Interaction of inside cracks 36
2.5.3 Interaction of surface cracks 37
2.5.4 Stiffness of damaged quasi-isotropic laminates 37
2.5.4.1 Quasi-isotropic laminates with cracks in inside layers 37
2.5.4.2 Quasi-isotropic laminates with cracks in surface layers 38

2.6 Conclusions 39

Chapter 3 43

3.1. Introduction 43

3.2. Material model of damaged symmetric laminates with intralaminar cracks 46
3.2.1 Distances between cracks 46
3.2.2 Stiffness Model 47
3.2.3 Elastic modulus of balanced laminates with cracks in 90-layer 49

3.3. Results and discussion 50
3.3.1 Formulation of calculation examples 50
3.3.2 COD parametric analysis at low crack density 53
3.3.2.1 Internal cracks 53

3.3.2.2 Surface cracks 55
3.3.3 Approximate COD determination from periodic solutions 56

3.4. Elastic modulus prediction and validation with FEM 60

3.5. Conclusions 66

Chapter 4 69

4.1. Introduction 69

4.2. Material model of damaged symmetric laminates with intralaminar cracks 72
4.2.1 Model formulation 72
4.2.2 Thermo-elastic constants of balanced laminates with cracks in 90-layers 74

4.3. Determination of COD 76
4.3.1 Crack face displacements 76
4.3.2 Average COD relation to stress perturbation 77
4.3.3 Shear-lag model 79
4.3.4 Hashin´s model 80
4.3.5 Ply discount model 80

4.4. Results and discussion 81
4.4.1 Material properties 81
4.4.2 Parametric analysis on cross-ply laminates 82
4.4.3 Comparison between simulations and experimental data 90
4.4.4 Comparison between analytical simulations and FEM data 93
4.4.5 Ply-discount model and the asymptotic behavior of stiffness reduction 99

4.5. Conclusions 101

Chapter 5 105

5.1. Introduction 105

5.2. Experimental technique and material 107
5.2.1 Experimental technique: ESPI 107
5.2.2 Material 110

5.3. Results 111
5.3.1 Normalized relative displacement measurement 111
5.3.2 Normalized crack opening displacement 114

5.4. Conclusions 117

Chapter 6 121
6.1. Introduction 121

6.2. Experimental technique and materials 124
6.2.1 ESPI measurements 124
6.2.2 Materials 125

6.3. Numerical parametric analysis of COD 125
6.3.1 Determination of COD 125
6.3.2 FEM analysis 126

6.4. Results 127
6.4.1 [90/0]s CF/EP laminate 127
6.4.1.1 Positions of intralaminar cracks 127
6.4.1.2 COD measurement using ESPI 128
6.4.1.3 Comparison with FEM for [90/0]s laminate 131
6.4.2 [903/0]s CF/EP laminate 133
6.4.2.1 Positions of cracks 133
6.4.2.2 COD measurement using ESPI and FEM calculations 134
6.4.3 The effect of the unsymmetrical crack distribution on the axial modulus 136

6.5. Conclusions 140

Chapter 7. Conclusions and perspectives 145

Appendix 151

References 157

Chapter 1

General Introduction

Composite is a material which has at least two distinct phases or constituents. This material has found usage in many industrial applications and more recently it is increasingly being used in aerospace panels and airframes. The use of composites in the aerospace industry is justified by their excellent specific modulus and strength (referred to the property divided by the density). Fig. 1.1 shows the increase in percentage of components made from composites for commercial airplanes.

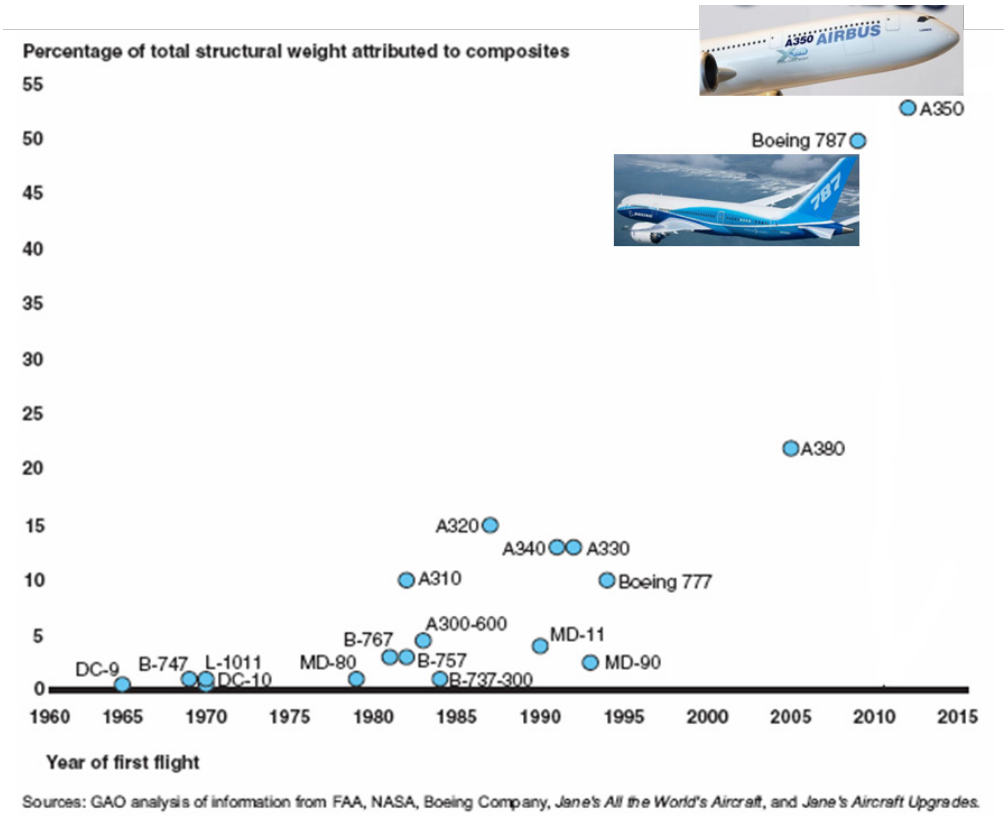

Figure 1.1. Commercial Airplane Models over time by percentage of composites

Fig. 1.2 shows the increase of composite use in commercial airplane from 1% (Boeing 747) in 1969 to 50% (Boeing 787) in 2009.

Recently the new generation commercial aircraft, the 787 (Dreamliner), was designed almost entirely with high performance carbon fiber materials including the stabilizers, wings, and fuselage, which represents 50% of aircraft structural weight (Fig. 1.3). Composite materials represent 53% of the Airbus A350.

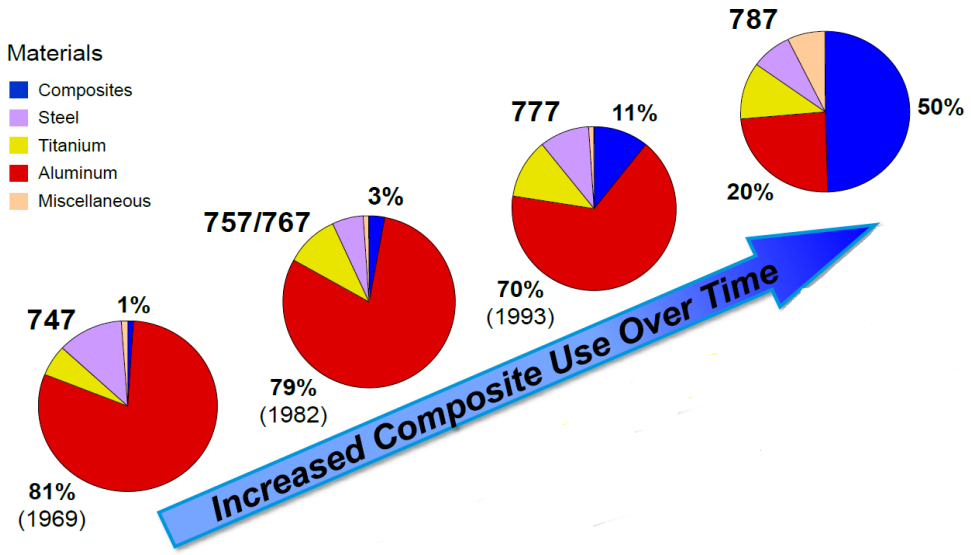

Figure 1.2. Composite materials trends [1]

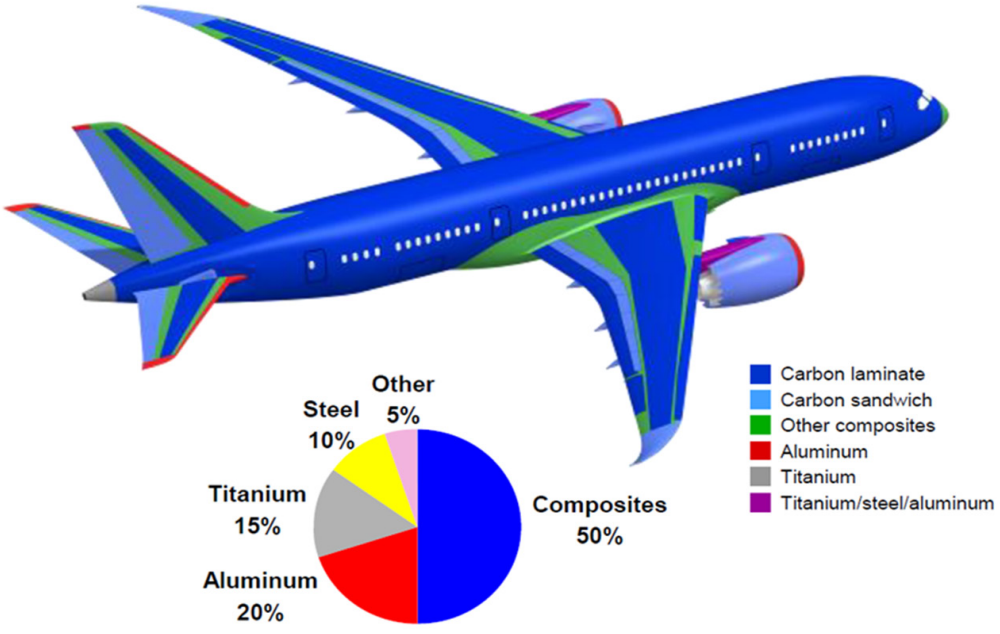

Figure 1.3. Composite structure content on the Boeing 787 [1]

When a composite is loaded in tension with increasing load it will eventually fail (macroscopically). The failure is preceded by initiation and evolution of several microdamage modes. On the microscale, a part of the matrix can fail, fibers can fail and there can be fiber/matrix interface debonding (Fig. 1.4(a)). On the mesoscale, three different modes of damage can be observed.

Matrix microcraking or intralaminar cracking (Fig. 1.4(b)):

Fiber-reinforced composites offer strength and stiffness properties in the longitudinal direction. Their properties, however, in the transverse direction are generally low. As results, they readily develop cracks along fibers. These cracks are usually the first mode of damage in fiber-reinforced composites. Such cracks are found to be caused by tensile loading, fatigue loading, as well as by changes in temperature or by thermal cycling. These cracks run parallel to fibers in the layer with the crack plane being transverse to the laminate midplane. Intralaminar cracks do not usually cause the final failure of a laminate, but may significantly impair the effective properties of the composite and serve as a source for other damage modes initiation, such as delamination.

Delamination or interlaminar cracking (Fig. 1.4(C)):

It is cracking in the interfacial plane between two adjoining plies in a laminate, causes separation of the plies and is referred to as delamination. The growth of delamination cracks under the subsequent application of external loads leads to a rapid deterioration of the mechanical properties and may cause catastrophic failure of the composite structure.

Fiber breaks (Fig. 1.4(d)):

The failure (separation) of a multidirectional fiber-reinforced composite ultimately comes from breakage of fibers. In a unidirectional composite loaded in tension along

fibers the individual fibers fail at their weak points and stress redistribution between fibers and matrix occurs, affecting other fibers in the local vicinity of the broken fibers and possibly broken some.

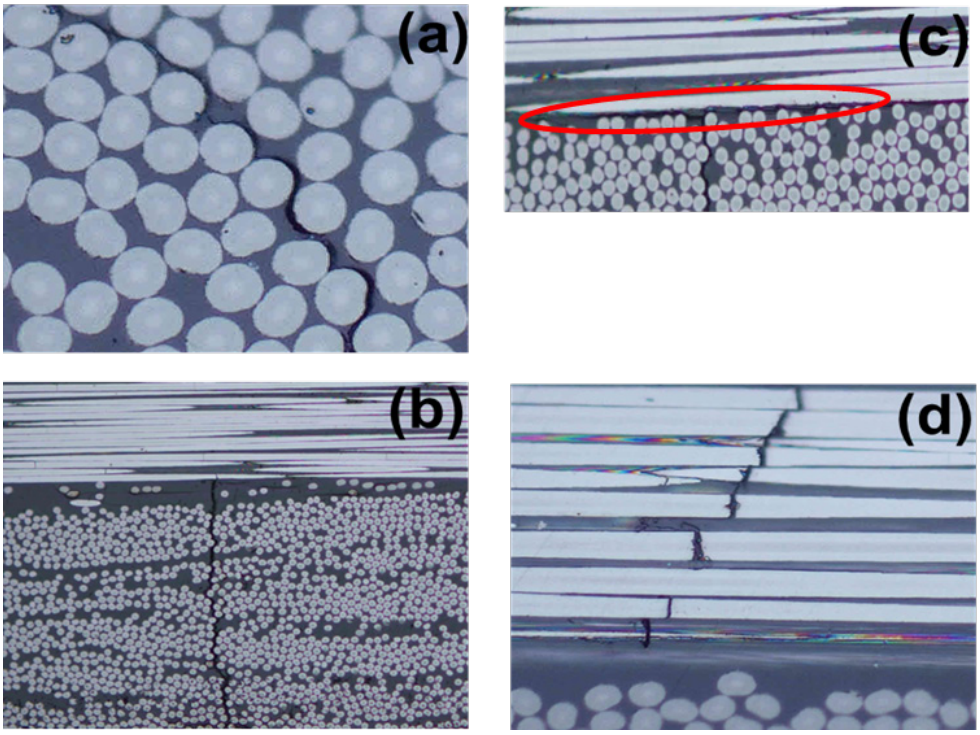

Figure 1.4. Various mechanics of damage in composite laminates
(a): Fiber/Matrix debonding, (b): Matrix cracking, (c): Delamination, (d): Fiber breaks

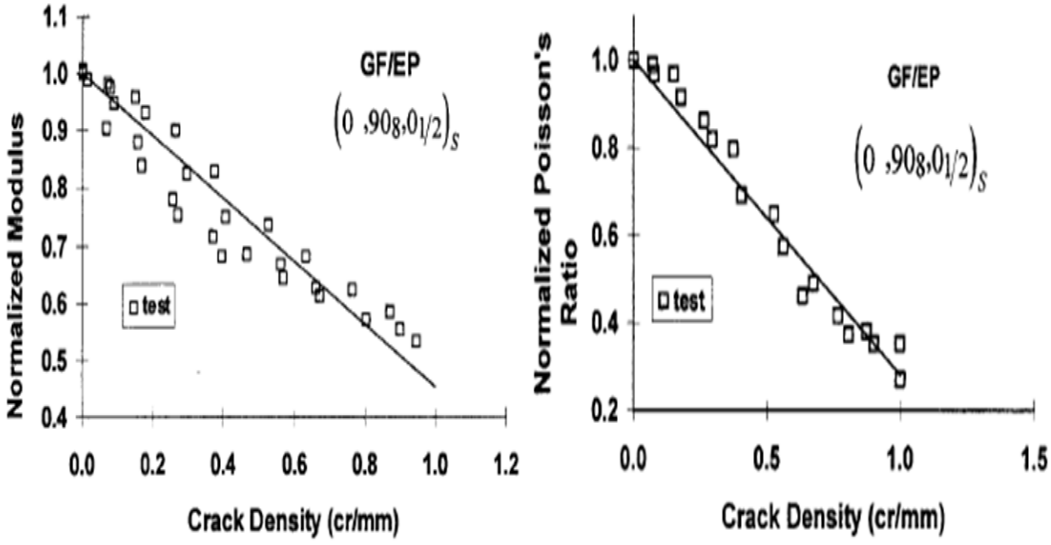

Figure 1.5. Elastic properties dependence on the microdamage level [2]

The number of cracks increases during service life reducing laminate thermo-elastic properties (Fig. 1.5). Many papers have been written on this subject, covering a broad range from "micromechanics" based to continuum damage mechanics based models (see review for example in [3-6]).

All models analyzing the stress state between two cracks are commonly referred as "micromechanics models". Most of the analytical stress distribution modeling has been performed for cross-ply laminates with cracks in the 90-layer.

The shear-lag type of analysis is the simplest way to describe intralaminar cracking in cross-ply laminates. This group of models was used by many authors, for example in [7-10], where a linear or parabolic shape of the crack face displacement or of the out-of-plane shear stress is assumed. In [10] a bi-linear distribution of the shear stress in the undamaged layer was suggested as more coherent with findings from FEM analysis. General drawbacks of these models are that the equilibrium equations are not satisfied in any point but only in average and that the shear stress is not zero on crack surface. The "shear lag parameter" governing the shape of stress distributions is often used as a fitting parameter.

Hashin [11] generalized his model [12] to the case when cracks are in both 0- and 90-layers of a cross-ply laminate. Solution for an orthogonally cracked cross-ply laminate under tension was found constructing a simple admissible stress field in the context of the principle of minimum complementary energy. The chosen stress field satisfies equilibrium equations and all boundary and interface conditions in tractions. The assumed constant in-plane normal stress distribution over each layer thickness leads to linear and parabolic through-the-thickness distributions of out-of-plane shear and normal stresses, respectively. The principle of minimum complementary energy (which for approximate stress distributions is equivalent satisfying the displacement continuity

equations in average) is used to calculate the stress distributions. Expressions for damaged laminate E-modulus and Poisson's ratio were derived. This model does not involve any fitting parameters and is simple to use.

As any model based on the principle of minimum complementary energy it overestimates the stiffness reduction. The accuracy has been improved using more sophisticated shape functions for stresses [13,14].

The most accurate local stress state comparable with a very fine FE solution and, therefore, also accurate stiffness prediction can be obtained using semi-analytical McCartney [15,16] and Schoeppner and Pagano [17] models.

In the McCartney model [15,16] each layer in the laminate is divided in a large number of thin sub-layers and in each sub-layer the stress assumptions are as in Hashin's variational model [12]. All displacement and stress continuity conditions at sub-layer interfaces are satisfied. The stress-strain relationships are also satisfied, except one, which is satisfied in an average sense. It was proven that satisfying in average is identical to asking for minimum of the Reissner energy functional in the used approximation of the stress-strain state.

The Schoeppner-Pagano model [17], which is also based on Reissners principle, considers a system of hollow concentric sub-cylinders with a radius approaching to infinity. Each layer is divided in a number of coaxial cylinders. These two methods have to be considered as numerical or semi-analytical. They render local stress state with accuracy comparable with a very fine FE solution and, therefore, also accurate stiffness prediction. However, the calculation routines in these models are extremely complex which limits the application for more general cases than cracks in one layer only.

Cross-ply laminates are a good configuration for analysis of basic phenomena in intralaminar cracking but they are seldom used in practical applications. Laminates with a general lay-up containing cracks in several layers of different orientation are, therefore, a challenge for any constitutive model. Analytical solutions except a straightforward generalization for [S/90]s laminates with homogenized sublaminate S, see [7,18], are not available.

In [19] the constitutive equations for a layer with cracks are presented. These expressions apart from lamina properties contain also so-called "in-situ damage effective functions -IDEF" which depend on crack density in the lamina and on the neighbouring layer constraint. In order to determine IDEF they introduced "an equivalent constraint model", which assumes that the constraint of the lay-ups above and below the analyzed lamina can be described by two sublaminates with properties calculated using laminate theory (CLT). Thereby the actual laminate was replaced by a cross-ply. The stress state in the repeating unit of the cross-ply laminate and the IDEF's were calculated using standard shear lag model with linear distribution of out-of-plane shear stresses. Then the constitutive relationships for damaged layers were used in the framework of the CLT to obtain the stiffness matrix of the damaged laminate.

The same micromechanics model was used also by Kashtalyan et al [20] where in the "equivalent constraint model" the effective properties of the constraint layer were adjusted for damage when analyzing the local stresses in another layer. This leads to an iterative procedure when cracks are present in both 0- and 90-layer of the cross-ply laminate. It was shown that a) the results are quite different when the shear stress localization model is used; b) the interaction of cracks in two layers leads to considerable additional reduction of the laminate shear modulus. It should be noted

that the methodology, which was developed and used for cross-ply laminates, could be rather easy generalized to more general lay-ups. Local delaminations at the tip of transverse cracks were included in the analysis by the same authors [21] were also a rather detailed analysis of the state of art on this subject is presented.

Two tracks may be distinguished in this type of modelling in recent years: a) generalizing analytical models to lay-ups where the lay-up supporting the damaged layer is monoclinic, leading to coupling of the normal and shear loading problems [22-25]; b) developing computational tools for calculating thermo-elastic properties of multidirectional laminates with cracks in several layers [26-30]. The iterative approach here is usually based on using effective constants of the damaged layers when cracks in another layer are explicitly analysed (generalized "equivalent constraint" model).

Generally speaking, the continuum damage mechanics (CDM) approach [5] also may be used to describe the stiffness of laminates with intralaminar cracks in off-axis plies of any orientation. The damage in CDM model is represented by internal state variables (ISV) and the laminate constitutive equations are expressed in general forms containing ISV and a number of material constants that must be for each laminate configuration determined experimentally measuring stiffness. Synergistic damage mechanics (SDM) version was published in [31] where micromechanics input in a form of calculated crack opening displacement (COD) is combined with the classical CDM.

The stiffness degradation phenomenon is indeed related to the opening and sliding of crack surfaces. Due to the relative displacement of both crack faces the average stress between cracks is reduced and, hence, the contribution of the damaged ply in bearing the applied load is reduced.

This relationship was used by Gudmundson et al. [32,33] considering laminates with general lay-up and using homogenization to derive expressions for stiffness and thermal

expansion coefficients of laminates with cracks in layers of a 3-D laminate. Their expressions in an exact form correlate damaged laminate thermo-elastic properties with parameters characterizing crack behavior: the average COD and the crack face sliding displacement (CSD). These parameters should be found solving the local boundary value problem. Gudmundson and co-workers suggested neglecting the effect of neighboring layers on COD and CSD. They were assumed equal to the known solution for a periodic system of cracks in an infinite homogeneous transversely isotropic medium (90-layer). FEM analysis in [28] shows that this approximation is not accurate for composites with stiff layers surrounding the damaged 90-layer.

A similar approach in the framework of the classical laminate theory (CLT) (called GLOB-LOC approach), which links the macro-constants of the damaged laminate with the geometry of the individual crack surface in deformed state, was developed in [28,29]. Exact analytical expressions for thermo-elastic constants of general symmetric laminates with cracks in layers were presented. In addition to laminate lay-up, layer properties and density of cracks in each layer they contain two parameters of the deformed crack surface: averaged relative opening (COD) and sliding displacements (CSD) normalized with respect to the far field stress in the layer. The largest advantage of this model is the transparency of derivations and the simplicity of application.

In [28,29,18] FEM analysis was used to identify parameters affecting these quantities. It was found that at low crack density (number of cracks per mm measured transverse to the fiber direction in a layer) the average COD and CSD are very robust parameters dependent only on the cracked and the neighboring layer stiffness and thickness ratios. The conclusion was that increasing modulus and thickness of the constraint layer leads to significant reduction of the average normalized COD and CSD. Simple but rather accurate fitting functions (“power laws”) were presented. Hence, the GLOB-LOC

approach can be used instead of FEM. The effect of material properties on the normalized COD was studied also experimentally using optical microscopy of loaded damaged specimens in [2,34]. It was shown that the measured COD profiles and average values are affected by the constraining layer orientation and stiffness. Experimental determination of the average COD and CSD needs the measurement of the displacement for all points of the crack surfaces, which justifies the use of full-field measurement technique Electronic Speckle Pattern Interferometry (ESPI). ESPI is an optical technique that provides the displacement for every point on a surface and offers the possibility to measure both, the in-plane and out-of-plane displacement without surface preparation [35].

This technique was used in [36,37] to measure the COD for cracks in internal layers on the specimen's edge. It was shown that the profile of the crack on the edge is very close to elliptical.

At higher density of transverse cracks the local stress states of individual cracks start to overlap and the effect of each individual crack on stiffness is reduced. This overlapping of stress perturbations is called "interaction" and cracks at high densities as "interactive". Interactive cracks have smaller opening. One can visualize it by imagining two existing cracks and a new crack (a "cut" in 90-layer) created between them. The "cut" will reduce the stress between existing cracks and the displacement of the corresponding faces of these two cracks.

The objectives of the presented doctoral thesis are the following:

The main objective of chapter 2 is to investigate the effect of crack interaction on COD using FEM and to describe the identified dependence on crack density in a simple and accurate form by introducing an interaction function.

In chapter 3, model with non-uniform crack distribution is used to calculate the axial modulus of cross-ply laminates with cracks in internal and surface layers.

In parametric analysis the COD and CSD are calculated using FEM, considering the smallest versus the average crack spacing ratio as non-uniformity parameter.

A "double-periodic" approach is presented in this chapter to calculate the COD of a crack in a non-uniform case as the average of two solutions for periodic crack systems.

The main objective of chapter 4 is to demonstrate the application of simple analytical models (shear lag, Hashin) to analyze the change of the whole set thermo-elastic properties of cross-ply and quasi-isotropic laminates with intralaminar cracks in layers. Predictions are performed using previously derived general expressions for stiffness of symmetric damaged laminates as dependent on crack density and crack face opening (COD) and sliding (CSD).

The main objective of chapter 5 is to measure experimentally the crack opening displacement (COD) and the crack sliding displacement (CSD) providing laminate stiffness reduction models with valuable information for validation of used assumptions and for defining limits of their application. In particular, the displacement field on the edges of a $[0/ +70_4/ -70_4]_s$ glass fiber/epoxy laminate specimens with multiple intralaminar cracks is studied and the COD and CSD dependence on the applied mechanical load is measured.

In chapter 6, the first objective is to measure experimentally the COD profile using the displacement field on the edge and on the surface of a $[90/0]_s$ and $[90_3/0]_s$ carbon fiber/epoxy laminates subjected to tension. The comparison between finite element method (FEM) and experimental results is the second objective of this chapter.

Chapter 2

Engineering expressions for thermo-elastic constants of laminates with high density of transverse cracks

2.1. Introduction

Intralaminar cracks are caused by in-plane transverse and shear stresses in layers with current understanding that the role of transverse stress is much more important. The number of cracks increases during service life reducing laminate thermo-elastic properties. Many papers have been written on this subject, covering a broad range from "micromechanics" based to continuum damage mechanics based models (see review for example in [3-6]).

All models analyzing the stress state between two cracks are commonly referred as "micromechanics models". Most of the analytical stress distribution modeling has been performed for cross-ply laminates with cracks in the 90-layer.

The shear-lag type of analysis is the simplest way to describe intralaminar cracking in cross-ply laminates. This group of models was used by many authors, for example in [7-10], where a linear or parabolic shape of the crack face displacement or of the out-of-plane shear stress is assumed. In [10] a bi-linear distribution of the shear stress in the undamaged layer was suggested as more coherent with findings from FEM analysis. General drawbacks of these models are that the equilibrium equations are not satisfied in any point but only in average and that the shear stress is not zero on crack surface. The "shear lag parameter" governing the shape of stress distributions is often used as a fitting parameter.

The variational model by Hashin [11], is free of any fitting parameters, but it is based on an oversimplified assumption that the axial stress in the cracked 90-layer does not

depend on the thickness coordinate. As any model based on the principle of minimum complementary energy it overestimates the stiffness reduction. The accuracy has been improved using more sophisticated shape functions for stresses [13,14].

In the McCartney model [15,16] each layer in the laminate is divided in a large number of thin sub-layers and in each sub-layer the stress assumptions are as in Hashin's variational model [11]. All displacement and stress continuity conditions at sub-layer interfaces are satisfied. The stress-strain relationships are also satisfied, except one, which is satisfied in an average sense. It was proven that satisfying in average is identical to asking for minimum of the Reissner energy functional in the used approximation of the stress-strain state. The Schoeppner-Pagano model [17], which is also based on Reissners principle, considers a system of hollow concentric sub-cylinders with a radius approaching to infinity. Each layer is divided in a number of coaxial cylinders. These two methods have to be considered as numerical or semi-analytical. They render local stress state with accuracy comparable with a very fine FE solution and, therefore, also accurate stiffness prediction. However, the calculation routines in these models are extremely complex which limits the application for more general cases than cracks in one layer only.

Cross-ply laminates are a good configuration for analysis of basic phenomena in intralaminar cracking but they are seldom used in practical applications. Laminates with a general lay-up containing cracks in several layers of different orientation are, therefore, a challenge for any constitutive model. Analytical solutions except a straightforward generalization for [S/90]s laminates with homogenized sublaminate S, see [7,18], are not available. In [19] "equivalent constraint" model was introduced, which assumes that the constraint of the lay-ups above and below the analysed lamina is

the same as from two homogenized orthotropic sublaminates and the actual laminate was replaced by a cross-ply.

Two tracks may be distinguished in this type of modelling in recent years: a) generalizing analytical models to lay-ups where the lay-up supporting the damaged layer is monoclinic, leading to coupling of the normal and shear loading problems [22-26]; b) developing computational tools for calculating thermo-elastic properties of multidirectional laminates with cracks in several layers [26-30]. The iterative approach here is usually based on using effective constants of the damaged layers when cracks in another layer are explicitly analysed (generalized "equivalent constraint" model).

Generally speaking, the continuum damage mechanics (CDM) approach [5] also may be used to describe the stiffness of laminates with intralaminar cracks in off-axis plies of any orientation. The damage in CDM model is represented by internal state variables (ISV) and the laminate constitutive equations are expressed in general forms containing ISV and a number of material constants that must be for each laminate configuration determined experimentally measuring stiffness. Synergistic damage mechanics (SDM) version was published in [31] where micromechanics input in a form of calculated crack opening displacement (COD) is combined with the classical CDM.

The stiffness degradation phenomenon is indeed related to the opening and sliding of crack surfaces. Due to the relative displacement of both crack faces the average stress between cracks is reduced and, hence, the contribution of the damaged ply in bearing the applied load is reduced.

This relationship was used by Gudmundson et al. [32,33] considering laminates with general lay-up and using homogenization to derive expressions for stiffness and thermal expansion coefficients of laminates with cracks in layers of a 3-D laminate. Their expressions in an exact form correlate damaged laminate thermo-elastic properties with

parameters characterizing crack behavior: the average COD and the crack face sliding displacement (CSD). These parameters should be found solving the local boundary value problem. Gudmundson and co-workers suggested neglecting the effect of neighboring layers on COD and CSD. They were assumed equal to the known solution for a periodic system of cracks in an infinite homogeneous transversely isotropic medium (90-layer). FEM analysis in [28] shows that this approximation is not accurate for composites with stiff layers surrounding the damaged 90-layer.

A similar approach in the framework of the classical laminate theory (CLT) (called GLOB-LOC approach), which links the macro-constants of the damaged laminate with the geometry of the individual crack surface in deformed state, was developed in [28,29]. Exact analytical expressions for thermo-elastic constants of general symmetric laminates with cracks in layers were presented. In addition to laminate lay-up, layer properties and density of cracks in each layer they contain two parameters of the deformed crack surface: averaged relative opening (COD) and sliding displacements (CSD) normalized with respect to the far field stress in the layer. The largest advantage of this model is the transparency of derivations and the simplicity of application.

In [18,28,29] FEM analysis was used to identify parameters affecting these quantities. It was found that at low crack density (number of cracks per mm measured transverse to the fiber direction in a layer) the average COD and CSD are very robust parameters dependent only on the cracked and the neighboring layer stiffness and thickness ratios. The conclusion was that increasing modulus and thickness of the constraint layer leads to significant reduction of the average normalized COD and CSD. Simple but rather accurate fitting functions ("power laws") were presented. Hence, the GLOB-LOC approach can be used instead of FEM. The COD and CSD have been measured also experimentally [34,37] and trends as well as values are confirmed.

At higher density of transverse cracks the local stress states of individual cracks start to overlap and the effect of each individual crack on stiffness is reduced. This overlapping of stress perturbations is called ”interaction” and cracks at high densities as ”interactive”. Interactive cracks have smaller opening. One can visualize it by imagining two existing cracks and a new crack (a “cut” in 90-layer) created between them. The “cut” will reduce the stress between existing cracks and the displacement of the corresponding faces of these two cracks.

We suggest accounting for interaction in a very simple way: introducing crack density dependent interaction function which multiplied by the COD and CSD of non-interactive cracks would give the opening and sliding at any crack density. Previously the crack interaction for COD was studied using FEM in [38], considering cracks in 90-layer of [0n/90m]s laminate. The FEM data were fitted with logarithmic function with limited range of applicability in terms of laminate lay-up and crack density.

The objectives of the presented chapter are

a) To use FEM to analyze COD’s in cross-ply laminates at high crack density in surface layers (“surface cracks”) and inside layers (“inside cracks”)
b) to present unified interaction functions for COD of surface and internal cracks to be used together with noninteractive crack COD
c) to adapt the methodology for more general laminate and to demonstrate the accuracy predicting stiffness of damaged quasi-isotropic laminates

Features of the crack face sliding, CSD in the interactive region as well as the interaction of cracks belonging to different layers in the laminate are not considered in this chapter. The GLOB-LOC model accounts for latter phenomena via changed COD and CSD. The determination of the COD and CSD change in that case is a very complex topic and generally speaking the solution has to be found in an iterative way.

However, see [28,29] for details, the level of interaction depends on the particular case and on the considered parameter. For example in cross-ply laminate with cracks in 0- and 90-layers, the COD of 90-cracks is almost not affected by cracks in the 0-layer. In contrary, CSD of the 90-crack is significantly higher in presence of cracks in the 0-layer.

2.2. Material model of damaged symmetric laminates with intralaminar cracks

2.2.1 Model formulation

The upper part of symmetric *N*- layer laminate is shown in Fig. 2.1. The *k*-th layer of the laminate is characterized by thickness t_k , fiber orientation angle with respect to the global x-axis θ_k and by stiffness in the local axes $[Q]$ (defined by thermo-elastic constants $E_1, E_2, G_{12}, \nu_{12}, \alpha_1, \alpha_2$). The total thickness of the laminate, $h = \sum_{k=1}^{N} t_k$. The crack density in a layer is $\rho_k = 1/(2l_k \sin\theta_k)$ where $2l_k \sin\theta_k$ is the average distance between cracks measured transverse to the crack plane. Dimensionless crack density ρ_{kn} is introduced as

$$\rho_{kn} = t_k \rho_k . \tag{2.1}$$

It is assumed that the damaged laminate is still symmetric; the crack density in corresponding symmetrically placed layers is the same. The stiffness matrix of the damaged laminate is $[Q]^{LAM}$ and the stiffness matrix of the undamaged laminate is $[Q]_0^{LAM}$. The compliance matrix of the undamaged laminate is $[S]_0^{LAM} = \left([Q]_0^{LAM}\right)^{-1}$, $\{\alpha\}_0^{LAM}$ is the thermal expansion coefficient vector. Constants of the undamaged laminate are calculated using CLT.

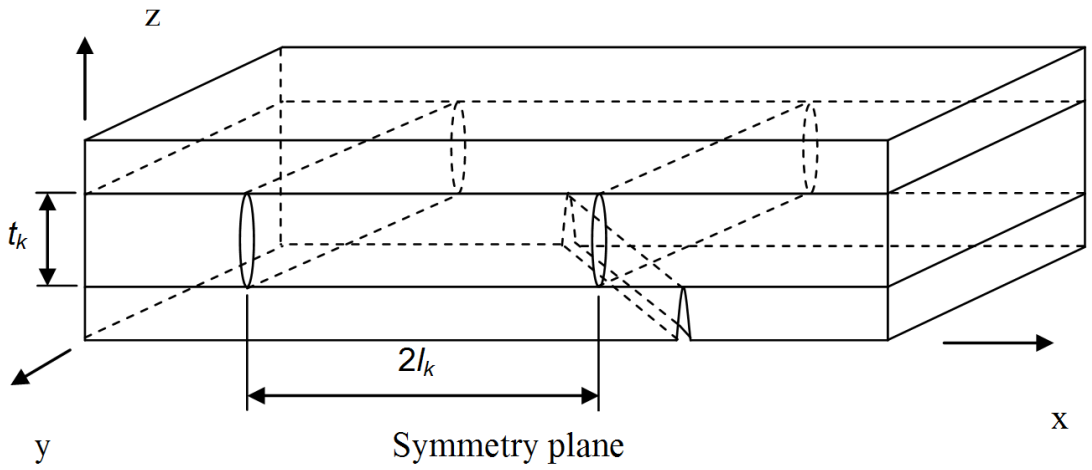

Figure 2.1. RVE of the damaged laminate with intralaminar cracks in layers

The expressions for thermo-elastic constants of the damaged laminate presented below are exact.

$$[S]^{LAM} = [S]_0^{LAM}\left([I] + \sum_{k=1}^{N} \rho_{kn} \frac{t_k}{h} [K]_k [S]_0^{LAM}\right) \tag{2.2}$$

$$\{\alpha\}^{LAM} = \left([I] + \sum_{k=1}^{N} \frac{t_k}{h} \rho_{kn} [S]_0^{LAM} [K]_k\right)\{\alpha\}_0^{LAM} - \sum_{k=1}^{N} \frac{t_k}{h} \rho_{kn} [S]_0^{LAM} [K]_k \{\overline{\alpha}\}_k \tag{2.3}$$

They were derived in [28,29] expressing the integral effect of cracks in terms of crack density and normalized average crack face opening (COD) and sliding displacements (CSD), u_{2an}, u_{1an} which may be different in different layers. In (2.3) $[K]_k$ is a 3X3 matrix-function dependent on ply properties. The $[K]_k$ matrix for a ply in a laminate is defined as

$$[K]_k = \frac{1}{E_2} [\overline{Q}]_k [T]_k^T [U]_k [T]_k [\overline{Q}]_k \tag{2.4}$$

The involved matrices $[T]_k$ and $[\overline{Q}]_k$ are defined according to CLT, upper index T denotes transposed matrix and bar over stiffness matrix indicates that it is written in global coordinates. For a layer with fiber orientation angle θ_k , $m = \cos\theta_k$ and $n = \sin\theta_k$

$$[T]_k = \begin{bmatrix} m^2 & n^2 & +2mn \\ n^2 & m^2 & -2mn \\ -mn & +mn & m^2 - n^2 \end{bmatrix} \qquad [\overline{Q}]_k = [T]_k^{-1}[Q]([T]_k^{-1})^T \tag{2.5}$$

The influence of each crack is represented in (2.4) by matrix $[U]_k$ which contains the normalized average COD and normalized average CSD of the crack surfaces in k-th layer

$$[U]_k = 2\begin{bmatrix} 0 & 0 & 0 \\ 0 & u_{2an}^k & 0 \\ 0 & 0 & \frac{E_2}{G_{12}} u_{1an}^k \end{bmatrix} \tag{2.6}$$

Simple and reliable determination of u_{2an}, u_{1an} in high crack density region is the main subject in this chapter. In (2.3) $\{\overline{\alpha}\}_k$ is the vector of thermal expansion coefficients of a damaged layer in global coordinates.

2.2.2 Thermo-elastic constants of balanced laminates with cracks in 90-layers

For balanced and symmetric laminates with cracks in 90-layers only, analytical expressions for $[K]_k$ can be obtained performing the multiplication in (2.4). Using the result in (2.2) and (2.3) the following expressions for the damaged laminate thermo-elastic constants were obtained

$$\frac{E_x}{E_x^0} = \frac{1}{1 + 2\rho_{90n}\frac{t_{90}}{h} u_{2an}^{90} c_2} \qquad \frac{E_y}{E_y^0} = \frac{1}{1 + 2\rho_{90n}\frac{t_{90}}{h} u_{2an}^{90} c_4} \tag{2.7}$$

$$\frac{\nu_{xy}}{\nu_{xy}^0} = \frac{1 + 2\rho_{90n}\frac{t_{90}}{h} u_{2an}^{90} c_1 \left(1 - \frac{\nu_{12}}{\nu_{yx}^0}\right)}{1 + 2\rho_{90n}\frac{t_{90}}{h} u_{2an}^{90} c_2} \qquad \frac{G_{xy}}{G_{xy}^0} = \frac{1}{1 + 2\rho_{90n}\frac{t_{90}}{h} u_{1an}^{90} \frac{G_{12}}{G_{xy}^0}} \tag{2.8}$$

$$\frac{\alpha_x}{\alpha_x^0} = 1 - 2\rho_{90n}\frac{t_{90}}{h}u_{2an}^{90}\frac{c_1}{\alpha_x^0}\left(\alpha_2 - \alpha_x^0 - \nu_{12}\left(\alpha_y^0 - \alpha_1\right)\right) \tag{2.9}$$

$$\frac{\alpha_y}{\alpha_y^0} = 1 - 2\rho_{90n}\frac{t_{90}}{h}u_{2an}^{90}\frac{c_3}{\alpha_y^0}\left(\alpha_2 - \alpha_x^0 - \nu_{12}\left(\alpha_y^0 - \alpha_1\right)\right) \tag{2.10}$$

$$c_1 = \frac{E_2}{E_x^0}\frac{1-\nu_{12}\nu_{xy}^0}{\left(1-\nu_{12}\nu_{21}\right)^2} \qquad c_2 = c_1\left(1-\nu_{12}\nu_{xy}^0\right) \tag{2.11}$$

$$c_3 = \frac{E_2}{E_y^0}\frac{\nu_{12}-\nu_{yx}^0}{\left(1-\nu_{12}\nu_{21}\right)^2} \qquad c_4 = c_3\left(\nu_{12}-\nu_{yx}^0\right) \tag{2.12}$$

Index 90 is used for 90-layer thickness, crack density and COD. The quantities with lower index x,y are laminate constants, quantities with additional upper index 0 are undamaged laminate constants. If the laminate contains several 90-layers, the term $\rho_{90n}\frac{t_{90}}{h}u_{2an}^{90}$ has to be replaced by $\sum_k \rho_{90n}^k \frac{t_{90}^k}{h}u_{2an}^{90(k)}$. It is noteworthy that

a) neglecting Poisson's effects leads to $c_3 = c_4 = 0$. Hence, in this approximation E_y and α_y do not change because of damage in 90-ply.

b) the shear modulus G_{xy} is not related to COD. It depends on the sliding displacement only.

The class of laminates covered by expressions (2.7)-(2.12) is broader than just cross ply laminates or laminates with 90-layers. For example, any quasi-isotropic laminate with an arbitrary cracked layer can be rotated to have the damaged layer as a 90-layer. The only limitation for applying (2.7)-(2.12) is that the laminate after rotation is balanced (zero coupling terms in $[S]_0^{LAM}$).

Application of (2.7)-(2.12) requires values of u_{2an}, u_{1an}. Simple and rather accurate expressions are presented in section 3 where FEM parametric analysis is used.

2.3. Numerical parametric analysis of COD

2.3.1 Definitions, interaction mechanisms and FEM model

Since the theory is developed to assess material thermo-elastic properties degradation (which is represented by the middle part of an infinite plate and not by a finite specimen) calculations have to exclude possible edge effects. It is assumed that all cracks in the same layer are equal and equidistant. The average CSD and COD are defined as

$$u_{1a}^{k} = \frac{1}{2t_k} \int_{-\frac{t_k}{2}}^{\frac{t_k}{2}} \Delta u_1^k(x_3)\, dx_3 \qquad u_{2a}^{k} = \frac{1}{2t_k} \int_{-\frac{t_k}{2}}^{\frac{t_k}{2}} \Delta u_2^k(x_3)\, dx_3 \tag{2.13}$$

Here Δu_i is the displacement gap between points at both crack faces. Index 1 denotes the displacement in fiber direction (sliding) and index 2 in the transverse direction (opening).

In a linear model the average displacements u_{2a}^{k} and u_{1a}^{k} are proportional to the applied stress and to the ply thickness (they are 2 times larger in $[0_2/90_2]_S$ than in $[0/90]_S$ laminate). Hence, a load and size independent parameters may be obtained normalizing (2.13) with respect to the far field (CLT) shear stress σ_{12}^{0k} and transverse stress σ_{2}^{0k} in the layer (resulting from the applied macro-load $\{\sigma\}_0^{LAM}$ and the temperature difference ΔT) and with respect to the thickness of the cracked layer t_k

$$u_{1an}^{k} = u_{1a}^{k} \frac{G_{12}}{t_k \sigma_{12}^{0k}} \qquad u_{2an}^{k} = u_{2a}^{k} \frac{E_2}{t_k \sigma_{2}^{0k}} \tag{2.14}$$

Elastic constants G_{12} and E_2 are introduced in (2.14) to have dimensionless descriptors u_{1an}^{k} and u_{2an}^{k} representing the crack face displacements. The influence of each crack on thermo-elastic laminate constants is represented by u_{2a}^{k} and u_{1a}^{k}, see (2.2)-(2.6) or (2.7)-(2.12). As demonstrated in [39], they can be deduced from simple stress models

like shear lag [7] or variational models [11], however the accuracy of these models is rather low. Instead, in this chapter we present expressions based on FEM parametric analysis for a wide range of material properties and crack density. Analysis in this chapter is limited to crack opening displacements leaving sliding for a separate studies.

The normalized average COD and CSD in the low crack density region are independent on crack density. Upper index 0 is used to indicate values in this region ($u_{1an}^{0k}, u_{2an}^{0k}$). Fitting expressions for $u_{1an}^{0k}, u_{2an}^{0k}$ are given in [28,29].

When the distance between cracks decreases the stress perturbation regions overlap and the normalized average COD and CSD start to decrease. This phenomenon was studied in [32], however, considering only COD for "inside cracks" (defined in Fig. 2.2a). Here we a) extend the analysis to damaged surface layers, see Fig. 2.2b) and b) present more reliable description of the interaction in inside layers.

As in [38] in this chapter we also express u_{2an}^{k} through COD of non-interactive cracks, u_{2an}^{0k} by introducing "interaction function" dependent on normalized crack density in the layer

$$u_{2an}^{k} = \lambda_k(\rho_{kn}) u_{2an}^{0k} \tag{2.15}$$

The interaction function λ depends also on elastic and geometrical parameters of the cracked and surrounding layers. For non-interactive cracks $\lambda_k = 1$.

In [38] a rather inaccurate logarithmic "master" curve was used with a good fit only for medium crack densities. The role of elastic constants and geometrical parameters on crack interaction was not really understood and therefore the "master curve" did not include these parameters. The outcome was a simple interaction function on the expense of reduced accuracy.

In the presented chapter we analyzed the effect of the dimensionless crack density ρ_n on u_{2an} using FEM for $[0_n/90_8]_S$ and $[90_8/0_n]_S$ laminates (n=2,8,24) shown in Fig. 2.2. To have large variation in elastic constants both CF/EP and GF/EP composites with constants given in Table 2.1 were analyzed. Since all expressions contain thickness ratios, the thickness of a single ply is irrelevant as long as dimensionless crack density is used.

In calculations the commercial code ABAQUS was used. In order to model the repeating volume element (see Fig. 2.2), a 3-D model was created. All plies are considered to be transversely isotropic, and hence the thickness direction related properties are taken as $E_2 = E_3; G_{12} = G_{13}$ and $\nu_{12} = \nu_{13}$.

Table 2.1. Material properties used in simulations, t is the ply thickness

Material	E_1(GPa)	E_2(GPa)	ν_{12}	ν_{23}	G_{12} (GPa)	G_{23} (GPa)	t (mm)
GF/EP	45	15	0.3	0.4	5	5.36	0.5
CF/EP	150	10	0.3	0.4	5	3.57	0.5

In order to mesh volumes, 3D continuum elements (C3D8) 8-node linear brick were used. The same fine mesh with 86400 elements was used in each FE model. The (X, Z) plane consisted of 21600 elements, with refined mesh near the crack surfaces. The number of elements in y-direction was 4 which as described below is more than sufficient for the used edge conditions.

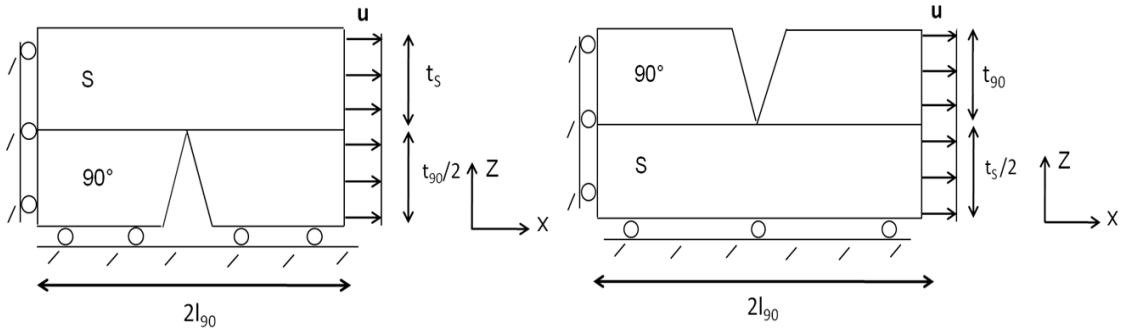

a) inside crack b) surface cracks

Figure 2.2. Models used for determination of average crack face opening displacement

Constant displacement corresponding to 1% average strain was applied to the repeating unit in x-direction. On the front edge (y=0) and the far-away edge (y=w) coupling conditions were applied for normal displacements (u_y = unknown constant). In this way edge effects are eliminated and the solution does not depend on y-coordinate. It corresponds to solution for an infinite structure in the width direction. Obviously these conditions correspond to generalized plane strain case and the size of the model in the y-direction could be reduced or 2D generalized plane strain elements used instead. Our choice was based on ambition to use the same mesh in shear loading studies. The displacement in x-direction for the nodes at the crack surface was used to calculate the average value of the COD. Varying length $2l_{90}$ of the repeating unit, the elastic modulus change and the average strain of 1% corresponds to different values of the applied load (laminate stress). Hence, performing normalization according to Equation (2.14) we have to use the corresponding far field stress σ_2^0 and σ_{12}^0 in the 90° layer.

The COD affects the axial stress distribution between neighbouring ply cracks. For high ply crack densities, compressive axial stresses can arise that might be associated with ply crack saturation.

Fig. 2.3 shows the normalized crack face opening displacement u_{2an} for $[90_8/0_n]_S$ and $[0_n/90_8]_S$ laminates made of GF/EP and CF/EP materials as a function of normalized crack density ρ_n in the 90-layer.

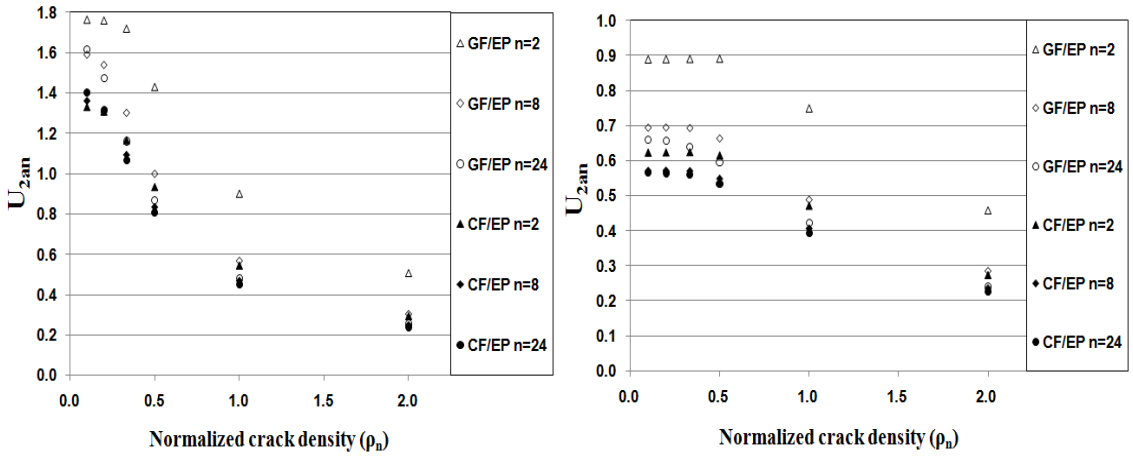

a) $[90_8/0_n]_s$ b) $[0_n/90_8]_s$

Figure 2.3. The FEM calculated u_{2an} dependence on crack density for **GF/EP** and **CF/EP** laminates with varying layer thickness ratio

A large variation in u_{2an} values dependent on the composite elastic properties and laminate lay-up is shown in Fig. 2.3. For a fixed value of the normalized crack density, u_{2an} is bigger for GF/EP than for CF/EP laminate because GF/EP 0-layer applies less constraint to the COD than the CF/EP 0-layer. The COD decreases with increasing crack density. The effect of increasing crack density is analyzed first normalizing the results in Fig. 2.3 with respect to the COD's of corresponding noninteractive cracks, u_{2an}^0, obtained by FEM. According to (2.15) the normalized values define the interaction function. As a result of many trials to fit these data we suggest the following form of the 'interaction function"

$$\lambda(\rho_n) = \tanh\left(\frac{\alpha}{\rho_n}\right) \tag{2.16}$$

The form (2.16) is similar to the corresponding term in shear lag model's solution for stiffness but the definition of α (see (2.17), (2.18)) is different.

2.3.2 Internal cracks

For internal cracks the constant α is defined by

$$\alpha^2 = C \times \left(\frac{t_s G_{23} + t_{90}/2 \, G_{12}}{(t_s + t_{90}/2) G_{23}} \right) \left(1 + \frac{t_{90}/2 \, E_2}{t_s E_s} \right) \qquad C = 0.52 \qquad (2.17)$$

In (2.17) and also in (2.18) E_s is the elastic modulus of the support layer in the transverse direction of the 90-layer. Obviously, $E_s = E_1$ for cross-ply laminates. C is a material and ply geometry independent fitting constant which has different value for "surface" and for "inside" cracks. To find C the FEM values of the interaction function $\lambda(\rho_n)$ for each lay-up and material separately were plotted versus ρ_n. Then the value of the parameter α in (2.16) was determined using free software REGRESSI. In this way α dependence on geometrical and elastic parameters was obtained. To calculate the constant C in (2.17), we plotted all α^2 data points versus the corresponding $\left(\frac{t_s G_{23} + t_{90}/2 \, G_{12}}{(t_s + t_{90}/2) G_{23}} \right) \left(1 + \frac{t_{90}/2 \, E_2}{t_s E_s} \right)$ value. According to (2.17) the relationship has to be linear. Indeed it was rather linear and fitting it with linear trend line gave the value in (2.17).

Using this value of C the inside crack interaction function may be calculated for any lay-up and material. For example in Fig. 2.4 values from direct FE calculations for internal cracks are compared with values according to expression (2.16) for [0/90]s laminates. The accuracy is good.

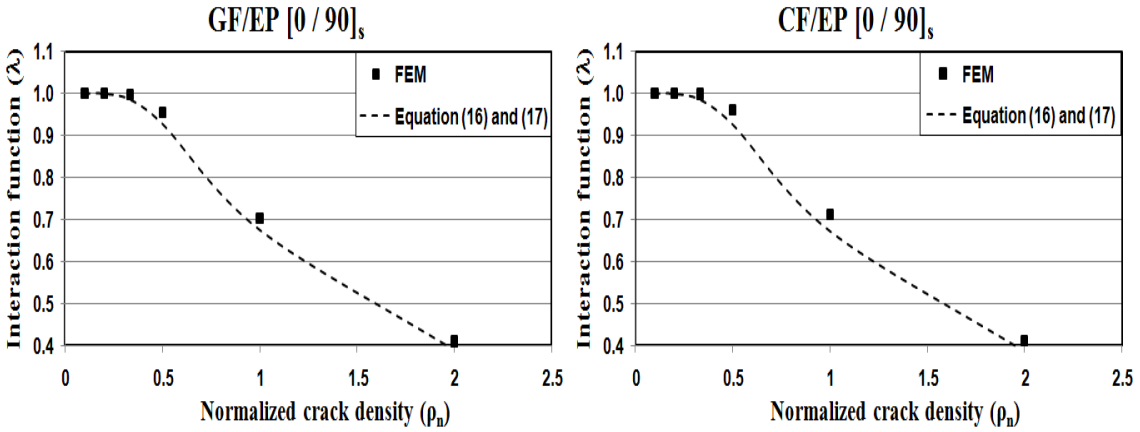

Figure 2.4. Interaction function according to FEM and equation (2.16) for inside cracks in **GF/EP** and **CF/EP** cross-ply laminates

2.3.3 Surface cracks

For surface cracks in cross-ply laminates

$$\alpha^2 = C \times \left(\frac{t_s/2 \; G_{23} + t_{90} G_{12}}{(t_s/2 + t_{90}) G_{23}} \right) \left(1 + \frac{t_{90} E_2}{t_s/2 \; E_s} \right) \qquad C = 0.085 \qquad (2.18)$$

The expression (2.18) is essentially the same as (2.17). The difference is because of the slightly different notation for ply thicknesses in Fig. 2.2a and Fig. 2.2b. In Fig. 2.5 the values of the interaction function from direct FE calculations for cracks in surface layer of GF/EP and CF/EP [90/0]s cross-ply laminate are compared with values according to the fitting expression (2.16), (2.18). Similar calculations for different layer thickness ratios showed as good agreement as in Fig. 2.5 except for relatively very thick 90-layer case with rather limited practical significance, where the crack interaction is overestimated by (2.16), (2.18) leading to too low COD values. As a consequence the elastic modulus reduction will be slightly underestimated.

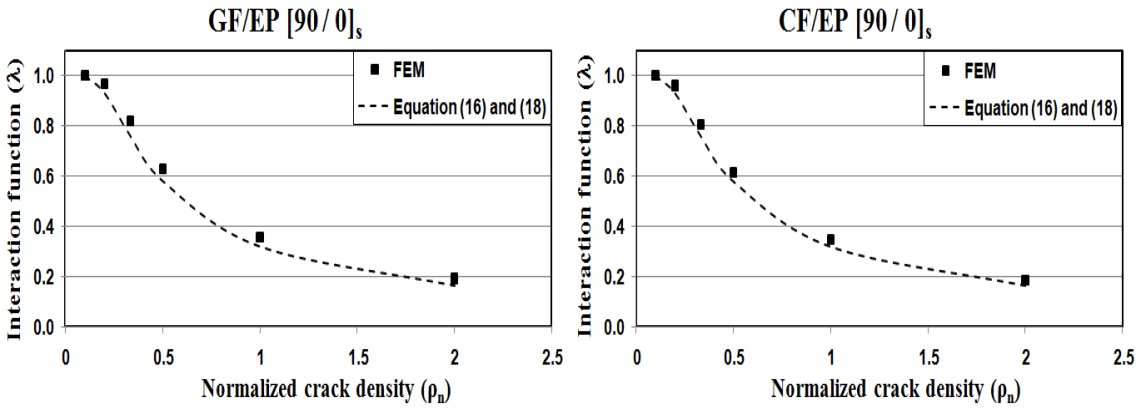

Figure 2.5. Interaction function according to FEM and equation (2.16) for surface cracks in **GF/EP** and **CF/EP** cross-ply laminates

2.4. Stiffness of cross-ply laminates

Elastic constants of the damaged laminates were calculated using (2.7) and (2.8). For cross-ply laminate with internal cracks the laminate thickness according to Fig. 2.2a is $h = t_{90} + 2t_S$. For laminate with surface crack the same laminate thickness according to Fig. 2.2b) is $h = 2t_{90} + t_s$. However, in the latter case we have two cracked surface layers with equal effect on stiffness. Hence, we have to consider two cracked layers in (2.7) to (2.12). We can achieve the same result dividing the laminate thickness in (2.7) to (2.12) by 2 and considering cracks in one layer. Calculations were performed with a half of the laminate thickness $h = t_{90} + {}^{t_s}\!/_{2}$ and cracks in one surface layer. The COD's of non-interactive cracks in (2.15) is taken from FEM considering the values as exact. Therefore the possible error in elastic constants is due to inaccuracy of (2.16) for $\lambda(\rho_n)$. The noninteractive COD's are given in Table 2.2.

Table 2.2. Values of u_{2an} for non-interactive cracks (FEM)

Laminate	CF/EP	GF/EP
$[0_2/90_8]_s$	0.6243	0.8880
$[0_8/90_8]_s$	0.5720	0.6941
$[0_{24}/90_8]_s$	0.5653	0.6593
$[90_8/0_2]_s$	1.3321	1.7654
$[90_8/0_8]_s$	1.3602	1.5915
$[90_8/0_{24}]_s$	1.4010	1.6174

For validation the elastic constants of the damaged cross-ply laminates were calculated also directly from FEM using the same mesh as for interactive COD determination: a) the total force and the applied axial strain were used to determine the axial modulus; b) the relative displacement of the coupled edge surfaces was used together with the applied axial strain to find the Poisson's ratio.

2.4.1 Stiffness of cross-ply laminates with damage in inside layers

The predicted axial modulus and Poisson's ratio of cross-ply laminates with cracks in inside layer is shown for GF/EP composite in Fig. 2.6 and for CF/EP in Fig. 2.7. The accuracy of predictions is good. Ply discount model predictions are also shown as dotted lines. It has to be reminded that the normalized crack density larger than 1 is extremely high and data in this region are shown to demonstrate the asymptotic approaching to the ply-discount value.

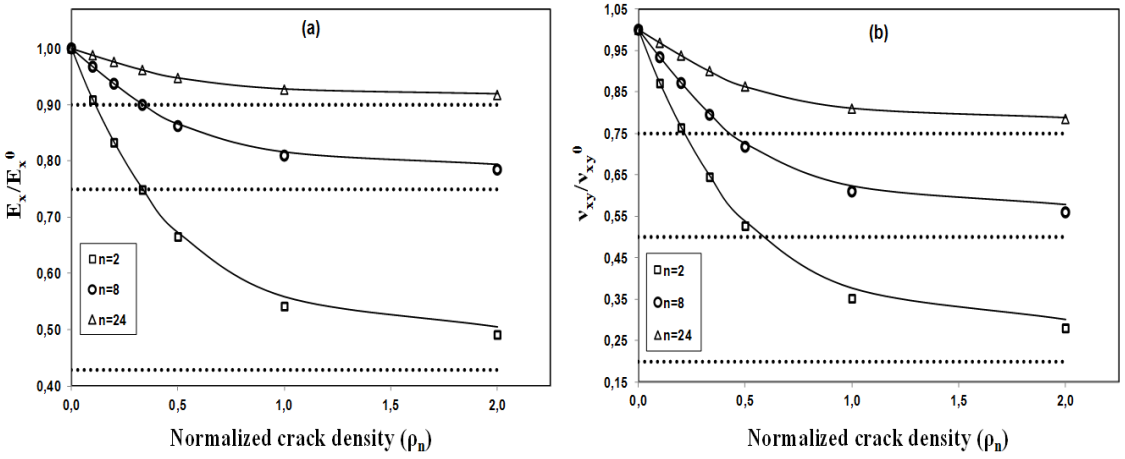

Figure 2.6. Elastic modulus (a) and Poisson's ratio (b) degradation in $[0_n/90_8]_S$ **GF/EP** laminate. FEM data are shown with symbols, predictions according to (2.16) by solid curves, dotted lines represent ply-discount model

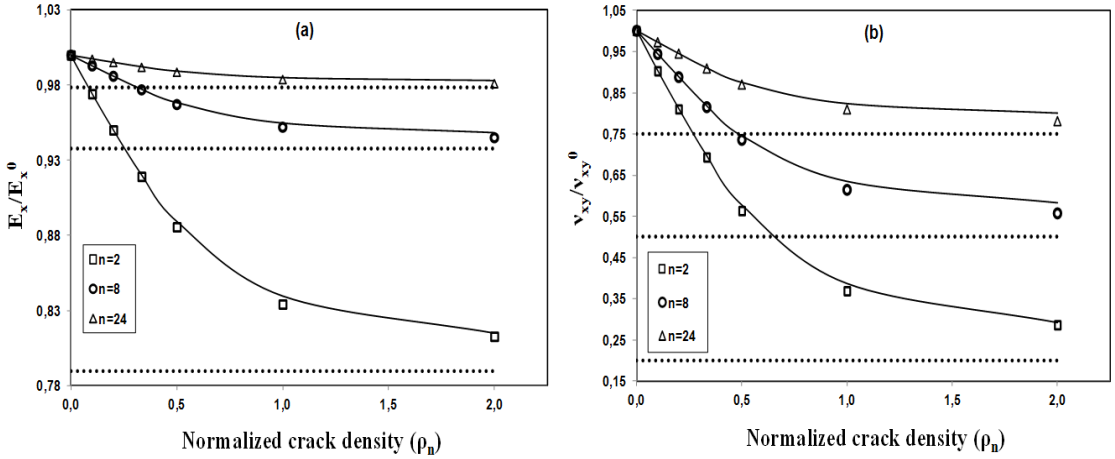

Figure 2.7. Elastic modulus (a) and Poisson's ratio (b) degradation in $[0_n/90_8]_S$ **CF/EP** laminate. FEM data are shown with symbols, predictions according to (2.16) by solid curves, dotted lines represent ply-discount model

2.4.2 Stiffness of cross-ply laminates with damage in surface layers

Elastic modulus and Poisson's ratio reduction with increasing crack density in $[90_8/0_n]_S$ GF/EP cross-ply laminates is presented in Fig. 2.8. The elastic modulus reduction calculated using (2.7) with non-interactive COD's in Table 2.2 and the interaction function (2.16) is slightly underestimated for $[90_8/0_8]$s laminates at very high crack density. The agreement is very good for $[90_8/0_{24}]$s laminate. The same observation holds for Poisson's ratio reduction.

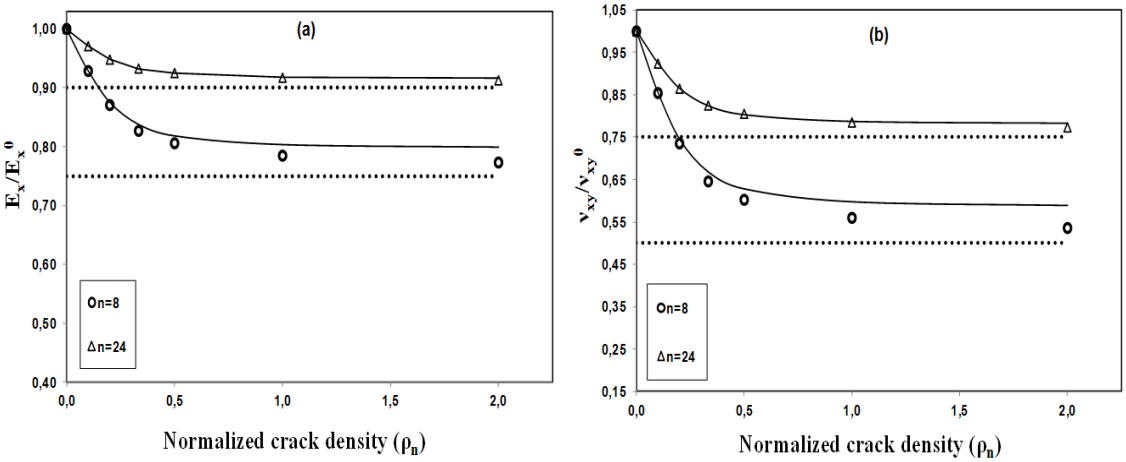

Figure 2.8 . Elastic modulus (a) and Poisson's ratio (b) degradation in $[90_8/0_n]_S$ **GF/EP** laminate due to cracking in 90-layer. FEM data are shown with symbols, predictions according to (2.16) by solid curves, dotted lines represent ply-discount model

In carbon fiber/epoxy laminates, see Fig. 2.9, the elastic modulus reduction due to cracks in 90-layer is much smaller, especially for relatively thin 90-layers. The accuracy using the interaction function is good also for Poisson's ratio prediction (except very high crack density).

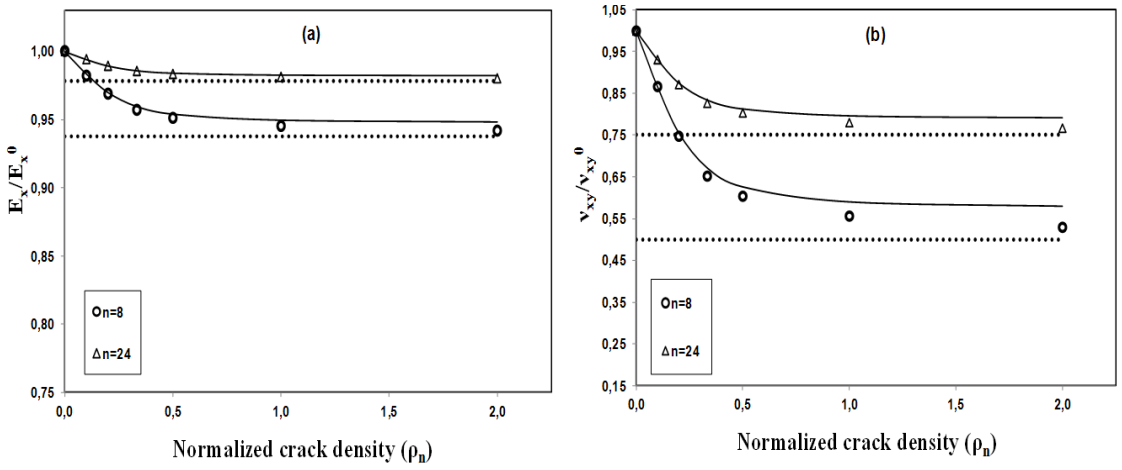

Figure 2.9. Elastic modulus (a) and Poisson's ratio (b) degradation in $[90_8/0_n]_S$ **CF/EP** laminate due to transverse cracking in 90-layer. FEM data are shown with symbols, predictions according to (2.16) by solid curves, dotted lines represent ply-discount model

2.5. Quasi-isotropic laminates

2.5.1 Generalization of the methodology

In section 3 we used FEM to analyze crack interaction and summarized the results in a simple but accurate interaction function. This analytical function together with expressions (2.7)-(2.12) can be used to predict stiffness of damaged laminates without any need to involve FEM. However, the value of the performed work finding COD interaction function would be rather limited if it can be applied for cross-ply laminates only. In this section we suggest to use the same interaction function $\lambda(\rho_n)$ also for more complex lay-ups. The necessary generalization and input parameters will be described. For quasi-isotropic laminates the predictions will be compared with numerical values of crack interaction and stiffness obtained directly from FE analysis.

In these calculations the commercial code ANSYS 12.1 was used. The 3-D 8-node structural solid element SOLID185 with three degrees of freedom for each node was used and the number of elements was 86400. Displacement coupling was applied. It means that points on the surface at y=0 has the same displacement in x- and z-directions as the corresponding points on the surface at y=w. In the same way, the points on the surface at x=0 and $x = 2l_{90}$ have the same displacement in y-direction. The coupling conditions were applied also for normal displacement (Uy=unknown constant) on all nodes at the front edge y=0 and the far-away edge y=w respectively.

CF/EP and GF/EP quasi-isotropic laminates with lay-up [90/0/45/-45]s and [90/45/-45/0]s containing cracks in surface layers as well as [45/-45/0/90]s and [0/45/-45/90]s laminates with cracks in the inside 90-layer were considered.

Applying (2.17) and (2.18) to "non-cross-ply" laminates further details have to be given with respect to the meaning of E_s and t_s. FEM results show that, when the neighboring layer is much stiffer than the 90-layer (for example 0-layer), the major part of the support is supplied by this layer and it is not really important what the following layers are. In contrary, when the layer closest to the 90-layer is less stiff (for example +45 or -45 layers), this layer alone can not govern crack interaction and the presence of following stiff layer is important (for example, the 0-layer in [0/45/-45/90]s laminate affects interaction of cracks in 90-layer). When this is the case, all neighboring layers have to be included in E_s (for example, considering [0/45/-45]s as sublaminate). Based on these observations the suggestion for E_s and t_s is as follows

$$E_s = \begin{cases} E_1 & \text{if 0-layer is the closest neighbor} \\ E_x^{subl} & \text{if not} \end{cases} \tag{2.19}$$

For surface cracks

$$t_s/2 = \begin{cases} t_{0°} & \text{if 0 - layer is the closest} \\ t_{subl}/2 & \text{if not} \end{cases} \tag{2.20}$$

For inside cracks

$$t_s = \begin{cases} t_{0°} & \text{if 0 - layer is the closest} \\ t_{subl}/2 & \text{if not} \end{cases} \tag{2.21}$$

2.5.2 Interaction of inside cracks

The fitting function (2.16) with (2.17) was adapted for [0/-45/45/90]s laminate as described above. Since the 0° layer is not the closest layer, E_s is calculated using LAP software for [0/45/-45]s sublaminate and t_s is ½ of its thickness. The obtained values (using data in Table 2.1) are: 62.622 GPa for CF/EP and 25.669 GPa for GF/EP. For [45/-45/0/90]s laminate where the 0° layer is the closest layer, $E_s = E_1$ and t_s is the thickness of the 0-layer. As shown in Fig. 2.10 the interaction function adapted from cross-ply case gives very good approximation of the crack interaction for CF/EP laminates. The agreement for GF/EP laminates is equally good.

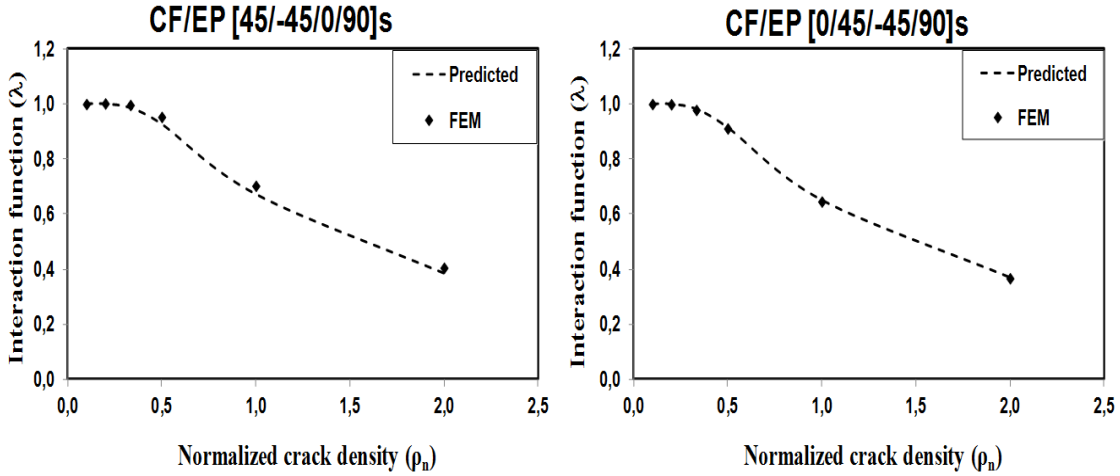

Figure 2.10. Interaction function according to FEM and equation (2.16), (2.17) for quasi-isotropic **CF/EP** laminates

2.5.3 Interaction of surface cracks

The fitting function (2.16) with (2.18) was adapted for [90/-45/45/0]s laminate as described above. Since the 0° layer is not the closest layer, E_s is calculated using LAP for [0/45/-45]s sublaminate and $t_s/2$ is ½ of its thickness. The obtained values are the same as for the inside crack case. For [90/0/45/-45]s laminate where the 0° layer is the closest layer, $E_s = E_1$ and $t_s/2$ is the thickness of the 0-layer. The values of interaction function are in a very good agreement with numerical values calculated directly from FEM, see Fig. 2.11 for GF/EP laminates.

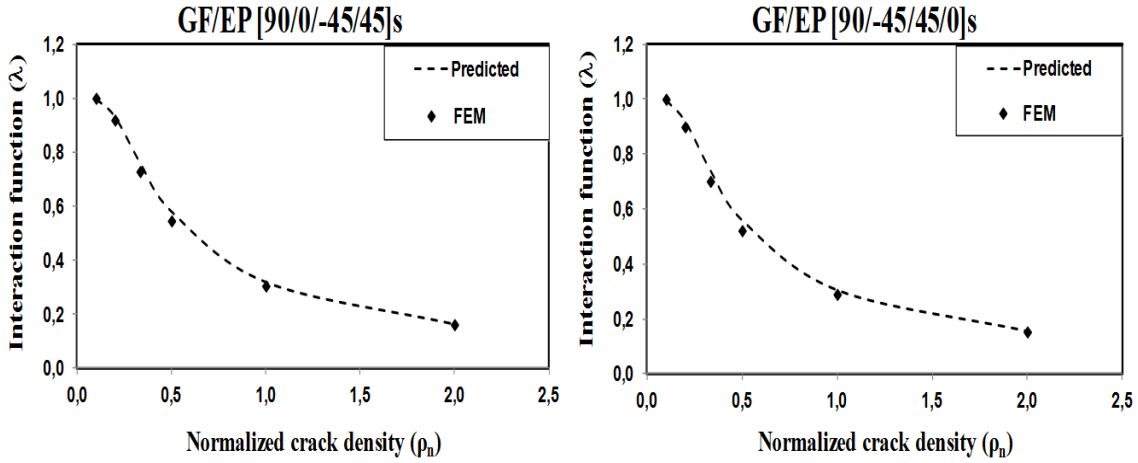

Figure 2.11. Interaction function according to FEM and equations (2.16),(2.18) for **GF/EP** laminates

2.5.4 Stiffness of damaged quasi-isotropic laminates

2.5.4.1 Quasi-isotropic laminates with cracks in inside layers

Predicted axial modulus and Poisson's ratio of quasi-isotropic laminates with cracks in inside layers is shown for CF/EP composite in Fig. 2.12 and for GF/EP in Fig. 2.13. Ply discount model predictions are also shown as dotted lines. The elastic modulus reduction is calculated using (2.7) and the Poisson's ratio is calculated using (2.8). The non-interactive COD's are from Table 2.2 and the interaction function (2.16) with

suggestions (2.19) and (2.21) is used. The accuracy of predictions is very high for both materials and for both cases of the closest support layer.

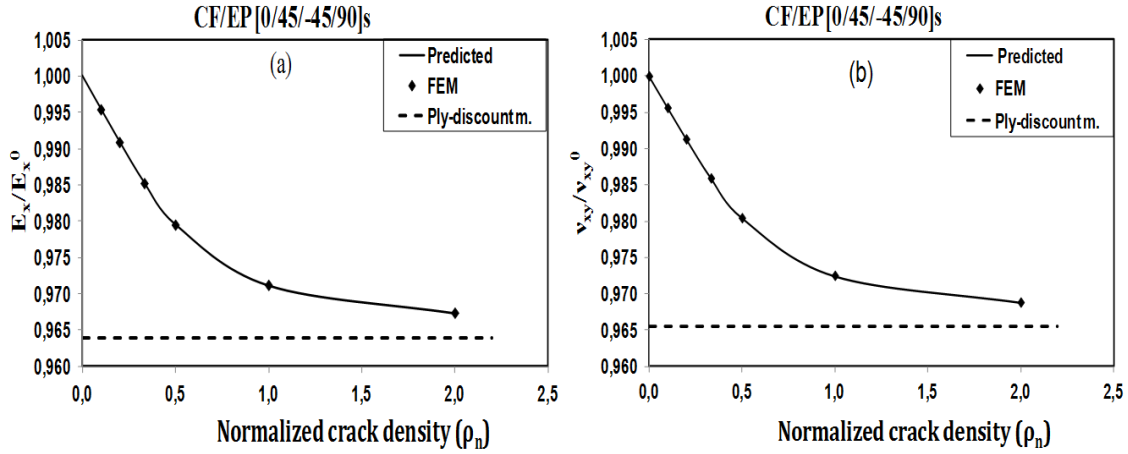

Figure 2.12. Elastic modulus (a) and Poisson's ratio (b) degradation in **CF/EP** quasi-isotropic laminate due to transverse cracking in 90-layer

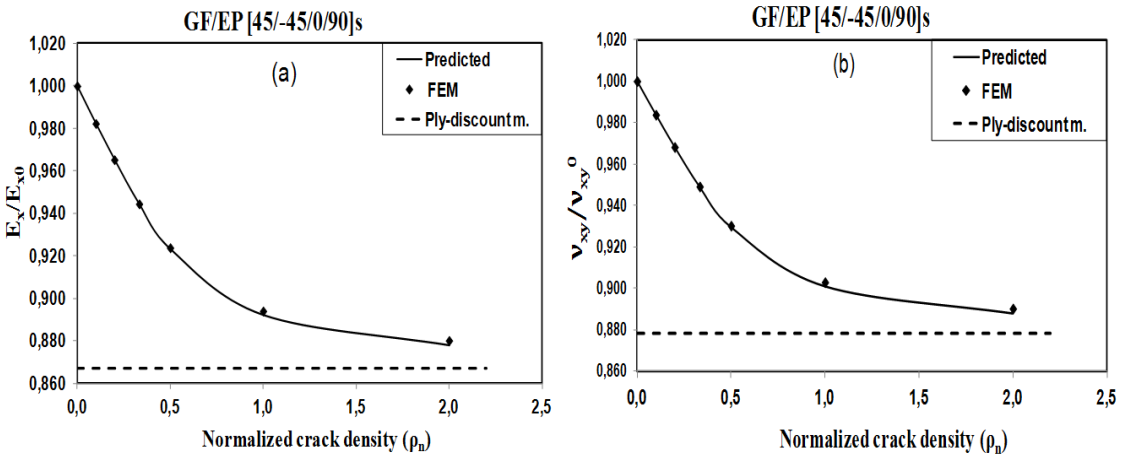

Figure 2.13. Elastic modulus (a) and Poisson's ratio (b) degradation in **GF/EP** quasi-isotropic laminate due to transverse cracking in 90-layer

2.5.4.2 Quasi-isotropic laminates with cracks in surface layers

Elastic modulus and Poisson's ratio reduction of quasi-isotropic laminates with cracks in surface layers is shown for GF/EP composite in Fig. 2.14 and for CF/EP in Fig. 2.15. For $[90/0/45/-45]_S$ laminate the calculated elastic modulus reduction is slightly overestimated, but the accuracy is good. For both lay-ups and materials the elastic properties predictions are slightly conservative, but the accuracy is good.

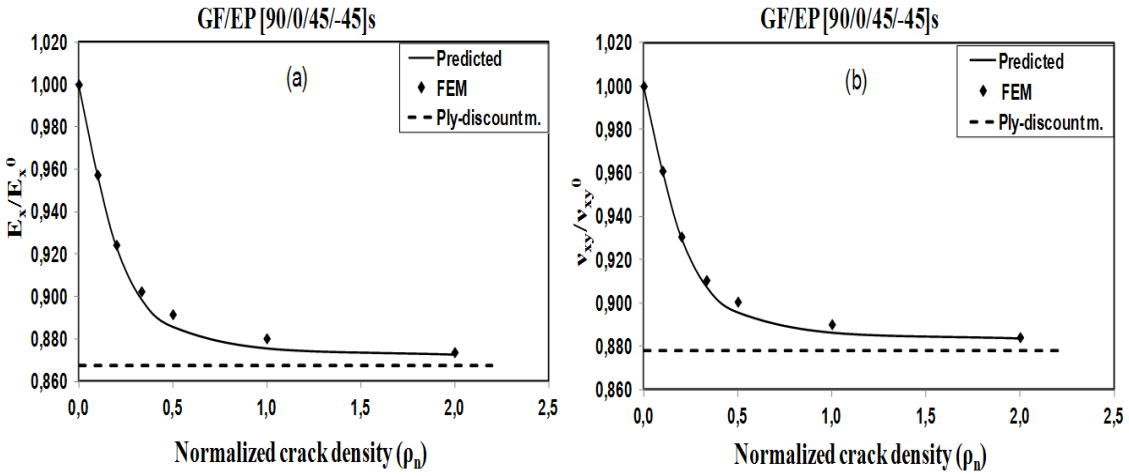

Figure 2.14. Elastic modulus (a) and Poisson's ratio (b) degradation in **GF/EP** quasi-isotropic laminate due to transverse cracking in 90-layer

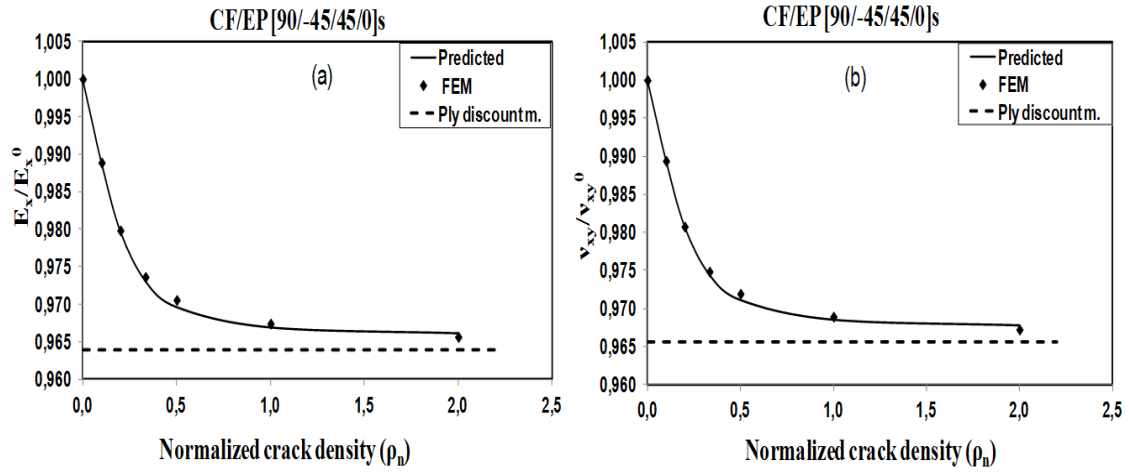

Figure 2.15. Elastic modulus (a) and Poisson's ratio (b) degradation in **CF/EP** quasi-isotropic laminate due to transverse cracking in 90-layer

2.6. Conclusions

Exact analytical expressions for thermo-elastic constants of symmetric and balanced laminates with intralaminar cracks in 90-layers are presented as a special case of the GLOB-LOC model developed in [28,29]. They can be used if simple and accurate expressions for normalized crack opening (COD) and sliding (CSD) displacements are available. At high crack density where cracks interact these parameters depend on distance between cracks.

The COD of an interactive crack is presented as a product of the COD of non-interactive crack and an interaction function which value is equal or smaller than one. In this chapter the tanh() form of the interaction function for COD is introduced and parameters determined using data generated by FEM for large variety of geometrical and material parameters considering cracks in surface as well as inside layers. Comparison with direct FEM calculations show that the interaction function gives a very good axial modulus and Poisson's ratio prediction for all possible crack densities and cross-ply laminates.

The interaction function derived for cross-ply laminates is adapted for more complex lay-ups and its accuracy is demonstrated for quasi-isotropic laminates.

Chapter 3

Applicability of solutions for periodic intralaminar crack distributions to non-uniformly damaged laminates

3.1. Introduction

Intralaminar cracking in laminates is the most typical mode of damage in laminates. Initiation, evolution and effect of these cracks on laminate stiffness has been discussed in many papers, see for example review papers [3,6]. Intralaminar cracks (called also matrix cracks, transverse cracks, inclined cracks) are orthogonal to the laminate midplane, they run parallel to fibers in the layer, usually cover the whole thickness and width of the layer in the specimen.

In the presence of cracks the average stress in the damaged layer is lower than in the same layer in undamaged laminate. The average stress between two cracks depends on the distance between them (normalized spacing). Usually the extent of cracking (number of cracks and distance between them) is characterized in an average sense by average crack spacing and crack density (cracks/mm). Most of the existing stiffness models, for example, [5,11,22,28] use this assumption. It is convenient for use and is expected to give sufficient accuracy.

However, the crack distribution in the layer may be highly non-uniform as schematically shown in Fig. 3.1. This is more pronounced in the beginning of the cracking process when the average crack density is relatively low. At high crack density close to saturation the cracks are more equidistant. The reason is the random distribution of transverse failure properties along the transverse direction of the layer. At low crack density the stress distribution between two existing cracks has a large

plateau region and any position there is a site of possible failure. At high crack density there is a distinct maximum in the stress distribution and a new crack most likely will be created in the middle between existing cracks.

The discussion in this chapter is focused on the possible inaccuracy introduced in laminate stiffness prediction by using assumption of uniform spacing between cracks in a layer. Numerical results presented here are for two cases: a) when the system of cracks is ”non-interactive” in average (low crack density) but some cracks are close to each other and interact; b) the crack density is high and cracks interact “in average”.

There are only a few studies where the effect of non-uniformity is addressed, see for example [25,40,41]. In [40] hypothesis was introduced that for a non-uniformly cracked laminate, the deformation field in the “element” between two neighbouring ply cracks separated by a distance l_k is identical to that in a uniformly cracked laminate where the crack spacing is l_k. Then, for example, the axial strain of the whole Representative Volume Element (RVE) can be calculated by the “rule of mixtures” of average strains of “elements” leading to simple expressions for RVE axial modulus. The high accuracy of this approach was demonstrated in [40] comparing results with another high accuracy semi-analytical methodology applied to the RVE. This assumption is reexamined in our chapter analyzing crack opening displacements (COD) of both crack faces and showing that the average stress in the “element” on one side, where the distance to the next crack is smaller, is overestimated by this assumption whereas on the other side it is underestimated. In [25,41] the non-uniform damage evolution is analyzed in a probabilistic way not discussing the effect of non-uniform distribution on stiffness.

The reduced average transverse stress and in-plane shear stress in the damaged layer are responsible for laminate stiffness changes. The average stress change between two cracks is proportional to the COD and sliding displacements (CSD) normalized with far

field stress [18,42]. The far-field stress at the given load is calculated using laminate theory (CLT). Therefore the damaged laminate stiffness can be expressed also in terms of density of cracks and two parameters: average COD a CSD as done in the GLOB-LOC model [28,29]. These two rather robust parameters depend on the normalized distance to neighboring cracks. Therefore for non-uniform crack distribution they are different for each individual crack. The values of COD and CSD in the commonly assumed uniform crack distribution case correspond to average spacing between cracks and are different than the calculated average over COD's and CSD's of all individual cracks.

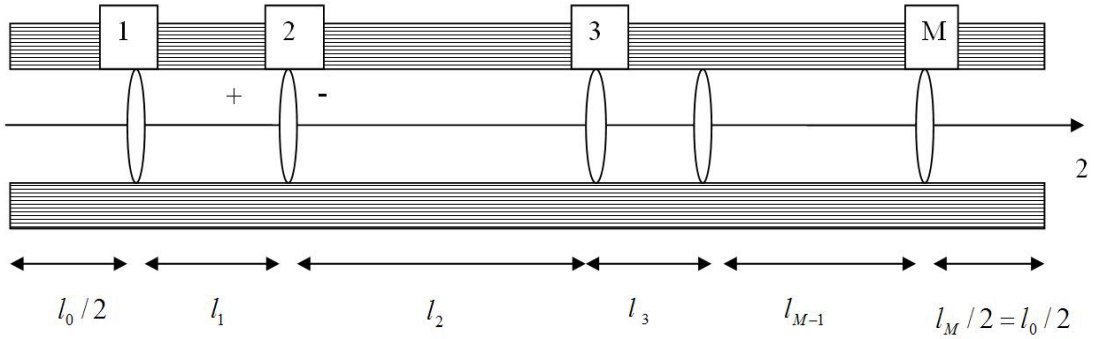

Figure 3.1. Non-uniform distribution of M cracks in damaged layer shown in its local coordinate system.

In this chapter we first will generalize the previously developed expressions for stiffness reduction in symmetric laminates (GLOB-LOC model [28]) for non-uniform spacing case. Then parametric analysis of the effect of geometrical non-uniformity in terms of COD and the laminate axial modulus will be performed for particular cases of $[90m/0n]_s$ and $[0n/90m]_s$ cross-ply laminates with cracks in 90-layers. Cases when sliding displacement CSD affects the stiffness are included in the stiffness expressions in Section 3.2.2 but they are not numerically analyzed in this chapter. Extreme layer thickness ratios and different material anisotropy levels comparing carbon fiber (CF) and glass fiber (GF) composites will be discussed. To simplify stiffness calculations for an arbitrary non-uniform distribution, routine allowing determination of COD's for any

crack as a sum of solutions for two periodic systems of cracks, will be formulated and its accuracy discussed (one solution is for periodic system with spacing as on the "+" side of the crack and another one for a periodic system with spacing as on the "-" side of the crack, see Fig. 3.1).

3.2. Material model of damaged symmetric laminates with intralaminar cracks

3.2.1 Distances between cracks

We consider RVE of a layer with M cracks as shown in Fig. 3.1. The RVE length is L, the average distance between cracks (spacing) is l_{av}, the crack density is ρ

$$L=\sum_{m=0}^{M-1} l_m \qquad l_{av}=\frac{L}{M} \qquad \rho=\frac{1}{l_{av}} \tag{3.1}$$

Stress state between two cracks in a layer, see Fig. 3.1 where the cracked layer is shown in its local coordinates, and also the opening and sliding displacements of crack faces depend on the normalized distance between cracks. Normalization is with respect to the layer thickness t

$$l_{mn}=\frac{l_m}{t}, \qquad \text{m=0,1,...,} M-1, \qquad l_{avn}=\frac{l_{av}}{t} \tag{3.2}$$

Index k, used in following sections to identify k-th layer in the laminate, is omitted here for simplicity. Crack with index m has two neighbors located at different distances l_{m-1} and l_m from this crack. Using notation u_{2an}, u_{1an} for the average normalized COD and CSD defined by (A2.3) – (A2.5), we can write for the m-th crack

$$u_{2an}^m=u_{2an}^m\left(l_{(m-1)n}, l_{mn}\right) \qquad u_{1an}^m=u_{1an}^m\left(l_{(m-1)n}, l_{mn}\right) \tag{3.3}$$

If $l_m > l_{m-1}$ the displacements on the "-" side will be larger than on the "+" side.

If the part of the layer shown in Fig. 3.1 is smaller than the RVE, the methodology of this chapter can still be applied but the unknown displacements of the outmost to the left (m=1) and the outmost to the right (m=M) positioned cracks are affecting the calculated

homogenized stiffness. The uncertainty is because COD and CSD of these two cracks depend on the distance to the next cracks not shown in Fig. 3.1 or, in other words, on boundary conditions. The uncertainty is avoided if the shown distribution is considered as "repeating super-element" with M cracks in it. In this case symmetry conditions can be applied on $x = 0$ and $x = L$. To model this periodic structure we have to assume $l_0 = l_M$.

3.2.2 Stiffness Model

The upper part of symmetric *N*- layer laminate with intralaminar cracks is shown in Fig. 3.2. The *k*-th layer of the laminate has thickness t_k, fiber orientation angle with respect to the global x-axis θ_k and stiffness matrix $[Q]$ in the material symmetry axes, calculated from elastic constants $E_1, E_2, G_{12}, \nu_{12}$. The total thickness of the laminate, $h = \sum_{k=1}^{N} t_k$. The crack density in a layer ρ_k is calculated using (3.1) where the average distance between cracks l_{av}^k is measured transverse to the fiber direction in the k-th layer. Dimensionless crack density ρ_{kn} in the layer is introduced as

$$\rho_{kn} = t_k \rho_k \tag{3.4}$$

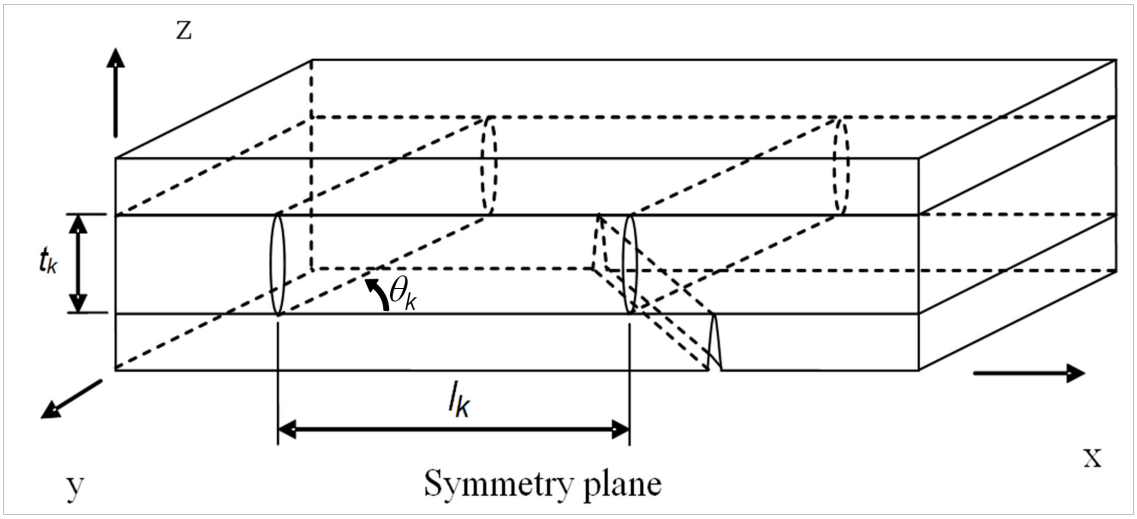

Figure 3.2. RVE of the damaged laminate with intralaminar cracks in layers.

It is assumed that in the damaged state laminate is still symmetric in other words the crack density in corresponding symmetrically placed layers is the same.

The stiffness matrix of the damaged laminate, $[Q]^{LAM}$ and the stiffness of the undamaged laminate, $[Q]_0^{LAM}$ are defined by the stress-strain relationships

$$\begin{Bmatrix} \sigma_{x0} \\ \sigma_{y0} \\ \sigma_{xy0} \end{Bmatrix}^{LAM} = [Q]^{LAM} \begin{Bmatrix} \varepsilon_x \\ \varepsilon_y \\ \gamma_{xy} \end{Bmatrix}^{LAM} \quad , \quad \begin{Bmatrix} \sigma_{x0} \\ \sigma_{y0} \\ \sigma_{xy0} \end{Bmatrix}^{LAM} = [Q]_0^{LAM} \begin{Bmatrix} \varepsilon_{x0} \\ \varepsilon_{y0} \\ \gamma_{xy0} \end{Bmatrix}^{LAM} \tag{3.5}$$

The compliance matrix of the undamaged laminate is $[S]_0^{LAM} = \left([Q]_0^{LAM}\right)^{-1}$.

The expressions below for thermo-elastic constants of the damaged laminate with non-uniform crack distribution are derived in Appendix 1 and 2

$$[Q]^{LAM} = \left([I] + \sum_{k=1}^{N} \rho_{kn} \frac{t_k}{h} [K]_k [S]_0^{LAM} \right)^{-1} [Q]_0^{LAM} \tag{3.6a}$$

$$[S]^{LAM} = [S]_0^{LAM} \left([I] + \sum_{k=1}^{N} \rho_{kn} \frac{t_k}{h} [K]_k [S]_0^{LAM} \right) \tag{3.6b}$$

$$\{\alpha\}^{LAM} = \left([I] + \sum_{k=1}^{N} \frac{t_k}{h} \rho_{kn} [S]_0^{LAM} [K]_k \right) \{\alpha\}_0^{LAM} - \sum_{k=1}^{N} \frac{t_k}{h} \rho_{kn} [S]_0^{LAM} [K]_k \left\{\overline{\alpha}\right\}_k \tag{3.7}$$

In (3.6a), (3.6b) and (3.7) the matrix-function $[K]_k$ for a layer with index k is defined as

$$[K]_k = \frac{1}{E_2} [\overline{Q}]_k [T]_k^T [U]_k [T]_K [\overline{Q}]_k \tag{3.8}$$

The involved matrices $[T]_k$ and $[\overline{Q}]_k$ are defined according to CLT, upper index T denotes transposed matrix and bar over stiffness matrix indicates that it is written in global coordinates. The influence of cracks in k-th layer is represented by matrix $[U]_k$.

$$[U]_k = 2 \begin{bmatrix} 0 & 0 & 0 \\ 0 & u_{2an}^k & 0 \\ 0 & 0 & \dfrac{E_2}{G_{12}} u_{1an}^k \end{bmatrix} \tag{3.9}$$

Elements of this matrix u_{2an}, u_{1an} are defined in Appendix 2. They are calculated, see (A2.8), using normalized and averaged crack face opening (COD) and sliding displacements (CSD) of all cracks as affected by varying spacing between them.

$$u_{1an} = \frac{1}{M}\sum_{m=1}^{M} u_{1an}^{m}\left(l_{(m-1)n}, l_{mn}\right) \qquad u_{2an} = \frac{1}{M}\sum_{m=1}^{M} u_{2an}^{m}\left(l_{(m-1)n}, l_{mn}\right) \tag{3.10}$$

Index for layer k is omitted in (3.10). Certainly, since u_{2an}, u_{1an} in k-th layer depend also on neighboring layer properties they are different in different layers. The methodology used in appendices is exactly the same as in [28]. The main difference is in Appendix 2 where the two crack faces of any crack may have different displacements due to nonuniformity. Appendix 1 which in a compact form contains the same information as given in [28] is included to insure consistency of explanation.

3.2.3 Elastic modulus of balanced laminates with cracks in 90-layer

In case of balanced laminates with damage in 90-layers only, expressions for $[K]_k$ and for $[S]^{LAM}$ have been obtained calculating the matrix products in (3.6) - (3.8) analytically. For example, the obtained expression for laminate normalized axial modulus is

$$\frac{E_x}{E_x^0} = \frac{1}{1 + 2\rho_{90n}\dfrac{t_{90}}{h}u_{2an}^{90}c} \qquad c = \frac{E_2}{E_x^0}\left(\frac{1-\nu_{12}\nu_{xy}^0}{1-\nu_{12}\nu_{21}}\right)^2 \tag{3.11}$$

Index 90 is used to indicate 90-layer. The quantities with lower index x,y are laminate constants, quantities with additional upper index 0 are undamaged laminate constants and (3.10) has to be used to calculate u_{2an}^{90}. In the case of uniform crack distribution all COD's in (3.10) are equal and (3.11) is just a different form of (31) in [28] leading to numerically identical results. In the following parametric analysis we consider COD related properties only and validation is based on axial modulus. Therefore shear

modulus expression of the damaged laminate which is related to CSD only is not presented here.

3.3. Results and discussion

3.3.1 Formulation of calculation examples

The effect of the non-uniform crack distribution on u_{2an}^{90} was analyzed using FEM for damaged $[0_n/90_8]_S$ and $[90_8/0_n]_S$ laminates (n=1,8) at fixed dimensionless crack density ρ_{90n}, see Fig. 3.3 where the repeating "super-element" with two cracks is shown. Parameter K is introduced as the ratio

$$K = \frac{l_0}{l_{av}} \tag{3.12}$$

to characterize the non-uniformity of the spatial distribution. This parameter has value 1 for uniform crack distribution. The average crack density, l_{av} was kept constant (two cracks over fixed distance $L = l_0 + l_1$ give $l_{av} = \frac{l_0 + l_1}{2}$) with average normalized spacing calculated according to (3.1) $l_{avn} = \frac{1}{2}(l_{0n} + l_{1n})$.

To cover large variation in elastic constants both CF/EP and GF/EP composites with constants given in Table 3.1 were analyzed. All results are presented in terms of dimensionless crack spacing and crack density. Results depend on layer thickness ratio, not on absolute value of ply thickness.

For laminates with cracks in surface layers staggered crack system, where the crack in the bottom layer is located in the middle between cracks in the top layer, could be analysed instead of symmetric damage state shown in Fig. 3.3. This case analyzed in [43] by J. Nairn is relevant when the failure analysis is deterministic and the small variation in stress state points on the locus of the next failure (always exactly in the middle between two existing cracks). However, the strength (or the fracture toughness)

is not one single value but follows certain statistical distribution. The variation of failure properties along the 90-layer transverse direction is often much larger than the stress perturbation in the bottom layer of the laminate due to crack in the top layer. Therefore the assumption of staggered cracks is as far from reality as the assumed symmetry of the damage with respect to the midplane used in this chapter. Starting with symmetric damage state in the stiffness analysis we are trying to create a simple reference case. The interaction effects between systems of cracks in different layers have to be analysed separately. Otherwise the number of parameters changing is too large to draw conclusions.

In all FE calculations the commercial code ABAQUS was used. In order to model the left half of the ”super-element” (see Fig. 3.3), a 3-D model was created. 3D continuum elements (C3D8) 8-node linear brick were used in order to mesh volumes. The same fine mesh with total number of elements 86400 was used in each FE model. The (x, z) plane consisted of 21600 elements, with refined mesh near the crack surfaces. In the ply with cracks the number of elements in the thickness direction was 120. The number of elements in y-direction was 4 which as described below is more than sufficient for the used edge conditions. The problem was solved by applying to the right boundary $x = 0$ of the model a given constant displacement in x-direction corresponding to 1% average strain and keeping at the left boundary $u_x = 0$. The top surface was free of tractions. On the front edge (y=0) and the edge y=w coupling conditions were applied for normal displacements (u_y= unknown constant). In this way edge effects are avoided and the solution does not depend on y-coordinate. It corresponds to solution for an infinite structure in the width direction. Obviously these conditions lead to generalized plane strain case and corresponding finite elements could be used obtaining the same results.

The displacements in direction x for the nodes at the crack surface were used to calculate the average value of the crack face displacement COD.

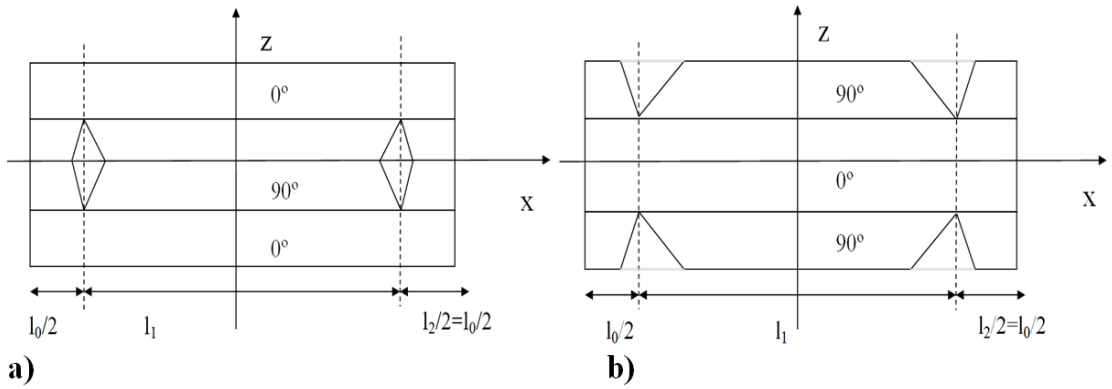

Figure 3.3. "super-element" models for COD studies with non-uniformly cracked 90-layers: a) cracks in inside layer; b) cracks in surface layer

All plies are considered to be transversally isotropic with $E_2 = E_3$, $G_{12} = G_{13}$ and $\nu_{12} = \nu_{13}$.

Table 3.1. Material properties used in simulations

Material	E_1(GPa)	E_2(GPa)	ν_{12}	ν_{23}	G_{12} (GPa)	G_{23} (GPa)
GF/EP	45	15	0.3	0.4	5	5.36
CF/EP	150	10	0.3	0.4	5	3.57

In calculations two values of the average normalized spacing were used: a) $l_{avn} = 10$ corresponding to $\rho_{90n} = 0.1$ where the interaction between uniformly spaced cracks would be negligible; b) $l_{avn} = 2$ corresponding to interactive crack region with crack density $\rho_{90n} = 0.5$.

Studying the effect of non-uniform distribution the normalized spacing l_{0n}, see Fig. 3.3, was used as a parameter which was lower or equal to the average spacing. In case a) $l_{0n} \in [0.5;10]$ and in case b) $l_{0n} \in [0.5;2]$. It is worth to remind here that at very high crack density (in the so called crack saturation region) the normalized average spacing

may be close to 1 (the distance between cracks is equal to the crack size (layer thickness)). Straight intralaminar cracks are almost never observed closer to each other than half of the cracked layer thickness.

3.3.2 COD parametric analysis at low crack density

In this section results for average normalized spacing $l_{avn} = 10$ ($\rho_{90n} = 0.1$) are presented.

3.3.2.1 Internal cracks

For internal cracks the profiles of normalized crack face displacements ($u_{2n}^{-}(z_n)$, $u_{2n}^{+}(z_n)$ defined in Appendix 2) along the thickness coordinate $z_n = z\dfrac{2}{t_{90}} + 1$ are shown in Fig. 3.4 and Fig. 3.5. The "+" face of the crack has smaller displacements than the "-" face and the difference is larger when the l_{0n} is smaller than 1 (the neighboring crack to the left is very close). The neighbor to the "-" face is at larger distance than the average spacing and therefore the displacement profile is almost unaffected. For the same geometry the COD's in CF composites are always significantly smaller.

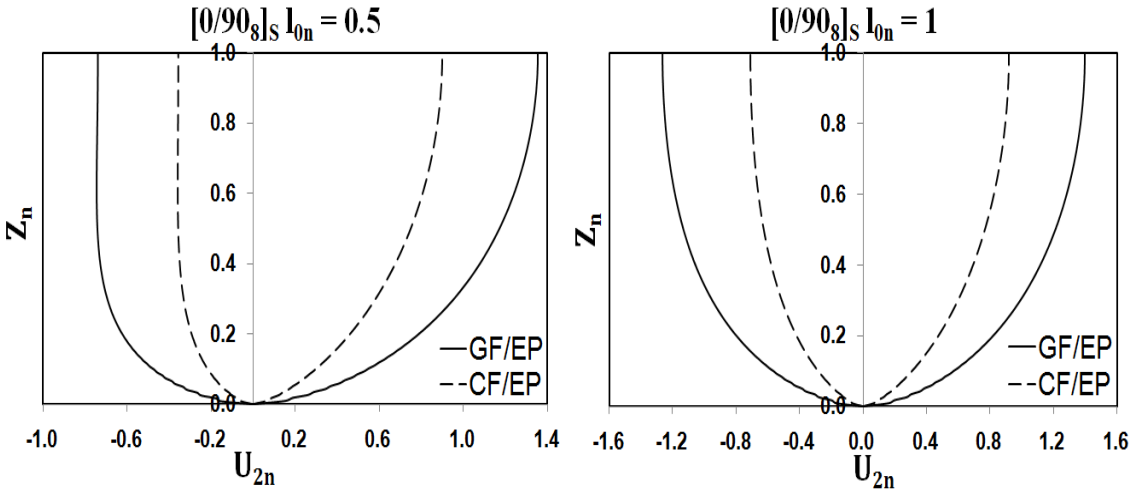

Figure 3.4. COD profiles of cracks in [0/90$_8$]s laminate with normalized crack density $\rho_{90n} = 0.1$

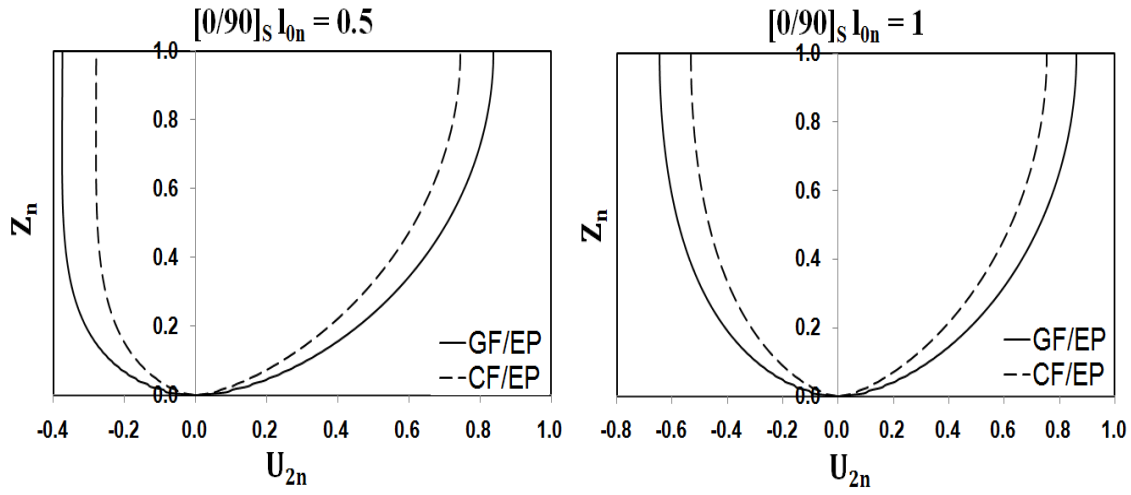

Figure 3.5. COD profiles of cracks in [0/90]s laminate with normalized crack density $\rho_{90n} = 0.1$

The displacements of both crack faces are significantly smaller when the relative thickness of the neighboring layer is higher, Fig. 3.5. This effect is more pronounced for GF composite where the 0-layer versus 90-layer modulus ratio is not very large.

Using crack face displacements the average normalized COD's u_{2an}^{90} are calculated by numerical integration using expressions in Appendix 2. The obtained dependence on the non-uniformity parameter K is shown in Fig. 3.6. The average normalized COD is larger if the spacing is uniform. However, the effect is negligible for $K > 0.2$ ($l_0 > 2t_{90}$).

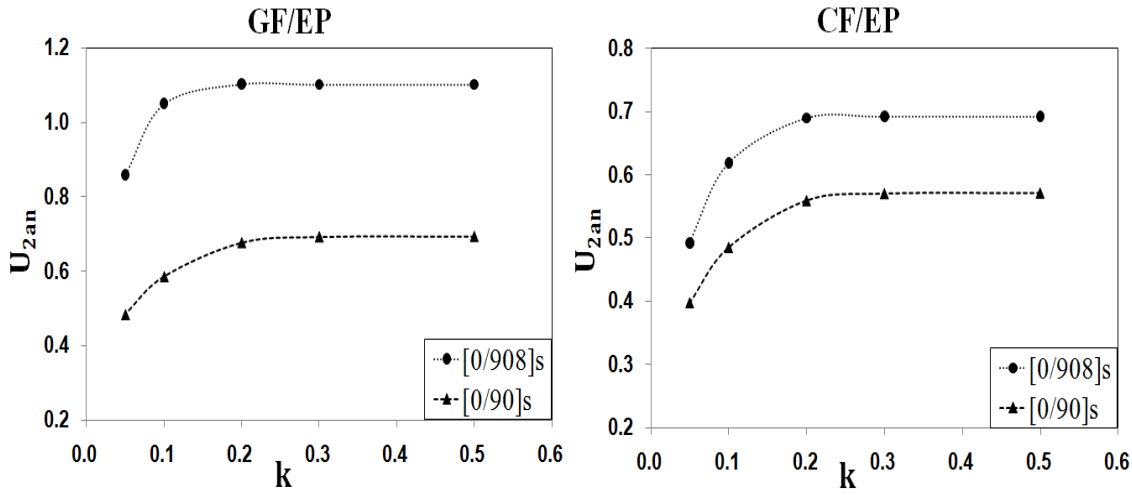

Figure 3.6. Effect of non-uniform spacing on COD of internal cracks in cross-ply laminates with normalized crack density $\rho_{90n} = 0.1$

3.3.2.2 Surface cracks

For surface cracks in [90_8/0]s and [90/0]s laminates the profiles of normalized crack face displacements, $u_{2n}^{-}(z_n)$, $u_{2n}^{+}(z_n)$ along the thickness coordinate $z_n = \dfrac{z - t_0/2}{t_{90}}$ (t_0 is 0-layer thickness) are shown in Fig. 3.7 and Fig. 3.8. The trends are the same as for internal cracks but the face displacements are larger and the shape of the profile, especially on the non-interactive side, is different not becoming vertical at outer surface, $z_n = 1$. Since the outer surface is not a symmetry surface this result was expected.

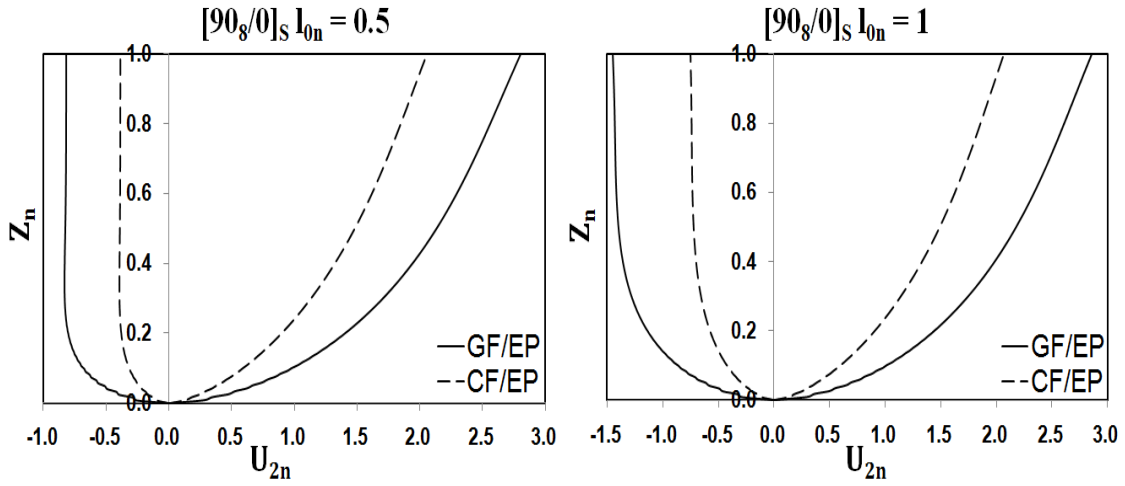

Figure 3.7. COD profiles of surface cracks in [90_8/0]s laminate with normalized crack density $\rho_{90n} = 0.1$

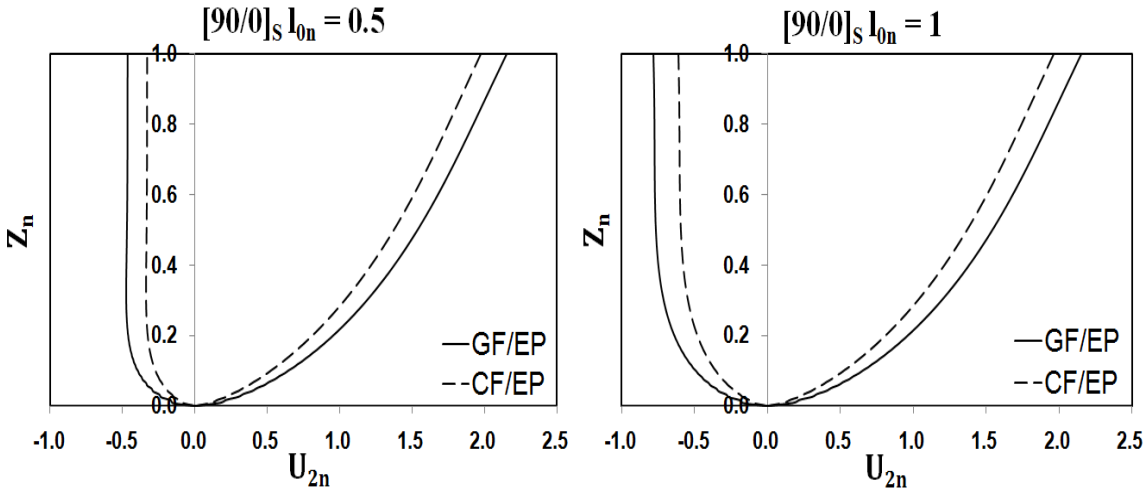

Figure 3.8. COD profiles of surface cracks in [90/0]s laminate with normalized crack density $\rho_{90n} = 0.1$

The average normalized COD's, u_{2an}^{90} are calculated as described in Section 3.2.1. The obtained dependence on the non-uniformity parameter K is shown in Fig. 3.9. The average normalized COD is smaller if the spacing is non-uniform. According to (3.11) it will lead to smaller axial modulus reduction. For [90_8/0]s laminate this effect becomes negligible for $K > 0.3$ ($l_0 > 3t_{90}$) whereas for [90/0]s laminate the transition values are slightly larger ($K > 0.5$, $l_0 > 5t_{90}$).

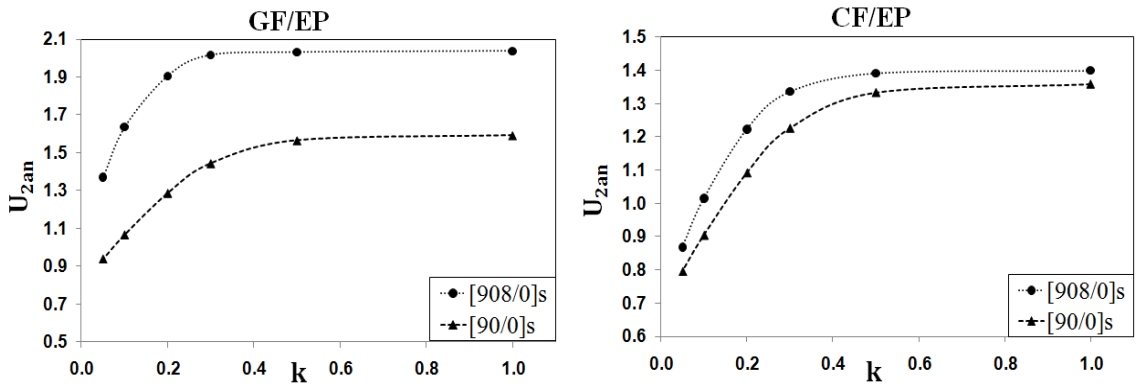

Figure 3.9. Effect of non-uniform spacing on COD of surface cracks in cross-ply laminates with normalized crack density $\rho_{90n} = 0.1$

3.3.3 Approximate COD determination from periodic solutions

The average normalized COD, u_{2an} of a crack in a layer with non-uniform crack distribution can be found considering separately the average normalized COD of the "-" face of the crack and "+" of the crack in Fig. 3.1.

$$u_{2an} = \frac{1}{2}\left(u_{2an}^{+} + u_{2an}^{-}\right) \tag{3.13}$$

In this section the following hypothesis will be analyzed:

" The COD of "-" face depends on the distance to the closest neighboring crack on the right only and can be calculated considering the region between these two cracks as a periodic element. The COD of the "+" face is obtained in a similar manner, considering the region on the left as periodic element"

This “double-periodic” approach with considering two periodic solutions states that

$$u_{2an} \approx u_{2an}^{p} \qquad u_{2an}^{p} = \frac{1}{2}\left(u_{2an}^{p-} + u_{2an}^{p+}\right) \tag{3.14}$$

The two values u_{2an}^{p+} , u_{2an}^{p-} are solutions of the two periodic models.

This hypothesis is equivalent to saying that in Fig. 3.3 symmetry conditions on the plane $x = \pm l_1/2$ can be applied. This would mean that even in the deformed state the line $x = \pm l_1/2$ in the 0-layer remains straight. Unfortunately there is no symmetry in Fig. 3.3 and this line will be deformed. The accuracy of the symmetry condition used in the “double-periodic” approach can be estimated only numerically. Hypothesis that the deviation can be neglected was used by Joffe et al in [18] calculating the work to close the crack for fracture mechanics based damage growth analysis.

If the “double-periodic” approach is accurate enough, the u_{2an} for any crack location with respect to other cracks could be calculated from a master curve for uniform crack distribution. This curve, which is expression of u_{2an} as a function of crack spacing in layer with uniformly distributed cracks, would be used twice to read the u_{2an}^{p+} , u_{2an}^{p-} values of the left and the right face of the crack.

In order to check the accuracy and validity of the “double-periodic” assumption, the u_{2an} for each value of non-uniformity parameter was calculated in two different ways: a) directly applying FEM to the non-uniform geometry; b) applying FEM two times and using (3.14), first, for periodic distribution with spacing as on the left from the crack and, second, for periodic distribution with spacing as on the right of the crack.

From Fig. 3.10 were displacement profiles according to a) and b) are presented we conclude that the trends in the double-periodic approach are described correctly but the values of face displacements are not accurate. On the left face where the interaction is

strongest the u_{2n}^{p+} is too small but on the right face, where the next crack is further away, u_{2n}^{p-} is too large. It seems that this result questions the validity of used hypothesis at low crack density.

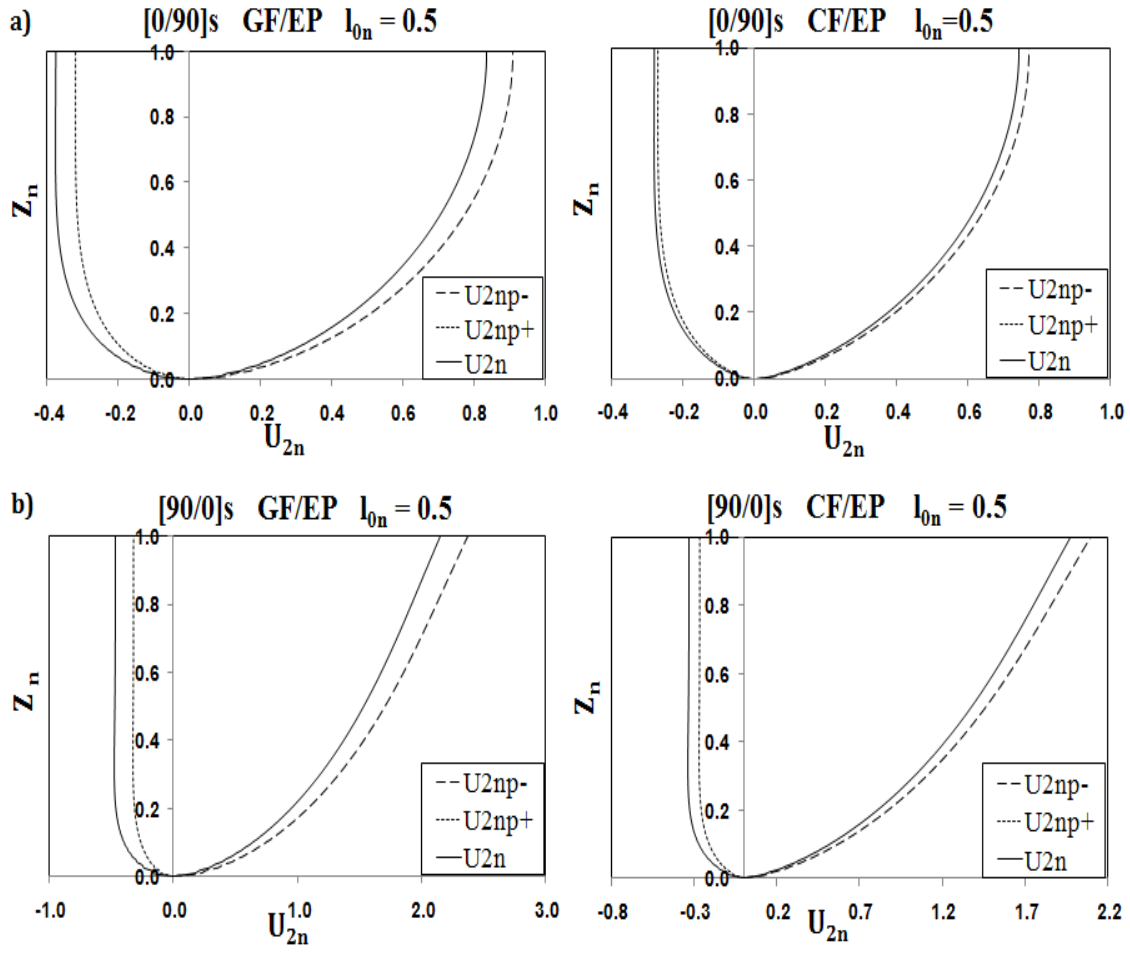

Figure 3.10. Calculated COD profiles: **a)** of internal cracks in [0/90]s laminate **b)** of surface cracks in [90/0]s laminate with normalized crack density $\rho_{90n} = 0.1$

However, for stiffness predictions the average of the COD of both faces, u_{2an}^{p} given by (3.14) is requested and not the value for each face separately. The values of u_{2an} and u_{2an}^{p} can be compared using results presented in Table 3.2 and Table 3.3 for all lay-ups, materials and non-uniformity parameter values. A very good agreement between values exists for all cases which validates the use of the "double-periodic" hypothesis.

Table 3.2. Average normalized COD of internal cracks from FEM and from "double-periodic" approach at normalized crack density $\rho_{90n} = 0.1$

	[0/90$_8$]s				**[0/90]s**			
	GF/EP		**CF/EP**		**GF/EP**		**CF/EP**	
K	u_{2an}	u^p_{2an}	u_{2an}	u^p_{2an}	u_{2an}	u^p_{2an}	u_{2an}	u^p_{2an}
1.00	1.1027	1.1027	0.6927	0.6927	0.6941	0.6941	0.5720	0.5720
0.50	1.1027	1.1030	0.6927	0.6927	0.6941	0.6943	0.5721	0.5722
0.30	1.1027	1.1030	0.6928	0.6931	0.6928	0.6935	0.5712	0.5716
0.20	1.1039	1.1045	0.6905	0.6907	0.6771	0.6786	0.5600	0.5607
0.10	1.0510	1.0537	0.6189	0.6230	0.5860	0.5910	0.4857	0.4894
0.05	0.8588	0.8811	0.4927	0.5091	0.4841	0.4890	0.3977	0.4035

Table 3.3. Average normalized COD of surface cracks from FEM and from "double-periodic" approach at normalized crack density $\rho_{90n} = 0.1$

	[90$_8$/0]s				**[90/0]s**			
	GF/EP		**CF/EP**		**GF/EP**		**CF/EP**	
K	u_{2an}	u^p_{2an}	u_{2an}	u^p_{2an}	u_{2an}	u^p_{2an}	u_{2an}	u^p_{2an}
1.00	2.0379	2.0379	1.3992	1.3992	1.5915	1.5915	1.3580	1.3580
0.50	2.0314	2.0378	1.3912	1.3930	1.5649	1.5661	1.3327	1.3318
0.30	2.0164	2.0169	1.3357	1.3364	1.4432	1.4471	1.2252	1.2256
0.20	1.9062	1.9221	1.2230	1.2268	1.2856	1.2958	1.0910	1.0964
0.10	1.6367	1.6421	1.0146	1.0184	1.0650	1.0798	0.9035	0.9141
0.05	1.3707	1.3915	0.8675	0.8744	0.9368	0.9477	0.7949	0.8040

The validity of enforcing symmetry in positions like $x = \pm l_1/2$ in Fig.3.3, is the basic assumption also in [40]. In our present chapter we have shown, see Fig. 3.10 that it can lead to noticeable inaccuracy in the displacement of each crack face. However the average COD of the crack presented in Fig. 3.2 and Fig 3.3 is very accurate. Since the COD values of the "double-periodic" approach coincide with exact values when the spacing is uniform, the accuracy increases with higher values of the non-uniformity parameter. To understand the real boundary conditions at $x = \pm l_1/2$ the intralaminar shear stress, σ_{xz} distribution along z-coordinate was calculated using FEM for different values of non-uniformity parameter K. For example, for GF/EP [0/90]s laminate with

$\rho_{90n} = 0.1$ and 1% applied strain the σ_{xz} in 0-layer at a distance from the crack tip equal to 10% of the 0-layer thickness changes from 0 to 3.8 MPa to 33 MPa when the non-uniformity parameter changes from 1 to 0.5 to 0.05 showing that the boundary conditions are noticeably violated only for high non-uniformity (low value of parameter K). The effect is stronger for cracks in surface layers.

Rephrasing the above in terms of average stresses and strains between two cracks calculated using similar assumption in [40], the accuracy in each element is reduced at high non-uniformity but the average values and the total values calculated in this way have as shown in [40] very high accuracy.

3.4. Elastic modulus prediction and validation with FEM

The effect of the non-uniform crack distribution on axial modulus of cross-ply laminates is shown in Fig. 3.11 for GF/EP laminates and in Fig. 3.12 for CF/EP laminates. All results are for the same normalized crack density $\rho_{90n} = 0.1$. The normalized axial modulus of the laminate is calculated in three different ways:

a) Calculating the average applied stress using FEM and using definition of E_x.

b) Applying (3.11) and using for u_{2an}^{90} values of u_{2an} obtained from FEM and presented in Table 3.2 and Table 3.3.

c) Applying (3.11) and using for u_{2an}^{90} values of u_{2an}^{p} obtained from "double-periodic" approach presented in Table 3.2 and Table 3.3.

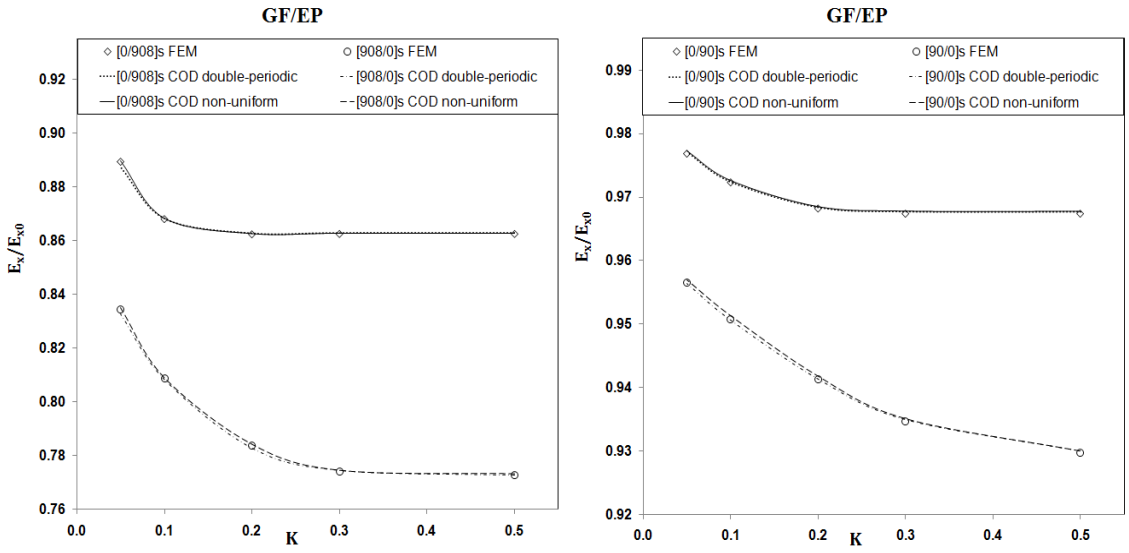

Figure 3.11. Effect of non-uniform crack distribution on axial modulus of GF/EP cross-ply laminates with normalized crack density $\rho_{90n} = 0.1$

The elastic modulus of the RVE with two non-equidistant cracks calculated directly from force (FEM) and the applied average strain (notation FEM in Fig. 3.11) is equal to the elastic modulus for this RVE calculated using (3.11) with u_{2an} input from the same FEM solution. Since (3.11) is an exact analytical expression this result was expected and some numerical discrepancy is possible only if the elastic modulus of the RVE is calculated with a different mesh than the u_{2an}. Since these two calculations always lead to coinciding results only one of them (called FEM) is shown in following figures.

On other side FEM values practically coincide with the ones where the "double-periodic" approach is used, proving the accuracy and potential of this approach for simulation of systems with multiple non-uniformly spaced cracks.

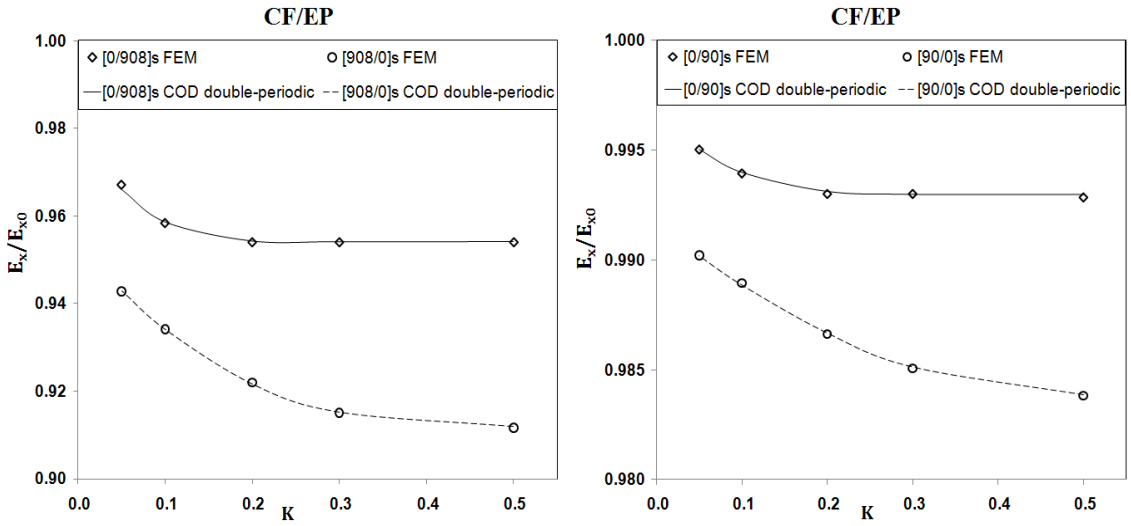

Figure 3.12. Effect of non-uniform crack distribution on axial modulus of CF/EP cross-ply laminates with normalized crack density $\rho_{90n} = 0.1$

For the used crack density and all investigated materials and lay-ups the axial modulus reduction is the highest if cracks have uniform distribution. For the reasons described in Introduction the experimental crack distribution at crack density $\rho_{90n} = 0.1$ is expected to be rather non-uniform and the axial modulus is higher than predicted by models based on periodic crack distribution. The normalized axial modulus value at the highest considered non-uniformity (K=0.05) and at uniform distribution (K=1) are given in Table 3.4.

The axial modulus of laminates with relatively thick damaged layers is more sensitive to non-uniform crack distribution: the highest value is 1.077 for GF/EP composite with lay-up [90_8/0]s.

The non-uniform distribution of internal cracks does not affect laminate modulus if the non-uniformity parameter $K > 0.2$. For laminates with cracks in surface layers the corresponding value is between 0.3 and 0.5. Note that K values given here are the same as the values when the non-uniformity stops to affect the average normalized COD.

Table 3.4. Normalized axial modulus of cross ply laminates with non-uniform and uniform (K =1) crack distributions calculated using FEM

		$\rho_{90n} = 0.1$			$\rho_{90n} = 0.5$		
Material	Lay-up	**K=0.05** $l_{0n} = 0.5$	**K=1** $l_{0n} = 10$	**Ratio**	**K=0.25** $l_{0n} = 0.5$	**K=1** $l_{0n} = 2$	**Ratio**
GF/EP	$[0/90_8]_s$	0.8894	0.8624	1.0312	0.6165	0.5556	1.1098
GF/EP	$[90_8/0]_s$	0.8345	0.7725	1.0804	0.5016	0.4337	1.1565
GF/EP	$[0/90]_s$	0.9768	0.9673	1.0098	0.8950	0.8619	1.0384
GF/EP	$[90/0]_s$	0.9566	0.9285	1.0303	0.8305	0.8057	1.0308
CF/EP	$[0/90_8]_s$	0.9671	0.9541	1.0136	0.8537	0.8070	1.0579
CF/EP	$[90_8/0]_s$	0.9428	0.9116	1.0342	0.7756	0.7321	1.0594
CF/EP	$[0/90]_s$	0.9950	0.9928	1.0022	0.9759	0.9672	1.0090
CF/EP	$[90/0]_s$	0.9902	0.9835	1.0068	0.9580	0.9510	1.0074

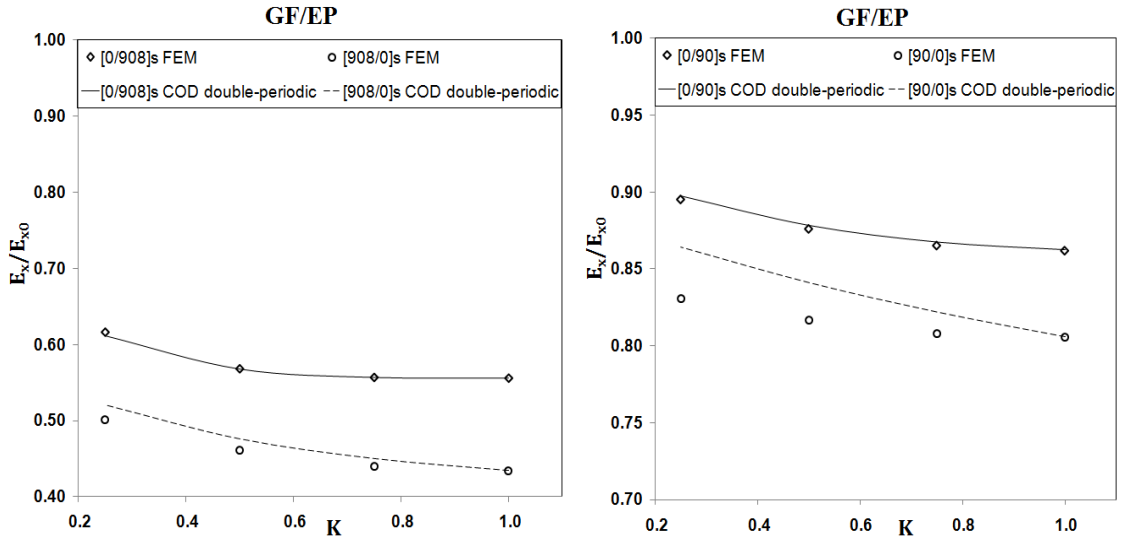

Figure 3.13. Effect of non-uniform crack distribution on axial modulus of GF/EP cross-ply laminates with normalized crack density $\rho_{90n} = 0.5$

Similar calculations as described above were performed for higher crack density $\rho_{90n} = 0.5$ Results are presented in Table 3.4 and in Fig. 3.13 and Fig. 3.14. Due to limitations for minimum possible spacing the range of the considered non-uniformity in calculations is narrower. Nevertheless the effect of non-uniform distribution is even larger than at low crack density. In contrast to low crack density case, there is no plateau

region in Fig. 3.13 and Fig. 3.14. The "double-periodic" approach at high crack density is still highly accurate for internal cracks. For surface cracks with high non-uniformity this approach underestimates the modulus reduction.

From section 3.2.2 follows that all elastic constants of the cross-ply laminate except the shear modulus can be analysed using the calculated u_{2an}. As shown in [40], the reduction of all properties in damaged laminate is linked and the same accuracy and trends as demonstrated for axial modulus apply for other constants. The shear modulus in our formulation depends on sliding displacements which have to be studied separately.

Calculations where performed also for carbon fiber/epoxy $[0/90_2]s$ laminate with non-uniformly distributed cracks in the 90 layer analyzed by McCartney et al in [40]. The used unidirectional composite properties are

$E_1 = 144.78GPa$, $E_2 = 9.58GPa$, $G_{12} = 4{,}785GPa$, $G_{23} = 3.090GPa$, $\nu_{12} = 0.31$,

$\alpha_1 = -0.72 \cdot 10^{-6} / C°$, $\alpha_2 = 27.0 \cdot 10^{-6} / C°$, $t_0 = 0.127mm$.

One of the numerical examples in [40] is for RVE between two cracks of length $2L = 1mm$ (notation as in [40]). The third crack is embedded in-between these two and the distance to the closest crack $2L_1 = 0.1mm$. Using our terminology the average spacing in the RVE is 0.5mm and the non-uniformity parameter $K = 0.2$. Elastic modulus of the RVE in [40] was calculated using LRAM and sub-dividing each layer in 7-8 sub-layers. In the analytical model which is based on similar assumptions as our "double-periodic" model each layer was sub-divided in 5-8 layers of equal thickness. Their results are compared with our results (FEM for the RVE and the "double-periodic" model) in Table 3.5. Our FEM results and LRAM results for E_x of the RVE are almost coinciding (our mesh had 120 elements in each layer in the thickness

direction).In addition also the ν_{xy} and the axial thermal expansion coefficient were calculated and for the latter the difference is slightly larger. Analytical expressions for these constants of the damaged cross-ply laminate one can find in [44].

Table 3.5. Thermo-elastic properties of damaged cross-ply laminates according to [40] and the present chapter with normalized crack density $\rho_{90n} = 1.016$

Method	FEM	LRAM [40]	Double-periodic	Error (%)	Analytical [40]	Error (%) [40]
$E_x(GPa)$	50.9606	50.9602	50.9224	-0.075	50.9111	-0.096
ν_{xy}	0.01746	0.01748	0.01736	-0.620	0.01733	-0.872
$\alpha_x(10^{-6} \cdot 1/C°)$	1.09622	1.10161	1.08213	-1.285	1.07685	-2.248

The results of the analytical method [40] and the "double-periodic" approach are very similar. In all cases they give slightly lower values than the values obtained by FEM or LRAM. Since our values are slightly higher the accuracy is slightly better than for the analytical model [40]. We believe that the accuracy of results in [40] could be improved by sub-division of layers in more sub-layers. Another observation from [40] is that even in the case when the third crack is exactly in the middle between the two cracks the results of LRAM and the analytical model [40] slightly differ. It can be explained only by different sub-division in sub-layers in both methods which has affected the accuracy.

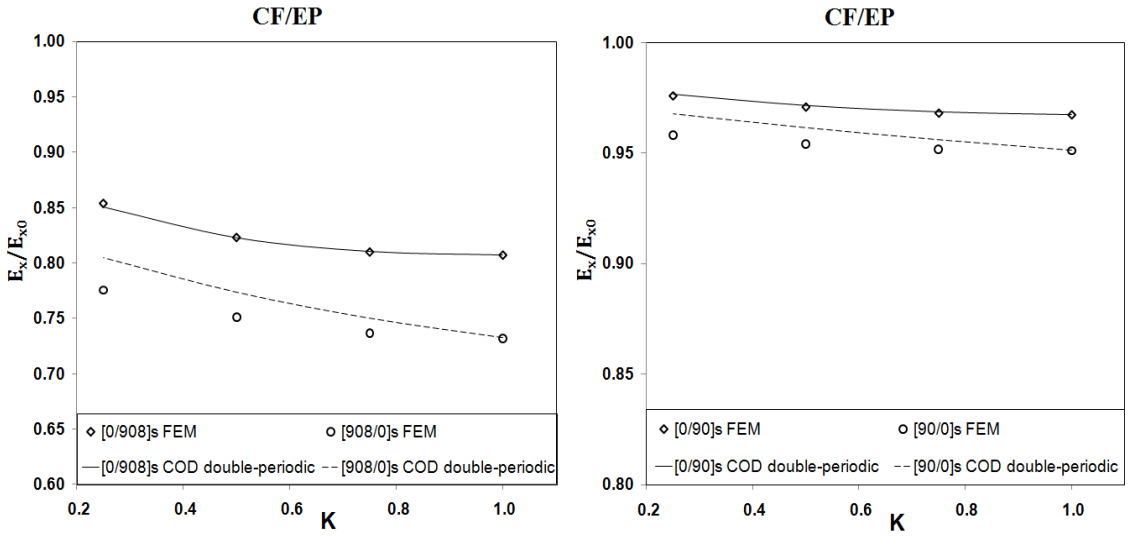

Figure 3.14. Effect of non-uniform crack distribution on axial modulus of CF/EP cross-ply laminates with normalized crack density $\rho_{90n} = 0.5$

3.5. Conclusions

Earlier developed model for elastic properties of damaged symmetric laminates was generalized for case when the intralaminar crack distribution is non-uniform and due to interactions each crack may have different opening (COD) and sliding (CSD) displacements. These displacements and the number of cracks per unit length in the layer are governing the laminate properties reduction. The obtained analytical expressions for elastic constants are exact. This model was applied to cross-ply laminates with cracks in 90-layers located in the middle or on the surface. The dependence of the damaged cross-ply laminate axial modulus (it depends on COD only) on the non-uniformity parameter in a repeating element containing two cracks was analyzed numerically. The non-uniformity parameter is defined as the ratio of the smallest and the average spacing between cracks. COD values needed as an input in the model were calculated using FEM in generalized plane strain formulation and stiffness calculations were performed for GF/EP as well as CF/EP laminates with low and also with high crack density. The trend is the same for all crack densities and lay-ups: assuming uniform crack distribution the damaged laminate modulus is underestimated.

An approximate “double-periodic” approach was proposed stating that the COD of a crack with different distances to the closest neighbors can be calculated as the average of two solutions for equidistant cracks. It was shown numerically for cross-ply laminates that in internal layers very accurate COD values for cracks with non-uniform spacing and elastic modulus values can be obtained using this approach. For cracks in surface layers this approach is accurate only for low crack densities. The applicability of the “double-periodic” approach to sliding displacement of non-uniformly distributed cracks has not been investigated.

Chapter 4

Thermo-elastic constants of symmetric laminates with cracks in 90-layer: application of simple models

4.1. Introduction

Composite laminates under service loading undergo complex combinations of thermal and mechanical loading leading to microdamage accumulation in layers. The most common damage mode is intralaminar cracking in layers. During service life, the number of these cracks, which are transverse to the midplane, increases reducing laminate thermo-elastic properties.

The stiffness degradation of composite laminates due to cracking can be explained in terms of opening and sliding of crack surface. The crack face relative displacement during loading reduces the average stress in the damaged layer, thus reducing the laminate stiffness.

Numerous analytical models have been developed to study the stiffness degradation due to transverse cracks. They are all based on approximate solution for the stress state between two cracks (repeating element). Reference is given only to papers with direct relevance to the current study [47-52].

The simplest type of models leading to linear second order differential equation with constant coefficients is called shear lag models [47-49]. General for all shear-lag models is that the equilibrium conditions are satisfied in average only and the shear stress free condition on crack surfaces is not satisfied. A “shear lag” parameter which is often a fitting parameter is needed in these models. The stress distribution and the stiffness degradation calculated according to these models in [39,51] are affected by the value of this parameter. The most typical modifications and values of the shear lag parameter

compared in [39,50,51] are: a) assuming a resin rich layer of unknown thickness between layers of different orientation where the out-of-plane shear deformation at the crack tip takes place. In this chapter we assume that this layer can not be thicker than fibre diameter; b) assuming that the shear strain acts in the cracked layer only and it is due to linear or parabolic crack opening displacement dependence on the thickness coordinate; c) assuming shear strain also in the constraint layer. The last model was refined by Zhang et al in [10] assuming that the intralaminar shear stress in 0-layer is present only in a part of the constraint layer. Unfortunately, unless experimental full field measurements or FEM are used, the thickness of this zone becomes a fitting parameter.

The first model based on the principle of minimum complementary energy which was free of these assumptions was developed by Hashin [11] to investigate the axial modulus reduction of cross ply laminate with cracks in inside 90 layers. The approximate stress field derived with this approach satisfies all the necessary equilibrium as well as the boundary conditions including zero tractions on the crack surfaces. Since the approximate nature of the selected stress functions lead to increase of the value of the complementary energy, it does not reach the minimum corresponding to the exact solution and the displacement continuity is satisfied only approximately. Hashin's model is relatively simple to use and it renders lower bond for the axial modulus of the damaged laminate. Refined variational models based on minimum principle of the complementary energy with more accurate predictions of axial modulus and Poisson's ratio were developed in [14,52]. However, higher accuracy of analytical solutions is always on the expense of significant increase of complexity. For example, use of the model [52] requires rather complex numerical minimization routine.

Therefore [52] as well as models by McCartney [16] and Shoeppner and Pagano [17] could rather be considered as numerical routines.

Two main problems/limitations related to the use of analytical solutions are: a) approximate analytical solutions are available for cross-ply laminates only; b) these models are developed to calculate only one or two of the whole set of laminate thermo-elastic constants (usually axial or shear modulus of the damaged laminate).

In practice a cross-ply laminate lay-up is rarely used. This limitation has been handled by several authors [19,28,29]. Zhang et al [10] introduced the concept of "an equivalent constraint" assuming that the constraint on the damaged layer of the lay-ups above and below the damaged lamina can be replaced by two sublaminates with properties calculated using laminate theory (CLT). Thereby the actual laminate, considered in the coordinate system related to the damaged layer symmetry, could be replaced by a cross-ply with orthotropic constraint layers. Similar approach was used in Lundmark et al [28,29] applying FEM to analyze the effect of surrounding layers. They demonstrated that the modulus and the thickness ratio of the closest neighbor to the damaged layer are the parameters governing the constraint.

In [28] a unique relationship between the damaged laminate thermo-elastic properties and the microdamage parameters was established (GLOB-LOC approach). Exact analytical expressions for thermo-elastic constants of general symmetric laminates with cracks in multiple layers were presented. These matrix expressions are given in Section 4.2. It was shown that the local parameters in these expressions are the normalized average values of crack opening displacement (COD) and crack sliding displacement (CSD). In addition the laminate lay-up, layer properties and density of cracks in layers has to be given. In this chapter we demonstrate how using this framework and the axial stress distributions obtained from shear lag or from Hashin's model one can calculate all

thermo-elastic constants of a damaged laminate (except shear modulus). The key point in the procedure is that the average COD can be related to the average stress in a layer between two cracks (see section 4.3.2).

The accuracy of predictions is evaluated comparing with direct FEM calculations.

4.2. Material model of damaged symmetric laminates with intralaminar cracks

4.2.1 Model formulation

The upper part of symmetric *N*- layer laminate is shown in Fig. 4.1. The *k*-th layer of the laminate is characterized by thickness t_k , fiber orientation angle with respect to the global x-axis θ_k and by stiffness matrix in the local axis $[Q]$ (defined by thermo-elastic constants $E_1, E_2, G_{12}, \nu_{12}, \alpha_1, \alpha_2$). The total thickness of the laminate, $h = \sum_{k=1}^{N} t_k$. The crack density in a layer is $\rho_k = 1/(2l_k \sin\theta_k)$ where average distance between cracks measured on the specimen edge is $2l_k$. Dimensionless crack density ρ_{kn} is introduced as

$$\rho_{kn} = t_k \rho_k \tag{4.1}$$

It is assumed that the damaged laminate is still symmetric: the crack density in corresponding symmetrically placed layers is the same. The stiffness matrix of the damaged laminate is $[Q]^{LAM}$ and the stiffness of the undamaged laminate is $[Q]_0^{LAM}$. The compliance matrix of the undamaged laminate is $[S]_0^{LAM} = \left([Q]_0^{LAM}\right)^{-1}$, $\{\alpha\}_0^{LAM}$ is the thermal expansion coefficient vector. Constants of the undamaged laminate are calculated using CLT.

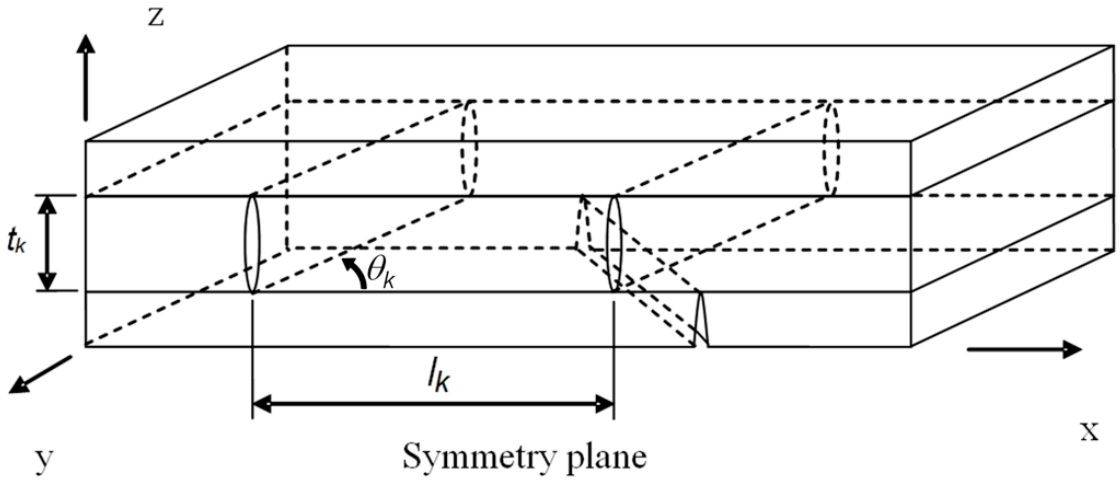

Figure 4.1. RVE of the damaged laminate with intralaminar cracks in layers

The expressions for compliance matrix and thermal expansion vector of the damaged laminate presented below are exact.

$$[S]^{LAM} = [S]_0^{LAM}\left([I] + \sum_{k=1}^{N} \rho_{kn} \frac{t_k}{h} [K]_k [S]_0^{LAM}\right) \tag{4.2}$$

$$\{\alpha\}^{LAM} = \left([I] + \sum_{k=1}^{N} \frac{t_k}{h} \rho_{kn} [S]_0^{LAM} [K]_k\right)\{\alpha\}_0^{LAM} - \sum_{k=1}^{N} \frac{t_k}{h} \rho_{kn} [S]_0^{LAM} [K]_k \{\overline{\alpha}\}_k \tag{4.3}$$

In (4.2) and (4.3) $[I]$ is identity matrix. These expressions were derived in [28] expressing the integral effect of cracks in terms of crack density and $[K]_k$, which is a known matrix-function dependent on ply properties and normalized and averaged crack face opening (COD) and sliding displacements (CSD), u_{2an}, u_{1an}, which may be different in different layers. In (4.3) $\{\overline{\alpha}\}_k$ is the vector of thermal expansion coefficients of the *k*-th layer in global coordinates. The $[K]_k$ matrix for a ply in a laminate is defined as

$$[K]_k = \frac{1}{E_2} [\overline{Q}]_k [T]_k^T [U]_k [T]_K [\overline{Q}]_k \tag{4.4}$$

The involved matrices $[T]_k$ and $[\overline{Q}]_k$ are defined according to CLT, superscript T denotes transposed matrix and bar over stiffness matrix indicates that it is written in global coordinates. For a layer with fiber orientation angle θ_k, $m = \cos\theta_k$ and $n = \sin\theta_k$

$$[T]_k = \begin{bmatrix} m^2 & n^2 & +2mn \\ n^2 & m^2 & -2mn \\ -mn & +mn & m^2 - n^2 \end{bmatrix}, \qquad [\overline{Q}]_k = [T]_k^{-1}[Q]\left([T]_k^{-1}\right)^T \tag{4.5}$$

The influence of each crack is represented in (4.4) by matrix $[U]_k$, which contains the normalized average COD and normalized average CSD of the crack surfaces in k-th layer

$$[U]_k = 2\begin{bmatrix} 0 & 0 & 0 \\ 0 & u_{2an}^k & 0 \\ 0 & 0 & \frac{E_2}{G_{12}}u_{1an}^k \end{bmatrix} \tag{4.6}$$

Correlation of u_{2an}, u_{1an} with the stress state between cracks is the key point in this chapter.

4.2.2 Thermo-elastic constants of balanced laminates with cracks in 90-layers

For balanced laminates with cracked 90-layer, $[K]_k$ can be calculated analytically. Using the result in (4.2) and (4.3) the following expressions for laminate thermo-elastic constants were obtained for the case with only one cracked 90-layer (if laminate has several cracked 90-layers summation is required in the denominator).

$$\frac{E_x^{LAM}}{E_{x0}^{LAM}} = \frac{1}{1 + 2\rho_{90n}\frac{t_{90}}{h}u_{2an}^{90}c_2} \qquad \frac{E_y^{LAM}}{E_{y0}^{LAM}} = \frac{1}{1 + 2\rho_{90n}\frac{t_{90}}{h}u_{2an}^{90}c_4} \tag{4.7}$$

$$\frac{\nu_{xy}^{LAM}}{\nu_{xy0}^{LAM}}=\frac{1+2\rho_{90n}\dfrac{t_{90}}{h}u_{2an}^{90}c_1\left(1-\dfrac{\nu_{12}}{\nu_{yx0}^{LAM}}\right)}{1+2\rho_{90n}\dfrac{t_{90}}{h}u_{2an}^{90}c_2},\qquad \frac{G_{xy}^{LAM}}{G_{xy0}^{LAM}}=\frac{1}{1+2\rho_{90n}\dfrac{t_{90}}{h}u_{1an}^{90}\dfrac{G_{12}}{G_{xy0}^{LAM}}} \tag{4.8}$$

$$\frac{\alpha_x^{LAM}}{\alpha_{x0}^{LAM}}=1-2\rho_{90n}\frac{t_{90}}{h}u_{2an}^{90}\frac{c_1}{\alpha_{x0}^{LAM}}\left(\alpha_2-\alpha_{x0}^{LAM}-\nu_{12}\left(\alpha_{y0}^{LAM}-\alpha_1\right)\right) \tag{4.9}$$

$$\frac{\alpha_y^{LAM}}{\alpha_{y0}^{LAM}}=1-2\rho_{90n}\frac{t_{90}}{h}u_{2an}^{90}\frac{c_3}{\alpha_{y0}^{LAM}}\left(\alpha_2-\alpha_{x0}^{LAM}-\nu_{12}\left(\alpha_{y0}^{LAM}-\alpha_1\right)\right) \tag{4.10}$$

$$c_1=\frac{E_2}{E_{x0}^{LAM}}\frac{1-\nu_{12}\nu_{xy0}^{LAM}}{\left(1-\nu_{12}\nu_{21}\right)^2},\qquad c_2=c_1\left(1-\nu_{12}\nu_{xy0}^{LAM}\right) \tag{4.11}$$

$$c_3=\frac{E_2}{E_{y0}^{LAM}}\frac{\nu_{12}-\nu_{yx0}^{LAM}}{\left(1-\nu_{12}\nu_{21}\right)^2},\qquad c_4=c_3\left(\nu_{12}-\nu_{yx0}^{LAM}\right) \tag{4.12}$$

Index 90 is used for thickness, crack density and COD in 90-layer. The quantities with subscripts x,y and superscript LAM are laminate constants, quantities with additional subscript 0 are undamaged laminate constants. It is noteworthy that

a) If Poisson's effects are neglected $c_3=c_4=0$. In this approximation E_y^{LAM} and α_y^{LAM} do not change because of damage in 90-ply.

b) Shear modulus is not related to COD and depends on sliding displacement only. It is not analyzed in the present chapter.

The class of laminates covered by these expressions is broader than just cross ply laminates or laminates with 90-layers. For example, any quasi-isotropic laminate with an arbitrary cracked layer can be rotated to have the damaged layer as a 90-layer. The only limitation of (4.7)-(4.12) is that the laminate after rotation is balanced with zero coupling terms in $[S]_0^{LAM}$.

Application of (4.7)-(4.12) requires values of u_{2an}, u_{1an}. Three different expressions of u_{2an} are presented in section 4.3 according to FEM, shear-lag and Hashin's models.

4.3. Determination of COD

4.3.1 Crack face displacements

It is assumed that all cracks in the same layer are equal and equidistant. The average CSD and COD are defined as

$$u_{1a}^{90} = \frac{1}{2t_{90}} \int_{-\frac{t_{90}}{2}}^{\frac{t_{90}}{2}} \Delta u_1^{90}(x_3)\, dx_3 \,, \qquad u_{2a}^{90} = \frac{1}{2t_{90}} \int_{-\frac{t_{90}}{2}}^{\frac{t_{90}}{2}} \Delta u_2^{90}(x_3)\, dx_3 \tag{4.13}$$

Here Δu_i is the displacement gap between corresponding points at both crack faces. Subscript 1 denotes the displacement in fiber direction (sliding) and subscript 2 in the transverse direction (opening).

In linear model the average displacements u_{2a}^{90} and u_{1a}^{90} are linear functions of the applied stress and the ply thickness. Therefore, they are normalized with respect to the far field (CLT) shear stress σ_{xy0}^{90} and transverse stress σ_{x0}^{90} in the layer (resulting from the macro-load $\{\sigma\}_0^{LAM}$ and temperature difference ΔT) and with respect to the thickness of the cracked layer t_{90}

$$u_{1an}^{90} = u_{1a}^{90} \frac{G_{12}}{t_{90}\sigma_{xy0}^{90}}, \qquad u_{2an}^{90} = u_{2a}^{90} \frac{E_2}{t_{90}\sigma_{x0}^{90}} \tag{4.14}$$

Elastic constants E_2 and G_{12} of the UD composite are introduced in (4.14) to have dimensionless descriptors. The influence of each crack on thermo-elastic laminate constants is represented by u_{2a}^{90} and u_{1a}^{90}.

4.3.2 Average COD relation to stress perturbation

Part of the deformed laminate with an open crack is shown in Fig. 4.2. Thickness of the supporting sublaminate is t_s and its effective modulus in the axial direction is E_x^s. Denoting the displacement of the undamaged sublaminate at $x = l_{90}$ (l_{90} is the half distance between cracks) by $u_s(l_0)$ and the displacement of the crack face by $u_{90}(l_0, z)$ we can write that the average COD is

$$u_{2a}^{90} = \frac{2}{t_{90}} \int_0^{\frac{t_{90}}{2}} [u_s(l_{90}) - u_{90}(l_{90}, z)] dz = u_s(l_{90}) - \frac{2}{t_{90}} \int_0^{\frac{t_{90}}{2}} u_{90}(l_{90}, z) dz \tag{4.15}$$

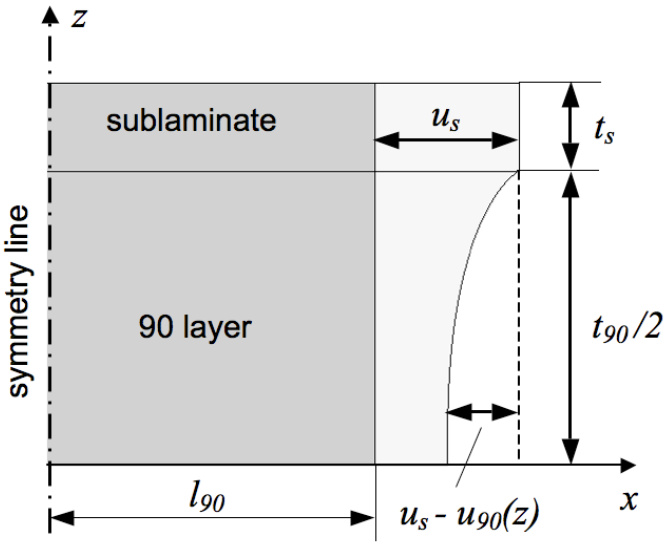

Figure 4.2. Schematic showing of the deformation of the laminate in the vicinity of transverse crack

The crack opening leads to reduction of axial stress in the 90-layer. The stress between two cracks in the 90-layer can be written in the following general form

$$\sigma_x^{90} = \sigma_{x0}^{90} [1 - f(x, z, l_{90})] \tag{4.16}$$

Function f in (4.16) represents the stress perturbation and σ_{x0}^{90} is the axial stress in the undamaged 90-layer (CLT). The average value of the stress between two cracks is defined as

$$\sigma_{xa}^{90} = \sigma_{x0}^{90}\left[1 - f_a\left(\rho_{90n}\right)\right] \tag{4.17}$$

$$f_a\left(\rho_{90}\right) = \frac{2}{l_{90}t_{90}}\int_0^{l_{90}}\int_0^{\frac{t_{90}}{2}} f\left(x,z,l_{90}\right)dxdz \tag{4.18}$$

The average stress in the sublaminate can be obtained from force balance

$$\sigma_{xa}^{s} = \sigma_{x0}^{s}\left(1 + \frac{t_{90}}{2t_s}\frac{E_2}{E_x^s} f_a\left(\rho_{90n}\right)\right) \tag{4.19}$$

In this section we will establish relationship between u_{2a}^{90} and f_a.

Neglecting Poisson's effects the $u_{90}\left(l_0, z\right)$ can be written as

$$u_{90}\left(l_{90}, z\right) = \int_0^{l_{90}} \varepsilon_x^{90}\left(x,z\right)dx = \frac{1}{E_2}\int_0^{l_{90}} \sigma_x^{90}\left(x,z\right)dx \tag{4.20}$$

Similarly for $u_s\left(l_{90}\right)$ we can write

$$u_s\left(l_{90}\right) = \int_0^{l_{90}} \varepsilon_x^{s}\left(x,z\right)dx = \frac{2}{t_{90}}\int_0^{\frac{t_{90}}{2}}\int_0^{l_{90}} \varepsilon_x^{s}\left(x,z\right)dxdz = \frac{2}{E_x^s t_{90}}\int_0^{\frac{t_{90}}{2}}\int_0^{l_{90}} \sigma_x^{90}\left(x,z\right)dxdz = \frac{l_{90}}{E_x^s}\sigma_{xa}^{s} \tag{4.21}$$

Substituting (4.20) and (4.21) in (4.15) we obtain

$$u_{2a}^{90} = l_{90}\left(\frac{\sigma_{xa}^{s}}{E_x^s} - \frac{\sigma_{xa}^{90}}{E_2}\right) \tag{4.22}$$

Substituting (4.17), (4.19) in (4.22) and using approximate expressions

$$\frac{\sigma_{x0}^{90}}{E_2} = \frac{\sigma_{x0}^{s}}{E_x^s}, \qquad E_{x0}^{LAM} = \frac{E_2\frac{t_{90}}{2} + E_x^S t_s}{\frac{t_{90}}{2} + t_s} \tag{4.23}$$

we obtain

$$u_{2a}^{90} = f_a \cdot l_{90}\sigma_{x0}^{90}E_{x0}^{LAM}\frac{\frac{t_{90}}{2} + t_s}{t_s E_2 E_x^s} \tag{4.24}$$

Using (4.14) the relationship between normalized average COD and stress perturbation f_a is written as

$$u_{2an}^{90} = f_a(\rho_{90n}) \cdot \frac{1}{\rho_{90n}} \frac{E_{x0}^{LAM}}{E_x^s} \frac{\frac{t_{90}}{2} + t_s}{2t_s} \tag{4.25}$$

4.3.3 Shear-lag model

The stress perturbation function for shear lag models is given in [50]. Using expression (40) from [50] in (4.25) we obtain (note that $f_a = \frac{\rho_{90n}}{2} R$ is used in [50])

$$u_{2an}^{90} = \frac{E_{x0}^{LAM}\left(t_s + \frac{t_{90}}{2}\right)}{2E_x^s t_s} \frac{1}{\xi} \tanh\left(\frac{\xi}{\rho_{90n}}\right) \tag{4.26}$$

The shear lag parameter ξ depends on the chosen modification of the shear lag model. Assuming existence of a resin rich layer with shear modulus G_m and thickness d_0 at the 0/90 interface we have the following expression

$$\xi^2 = \frac{G_m}{d_0} \frac{\frac{t_{90}}{2}\left(E_2 \frac{t_{90}}{2} + E_x^s t_s\right)}{t_s E_2 E_x^s} \tag{4.27}$$

Usually the thickness of the resin layer is taken equal to one fiber diameter. It seems physically unrealistic to have it larger than that (if any). In other modifications of the shear lag model [7,49] the expressions for the shear lag parameter are different. In one of the most common modifications G_m / d_0 in (4.27) is replaced by $2G_{23} / t_{90}$, whereas in modification assuming parabolic displacement distribution it is equal to $6G_{23} / t_{90}$.

4.3.4 Hashin´s model

Expressions for Hashin's model for the case when 90-layer is supported by orthotropic sublaminate are given in [50]. Expression for stress perturbation function is also given there. After substituting these expressions in (4.25) and using our notation we obtain

$$u_{2an}^{90} = \frac{E_{x0}^{LAM}\left(t_s + \frac{t_{90}}{2}\right)}{2E_x^s t_s} \frac{2\alpha\beta}{\alpha^2+\beta^2} \frac{\cosh\left(\frac{2\alpha}{\rho_{90n}}\right) - \cos\left(\frac{2\beta}{\rho_{90n}}\right)}{\beta\sinh\left(\frac{2\alpha}{\rho_{90n}}\right) + \alpha\sin\left(\frac{2\beta}{\rho_{90n}}\right)} \tag{4.28}$$

$$\text{Here } \alpha = q^{1/4}\cos\frac{\theta}{2},\ \beta = q^{1/4}\sin\frac{\theta}{2},\ \tan\theta = \sqrt{\frac{4q}{p^2}-1} \tag{4.29}$$

$$p = \frac{C_{02}-C_{11}}{C_{22}}, \qquad q = \frac{C_{00}}{C_{22}} \tag{4.30}$$

$$C_{00} = \frac{1}{E_2} + \frac{t_{90}}{2E_x^s t_s}, \qquad C_{02} = \frac{\nu_{23}}{E_2}\left(\frac{2t_s}{t_{90}} + \frac{2}{3}\right) - \frac{\nu_{xz}^s}{3E_x^s}\frac{2t_s}{t_{90}} \tag{4.31}$$

$$C_{11} = \frac{1}{3G_{23}} + \frac{1}{3G_{xz}^s}\frac{2t_s}{t_{90}}, \qquad C_{22} = \frac{1}{E_2}\left(\left(\frac{t_s}{t_{90}}\right)^2 + \frac{2t_s}{3t_{90}} + \frac{8}{60}\right) + \frac{2}{5E_z^s}\left(\frac{t_s}{t_{90}}\right)^3 \tag{4.32}$$

For cross-ply laminates $E_x^s = E_1$, $E_z^s = E_2$, $G_{xz}^s = G_{12}$, $\nu_{xz}^s = \nu_{12}$ and t_s is equal to the thickness of 0 layer.

For "non cross-ply laminate", GF/EP2 [±15/90$_4$]s laminate (in section 4.4.3) and GF/EP [0/±45/90]s laminate (in section 4.4.4) E_x^s is calculated using CLT, t_s is the thickness of the sublaminate. E_z^s, G_{xz}^s and ν_{xz}^s in this case are calculated using FEM.

4.3.5 Ply discount model

In the ply discount model it is assumed that as soon as damage appears in a layer its load bearing capacity reduces to zero. This assumption corresponds to infinite number of cracks in the layer. Zero load bearing by the layer can be obtained by changing

elastic properties of the layer to zero. In the most conservative form of this model all elastic constants are assumed zero. More representative for the case of transverse cracking is assumption used in this chapter stating that the transverse and the shear modulus of the damaged layer is close to zero whereas the longitudinal modulus and Poisson's ratio have not changed. The stiffness of the damaged laminate is calculated using CLT.

The transverse elastic modulus E_2 and shear modulus G_{12} were reduced to 0.01 of their initial values. In section 4.4.5, where the ply discount model is used for case with neglected Poisson's effects the CLT analysis is reduced to the rule of mixtures.

4.4. Results and discussion

4.4.1 Material properties

The elastic properties of the unidirectional composites relevant to this study are given in Table 4.1. Elastic properties of GF/EP and CF/EP used in simulations were arbitrary assumed to represent materials like glass fiber/epoxy and carbon fiber/epoxy respectively.

Elastic properties of GF/EP2 were taken from [50] where the properties (except the out-of-plane Poisson's ratio ν_{23}, which was assumed) were obtained experimentally.

It has to be noted that the GF/EP and CF/EP in Table 4.1 do not have isotropy in the transverse plane and the out-of-plane shear modulus is slightly different than it would be for transverse isotropic material. Reason for the increased anisotropy could be through the thickness stitching observable in many composites. However, shear lag model does not contain G_{23} and Hashin's model, which has it in C_{11} is insensitive to it.

Table 4.1. Ply properties of the studied materials

	E_1	E_2	ν_{12}	ν_{23}	G_{12}	G_{23}	α_1	α_2	t_0	d_0
Material	[GPa]	[GPa]	[-]	[-]	[GPa]	[GPa]	[°C^{-1}]	[°C^{-1}]	[mm]	[mm]
GF/EP	45	15	0.3	0.4	5	6	1.0e-5	2.0e-5	0.13	0.007
CF/EP	150	10	0.3	0.4	5	6	4.3e-7	2.6e-5	0.13	0.0035
GF/EP2	44.73	12.76	0.297	0.42	5.8	4.49	-	-	0.144	0.007

d_0 is the thickness of the shear layer ($d_0 = 0.5 \cdot d_f$, where d_f is the diameter of one fiber)

4.4.2 Parametric analysis on cross-ply laminates

In all figures below the notation "Shear-lag" is used to indicate results calculated using COD obtained from shear lag stress analysis (4.26) in expressions (4.7)-(4.12). The thickness of the shear layer is given in Table 4.1 or indicated in figures if selected differently. The notation "Hashin" is used for predictions where the stress perturbation function from Hashin's model (generalized for orthotropic support layers/sublaminates) (4.28) is used. The notation used for considered cross-ply lay-ups is shown in Table 4.2.

Table 4.2. Cross-ply laminate lay-ups and used notation

Notation	Lay-up
{1}	[0/90/0]
{2}	[0/90]s
{3}	[0/90$_2$]s

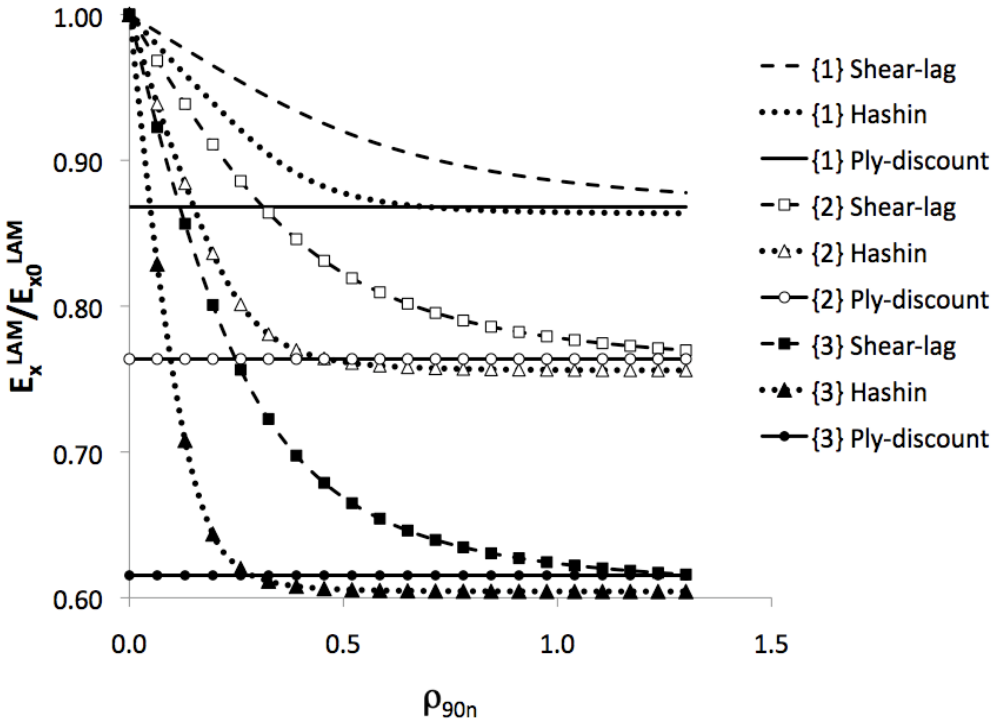

Figure 4.3. Simulation results showing changes in the axial modulus of the laminate E_x^{LAM} for GF/EP.

In Fig. 4.3 and Fig. 4.4 the axial modulus reduction normalized with respect to its initial value is shown for all three lay-ups and for GF/EP and CF/EP composites. Predictions of the ply-discount model are shown as horizontal lines. The modulus reduction behavior is well known and described in literature: a) more modulus reduction in laminates with relatively thick cracked plies; b) much more modulus reduction in GF/EP composites because the damaged layer has relatively high modulus as compared with the longitudinal modulus; c) more modulus reduction according to Hashin's model which as a consequence of the used minimum principle always gives conservative results.

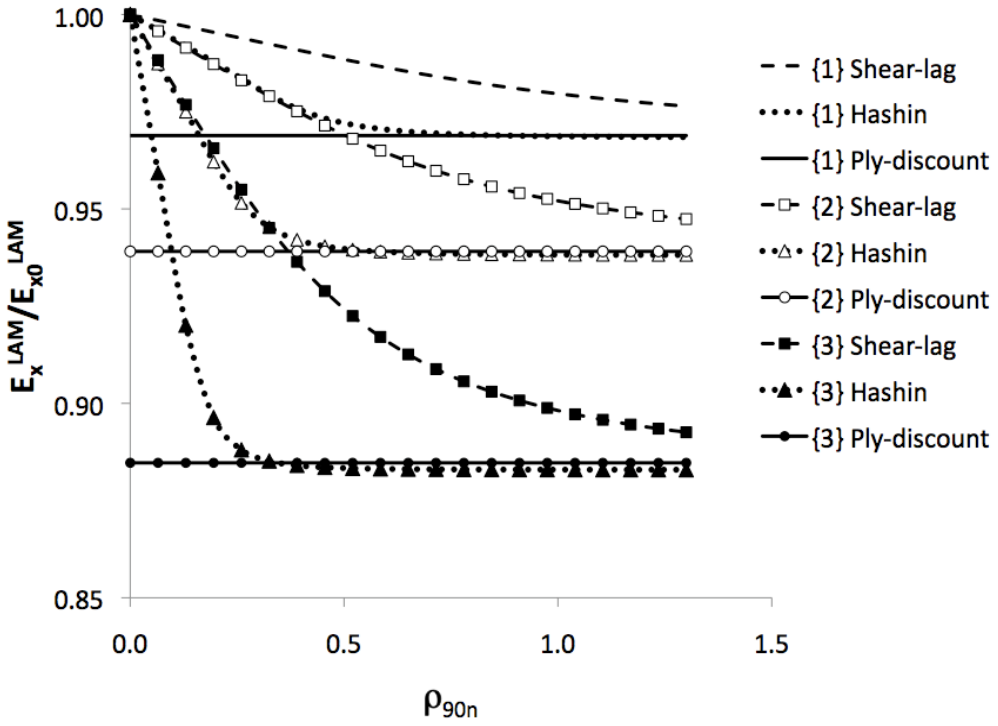

Figure 4.4. Simulation results showing changes in the axial modulus of the laminate E_x^{LAM} for CF/EP

The rate of the modulus reduction according to the shear lag model depends on the shear lag parameter (related to the thickness of the resin layer d_0). The values given in Table 4.1 lead to much slower decrease rate than in Hashin's model. All simulated curves approach to the ply discount value. Surprisingly, the asymptotic values of both models go slightly below the ply-discount value. Since ply-discount model corresponds to an infinite number of cracks this trend needs an explanation which is given in section 4.4.5.

The normalized transverse modulus E_y^{LAM} / E_{y0}^{LAM} of the damaged laminate reduction is marginal, see Fig. 4.5 and Fig. 4.6, which validates the usual assumption that due to cracks in 90-layer it is not changing at all. Also for this elastic property the Hashin's model predicts faster reduction with increasing crack density than the shear lag model. The change is very similar for GF/EP and CF/EP and the asymptotic values are very insensitive to the damaged ply thickness.

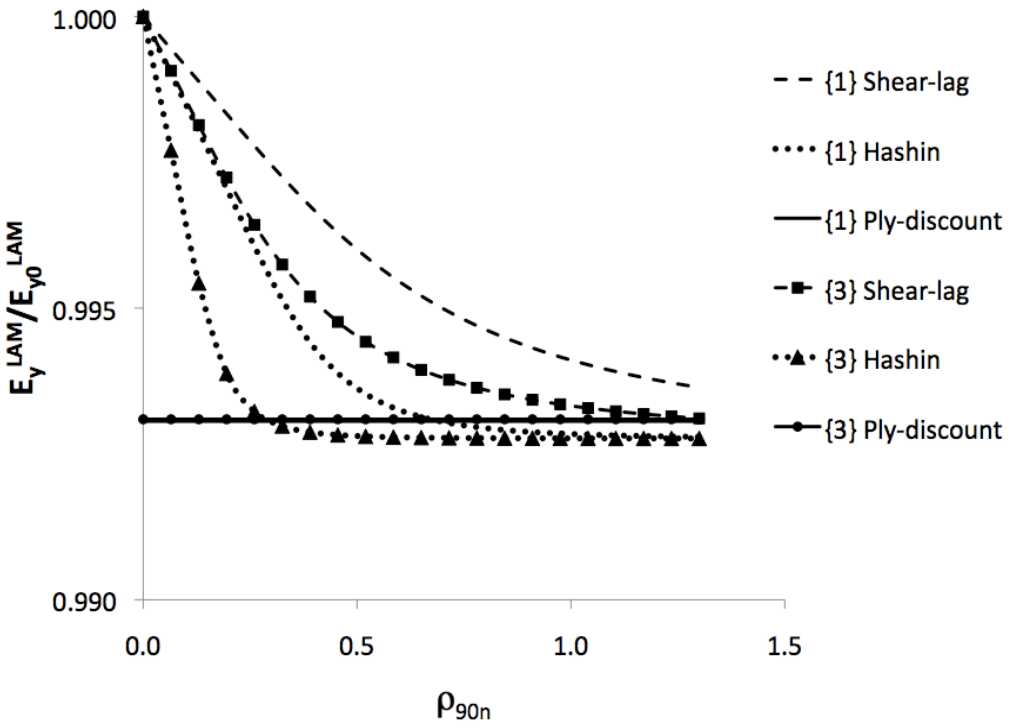

Figure 4.5. Simulation results showing changes in the transverse modulus of the laminate E_y^{LAM} for GF/EP

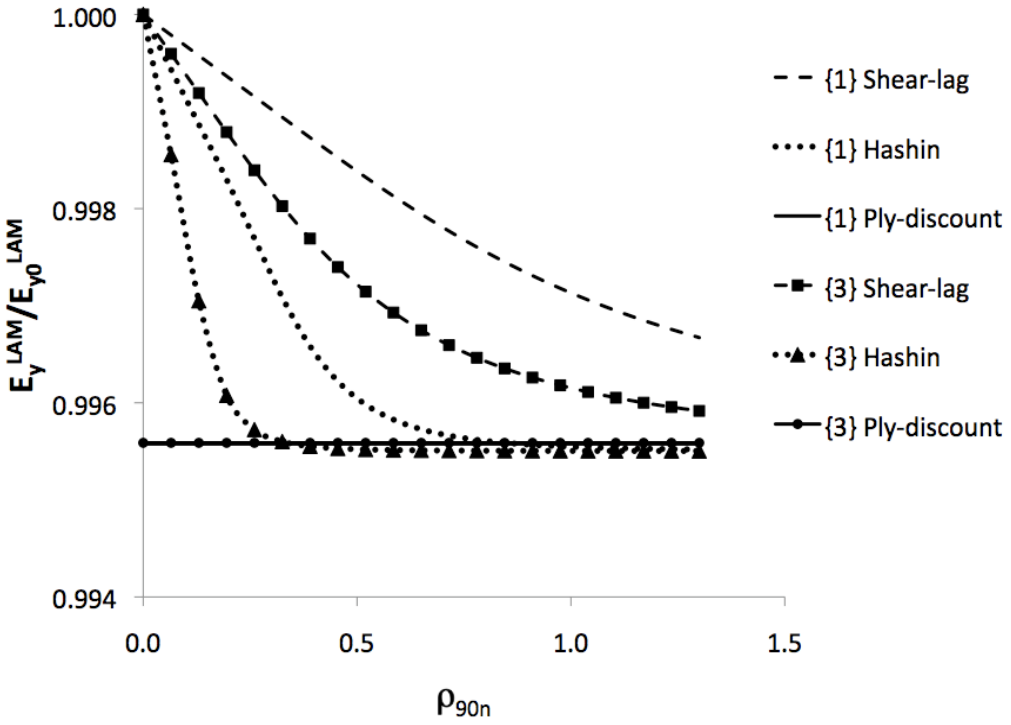

Figure 4.6. Simulation results showing changes in the transverse modulus of the laminate E_y^{LAM} for CF/EP

Similar results for the normalized Poisson's ratio are given in Fig. 4.7 and Fig. 4.8. For this property the asymptotic values does not depend on the used material but the rate of approaching to these values is material dependent, especially according to the shear lag model. The asymptotic value for damaged cross-ply laminate depends only on ply-thickness ratio.

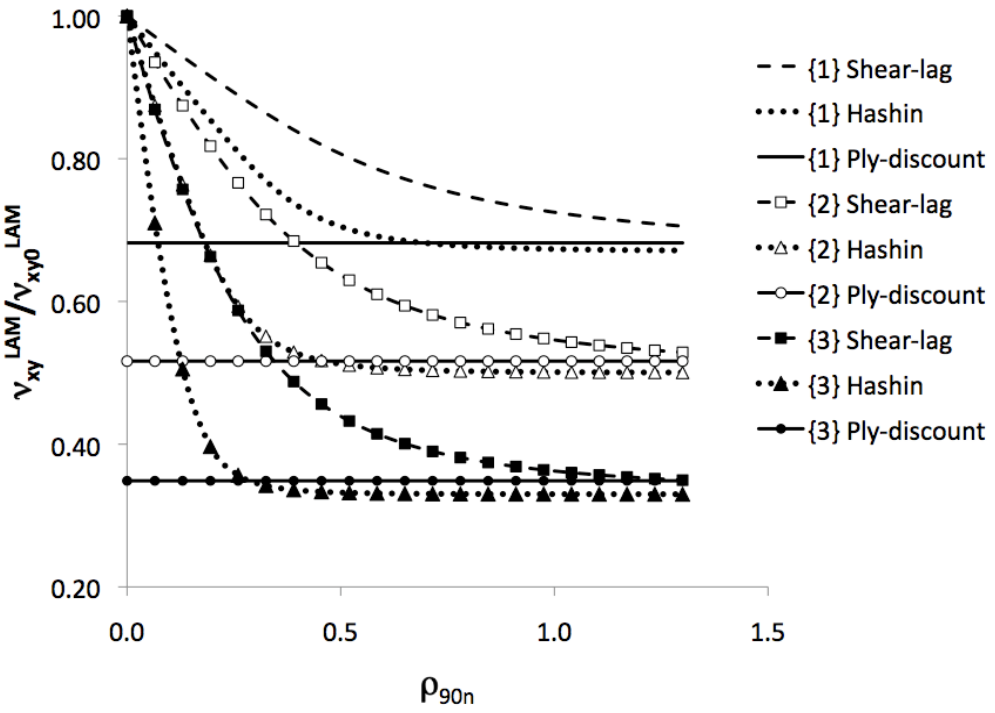

Figure 4.7. Simulation results showing change in Poisson's ratio of the laminate ν_{xy}^{LAM} for GF/EP

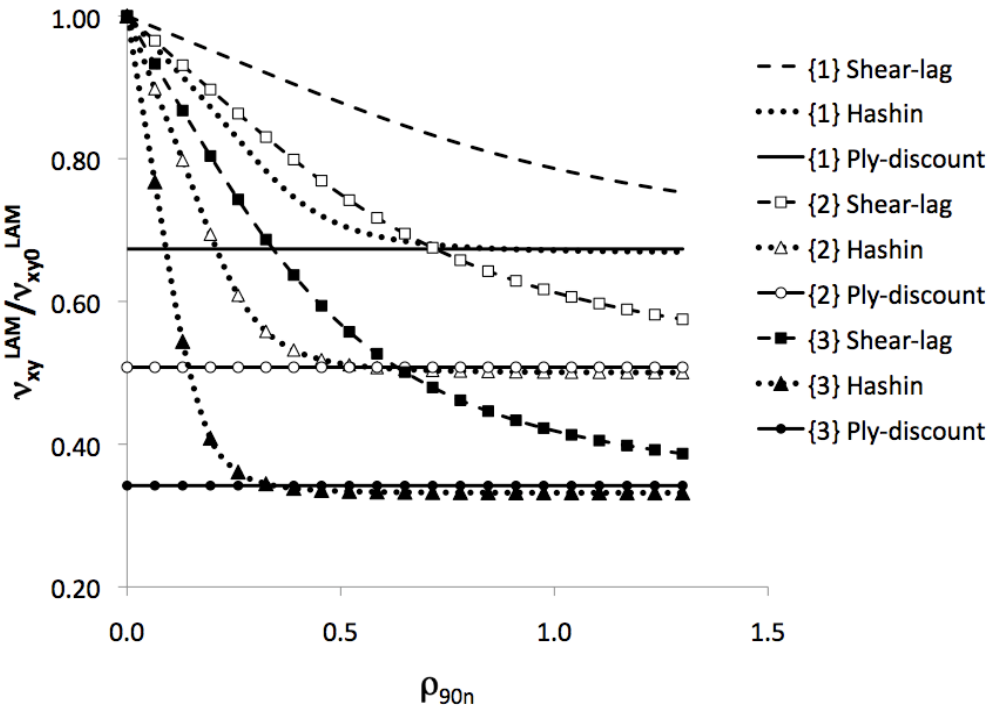

Figure 4.8. Simulation results showing change in Poisson's ratio of the laminate ν_{xy}^{LAM} for CF/EP

Change of thermal expansion coefficients, which is seldom discussed in analytical models is shown in Fig. 4.9 and Fig. 4.10 for $\alpha_x^{LAM}/\alpha_{x0}^{LAM}$ and in Fig. 4.11 and Fig. 4.12 for $\alpha_y^{LAM}/\alpha_{y0}^{LAM}$. The relative change is much larger for CF/EP laminates but the absolute values are, certainly, much smaller. The trend is the same: Hashin's model predicts much faster properties reduction. It is noteworthy that for CF/EP laminate the transverse thermal expansion coefficient change is more than 20% (for lay-up with thickest 90-layer).

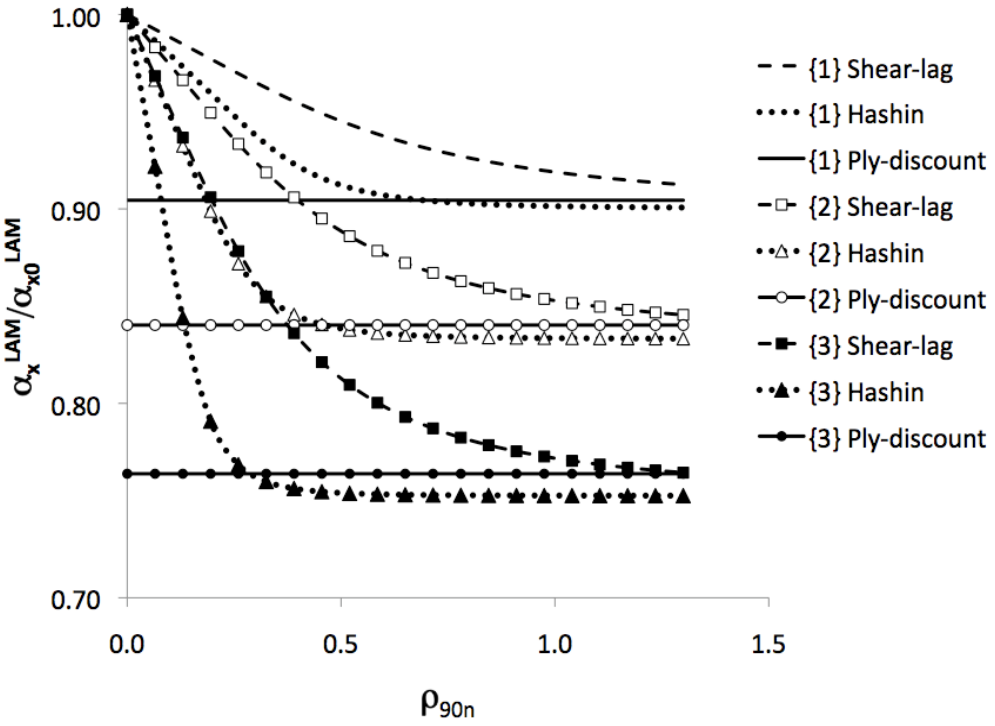

Figure 4.9. Simulation results showing change in the axial coefficient of thermal expansion of the laminate α_x^{LAM} for GF/EP

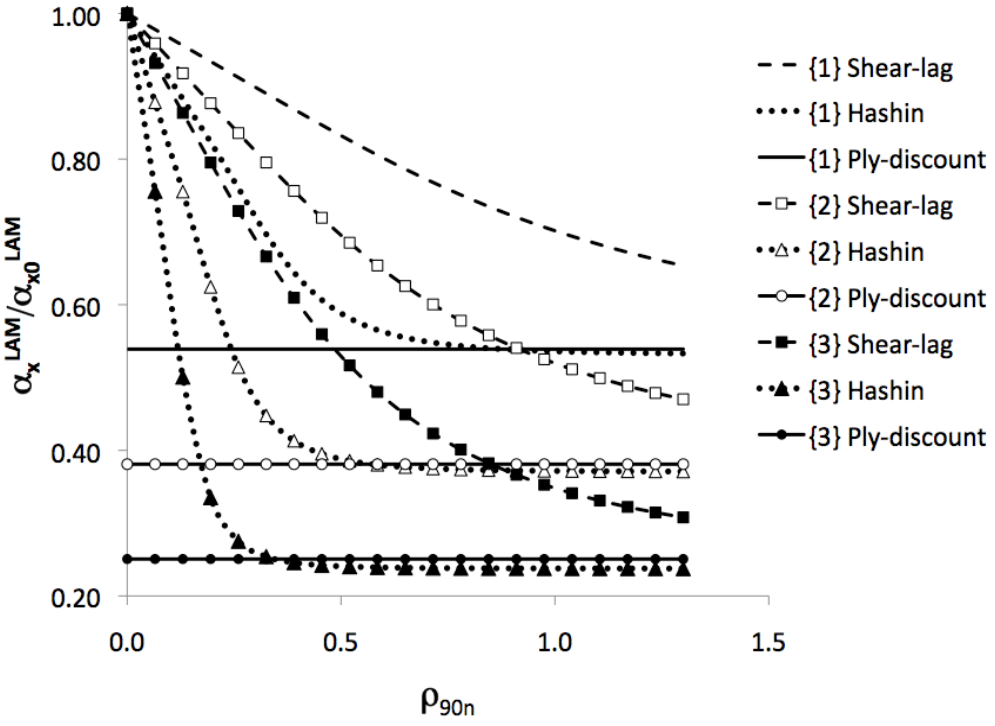

Figure 4.10. Simulation results showing change in the axial coefficient of thermal expansion of the laminate α_x^{LAM} for CF/EP

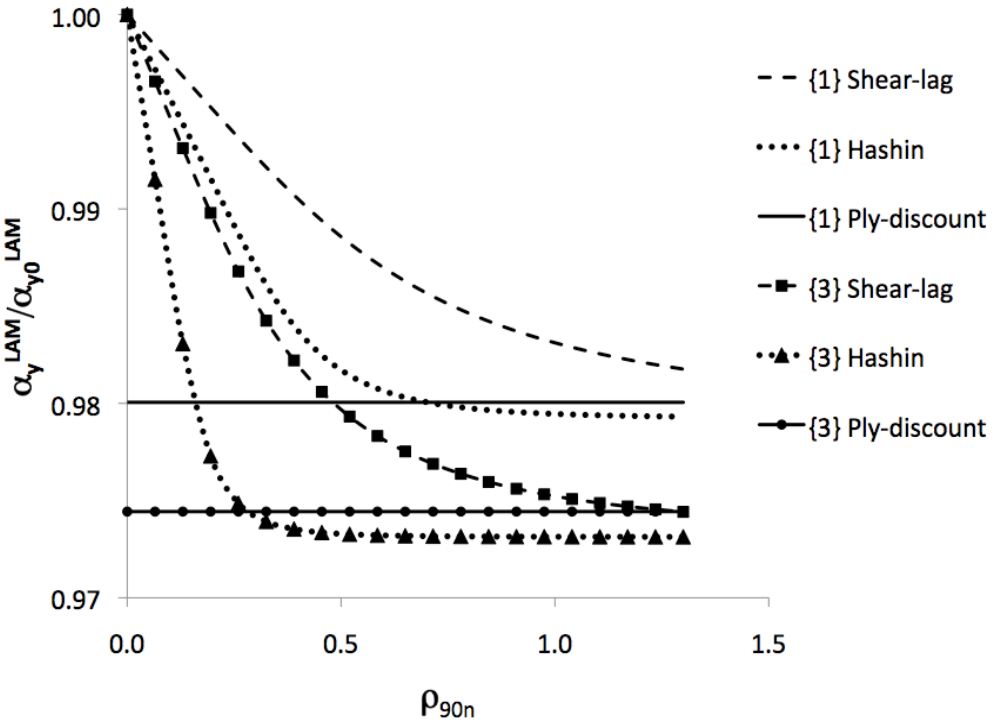

Figure 4.11. Simulation results showing change in the transverse coefficient of thermal expansion of the laminate α_y^{LAM} for GF/EP

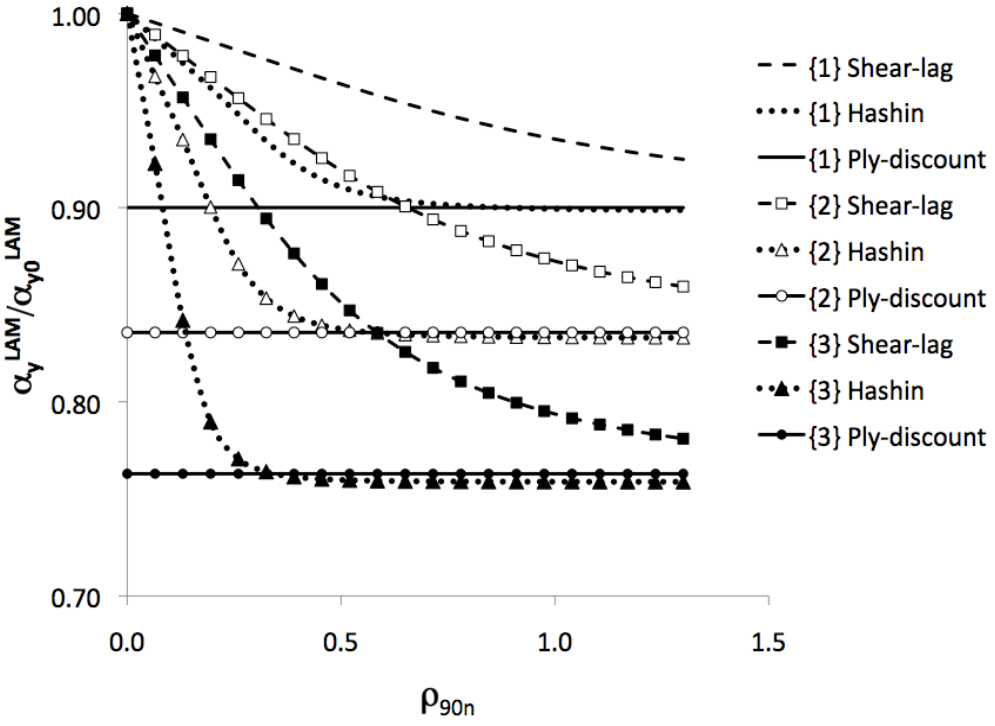

Figure 4.12. Simulation results showing change in the transverse coefficient of thermal expansion of the laminate α_y^{LAM} for CF/EP

4.4.3 Comparison between simulations and experimental data

The shear lag model and the Hashin's model predictions are compared with experimental data in Fig. 4.13 to Fig. 4.16. It is obvious that for both GF/EP2 laminate lay-ups ($[0_2/90_4]$s and $[\pm15/90_4]$s) Hashin's model describes the axial modulus and Poisson's ratio reduction more accurate than the shear lag model. Still, the Hashin's model gives conservative values, especially for the $[\pm15/90_4]$s lay-up. The shear lag model by far under-predicts the reduction of these constants.

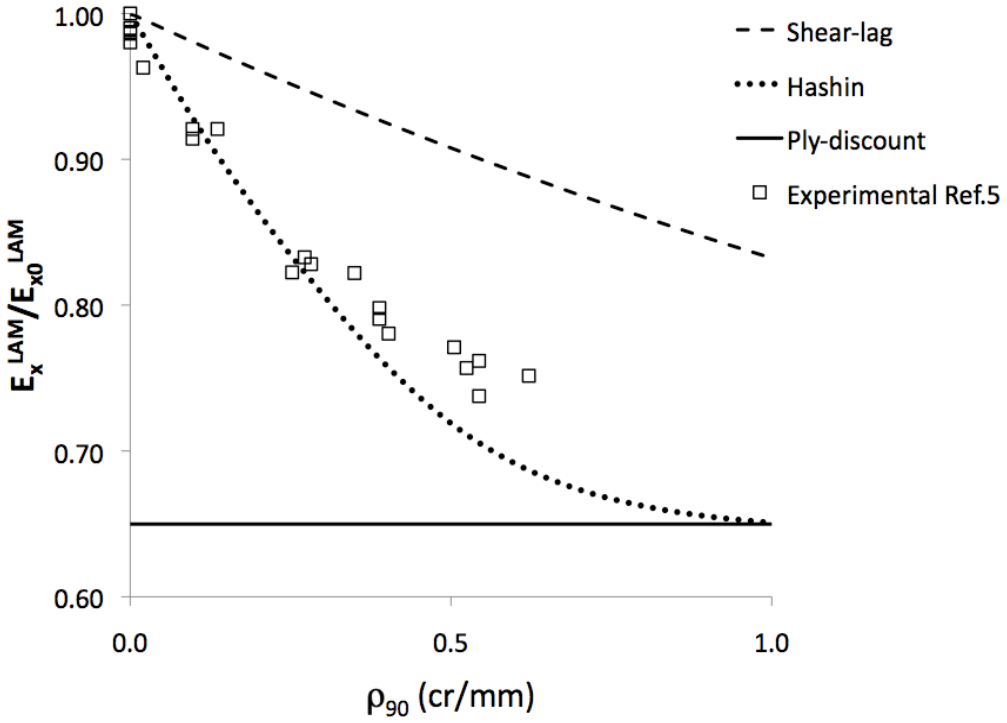

Figure 4.13. Simulations and experimental data showing the change in axial modulus E_x^{LAM} of GF/EP2 $[0_2/90_4]$s laminate

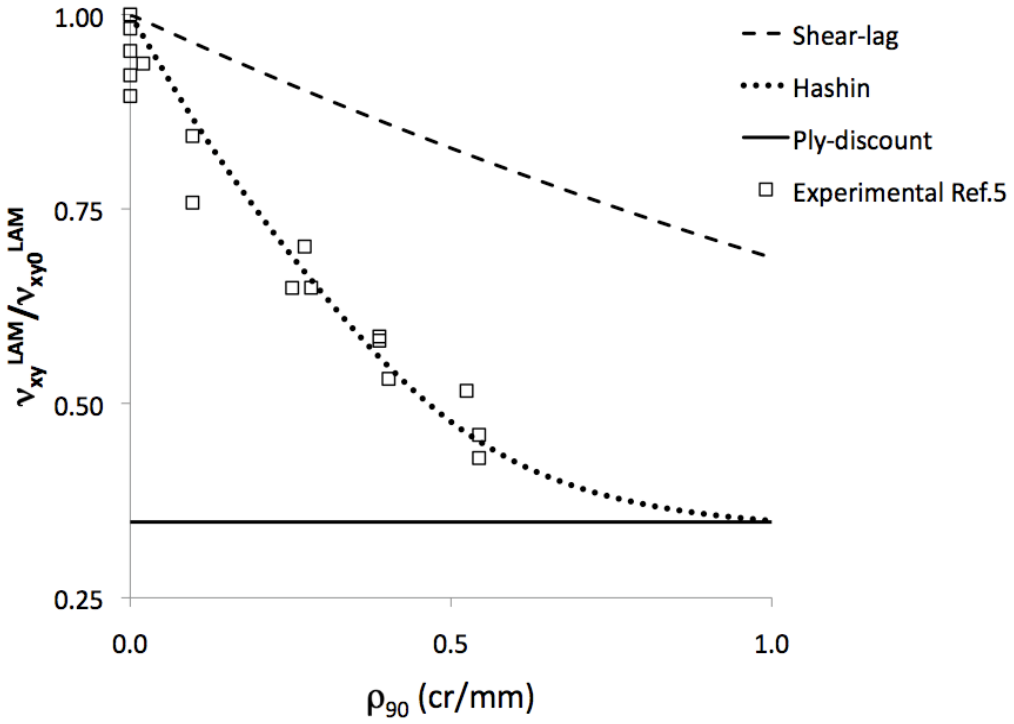

Figure 4.14. Simulations and experimental data showing the change in Poisson's ratio ν_{xy}^{LAM} of GF/EP2 $[0_2/90_4]$s laminate.

The excellent agreement between the test results and the predictions of the Hashin's model, which suppose to give a lower bond to stiffness, requires an explanation. 90-layer thickness was rather large (1.15mm) and much thicker than the constraint layer. Laminates with such geometry are prone to local delaminations starting from transverse crack tip. These local delaminations would increase the crack opening and lead to more modulus reduction than in the case without delaminations and improve the agreement with Hashin's model. FEM results for this laminate presented in [50] are higher than experimental data indicating that in this case indeed the crack model without delaminations may not correspond to reality.

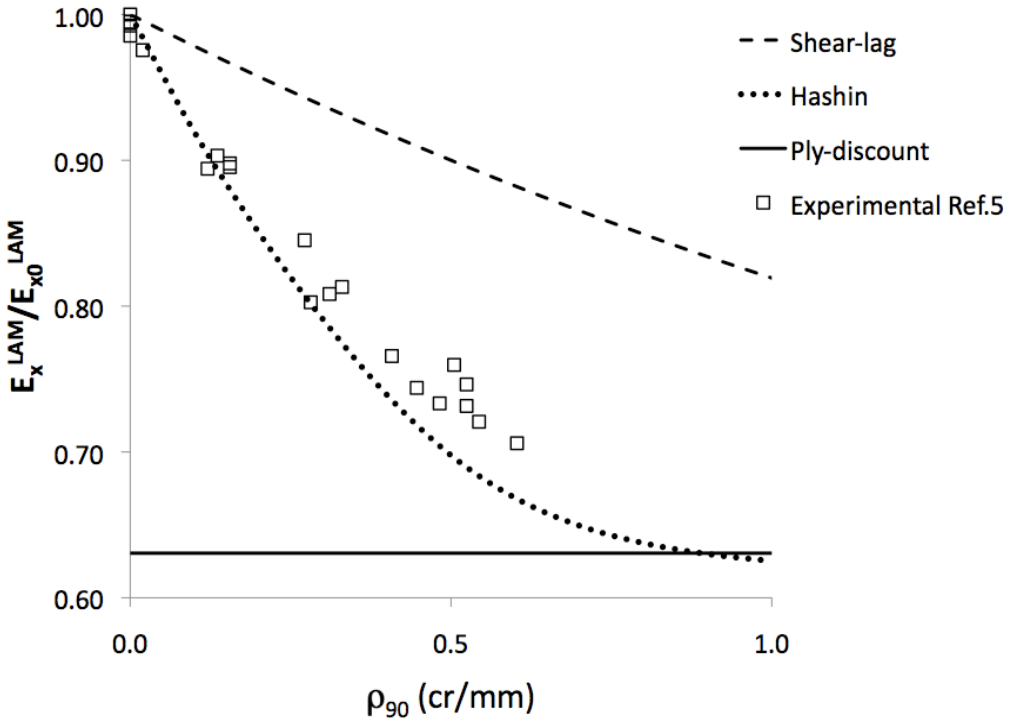

Figure 4.15. Simulations and experimental data showing the change in axial modulus E_x^{LAM} of GF/EP2 [±15/90$_4$]s laminate

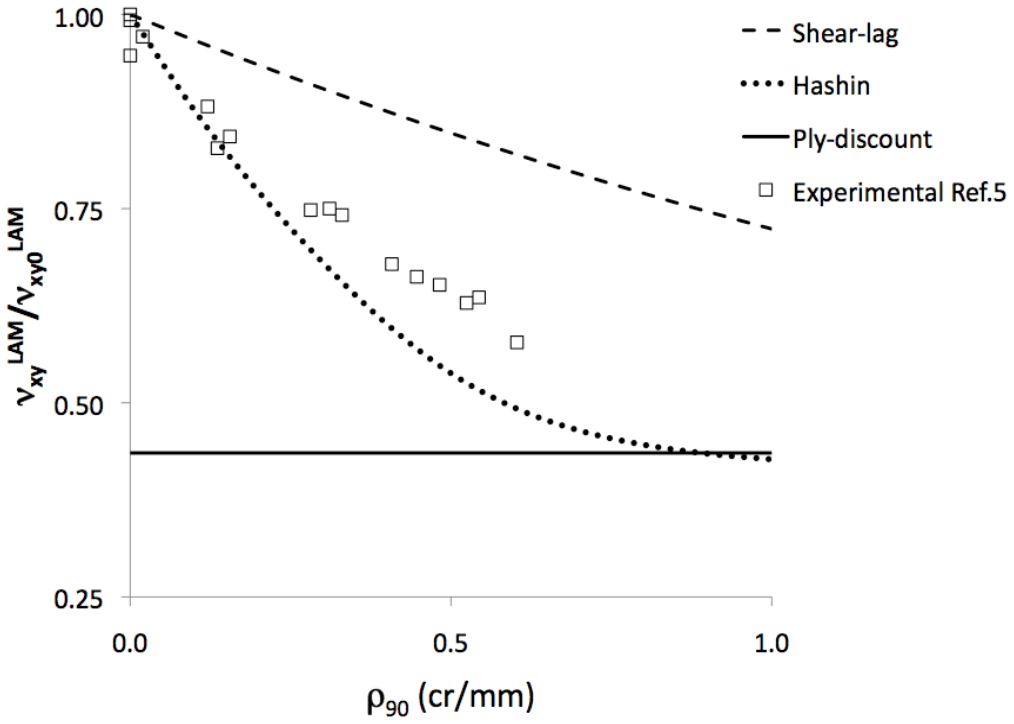

Figure 4.16. Simulations and experimental data showing the change in Poisson's ratio ν_{xy}^{LAM} of GF/EP2 [±15/90$_4$]s laminate

4.4.4 Comparison between analytical simulations and FEM data

To validate the results and trends presented in section 4.4.2 FEM analysis was performed and the thermo-elastic properties of damaged laminates were analyzed directly from the FEM model or indirectly (for example, thermal expansion coefficients) determining COD with FEM and using (4.7)-(4.12). Results are presented in Fig. 4.17 to Fig. 4.24.

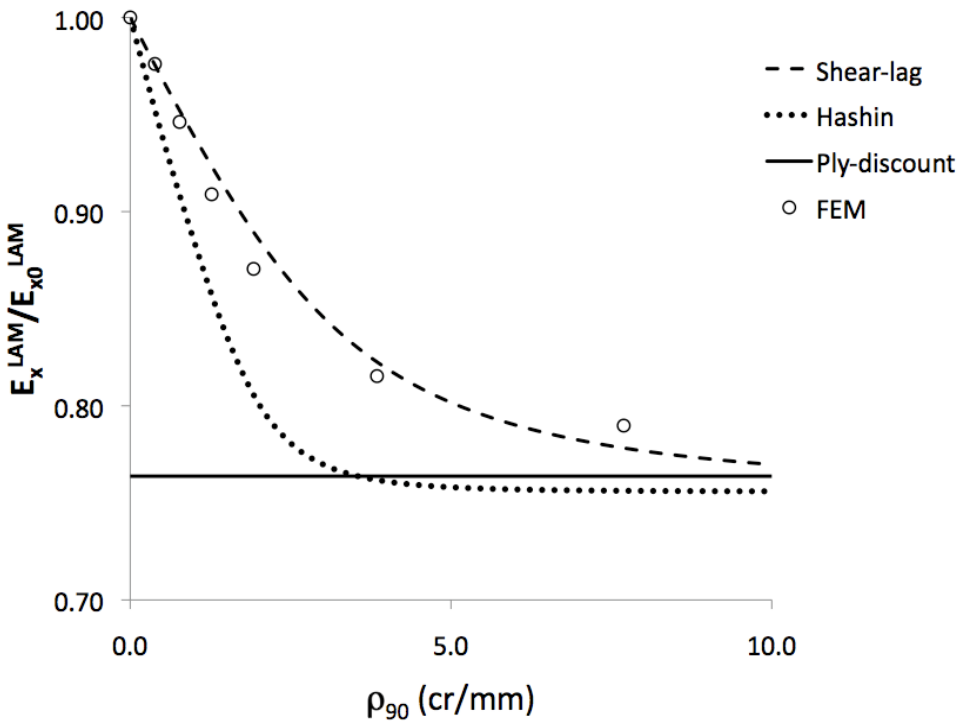

Figure 4.17. Simulations and FEM data showing the change in axial modulus E_x^{LAM} of GF/EP [0/90]s laminate

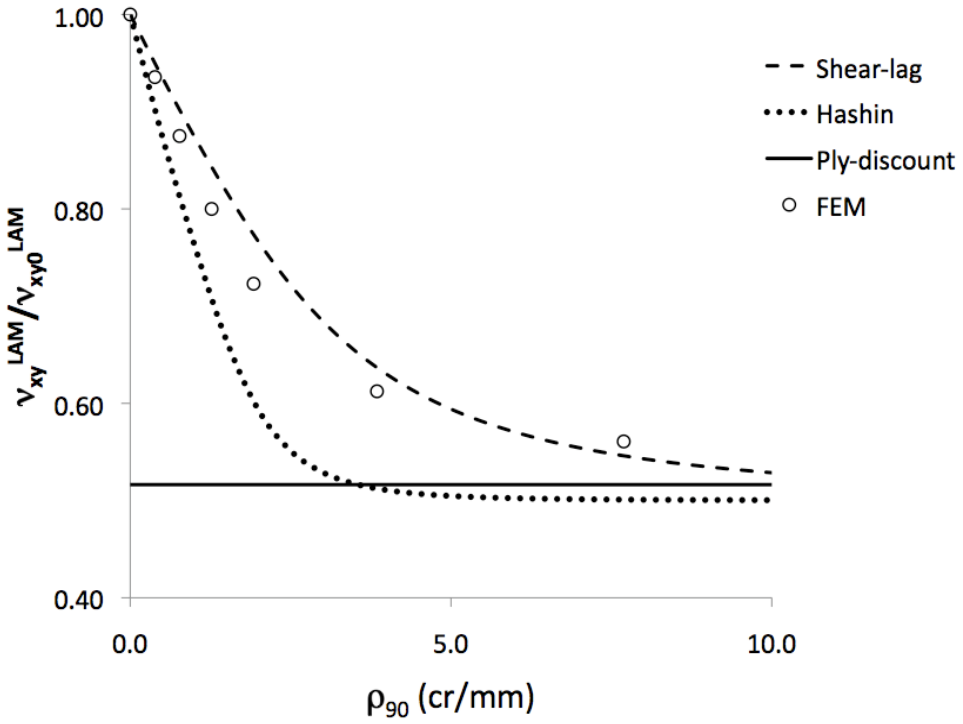

Figure 4.18. Simulations and FEM data showing the change in Poisson's ratio ν_{xy}^{LAM} of GF/EP [0/90]s laminate

Comparison for GF/EP [0/90]s laminates can be based on data presented in Fig. 4.17 to Fig. 4.19. The shear lag model with the selected resin layer thickness of 0.007 mm gives excellent accuracy for axial modulus and for thermal expansion coefficient and slightly larger differences for Poisson's ratio. Noteworthy, the differences have the same trends with crack density change for all three properties. Hashin's model largely overestimates changes of all three properties.

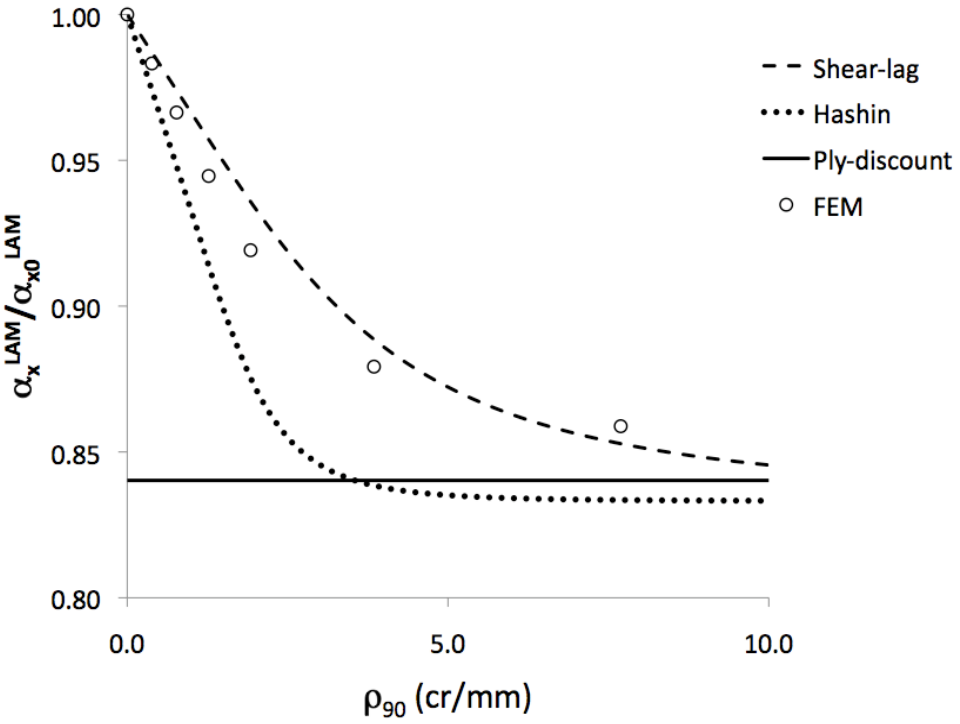

Figure 4.19. Simulations and FEM data showing the change in axial coefficient of thermal expansion α_x^{LAM} of GF/EP [0/90]s laminate

In CF/EP [0/90]s laminate, see Fig. 4.20 to Fig. 4.22, the situation is different: the shear lag model with $d_0 = 0.0035$ mm (half of the carbon fiber diameter) gives very poor prediction. Voluntarily taking it two times larger (equal to the value for glass fiber radius) improves the agreement but it still underestimates the properties reduction.

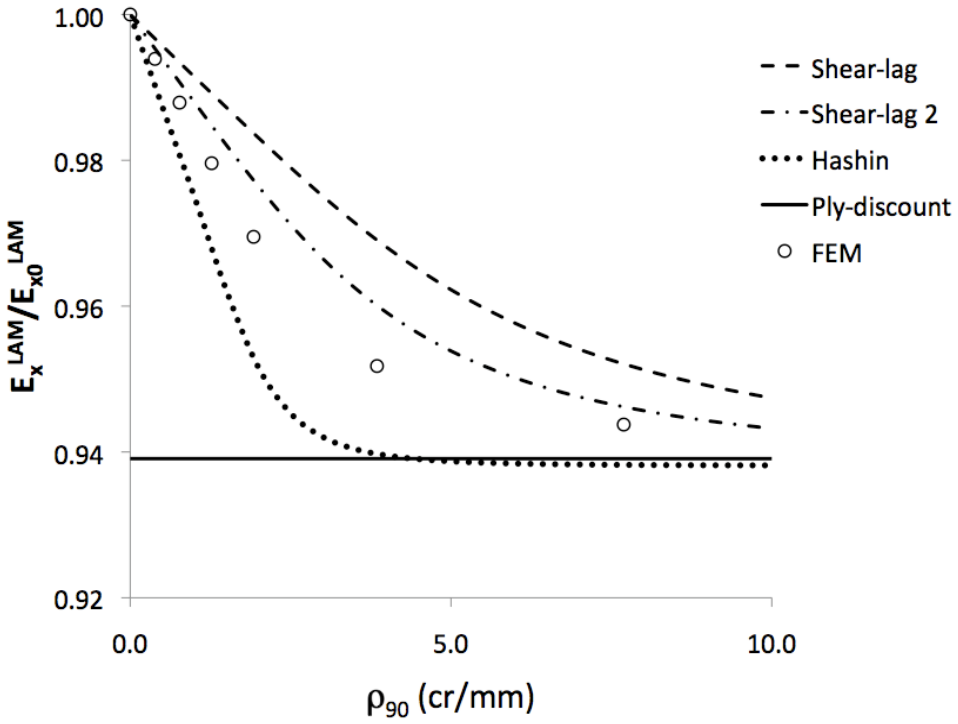

Figure 4.20. Simulations and FEM data showing the change in axial modulus E_x^{LAM} of CF/EP [0/90]s laminate. "Shear-lag" corresponds to $d_0 = 0.0035\,\text{mm}$, "Shear-lag 2" to $d_0 = 0.007\,\text{mm}$

The lower bond from Hashin's model is much lower than the FEM data. Fig. 4.20 to Fig. 4.22 reveal the features of the shear lag model: using the resin layer thickness as a fitting parameter we could find a value which gives a very good fitting for all three considered properties. This is useful result suggesting approximate procedure: find this fitting parameter from FEM data for axial modulus and use it for all thermo-elastic properties.

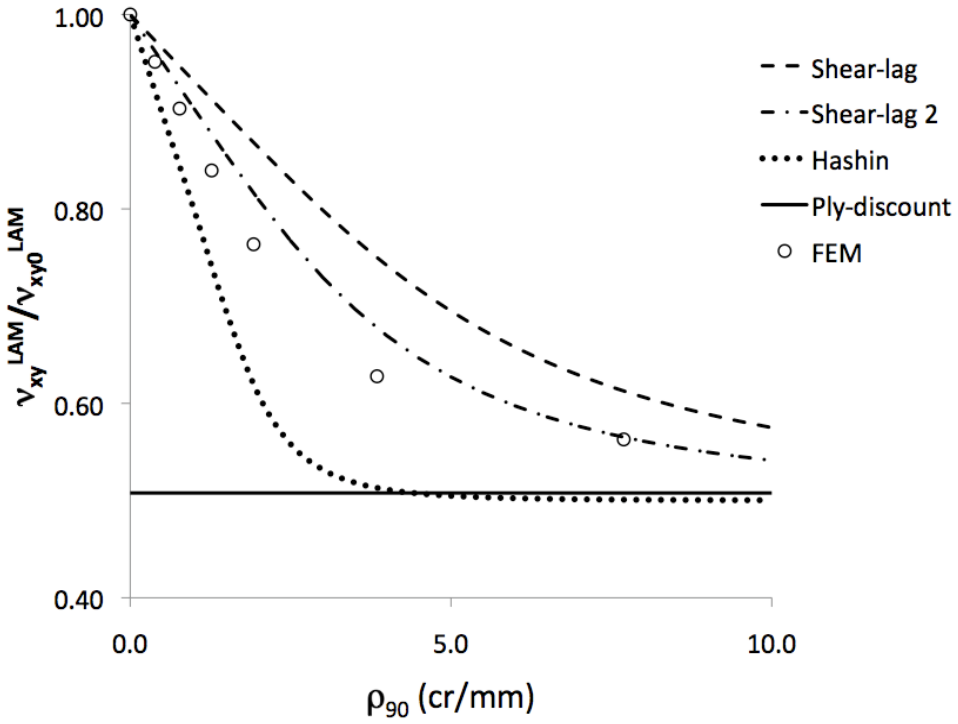

Figure 4.21. Simulations and FEM data showing the change in Poisson's ratio ν_{xy}^{LAM} for CF/EP [0/90]s laminate. "Shear-lag" corresponds to $d_0 = 0.0035\,\text{mm}$, "Shear-lag 2" to $d_0 = 0.007\,\text{mm}$

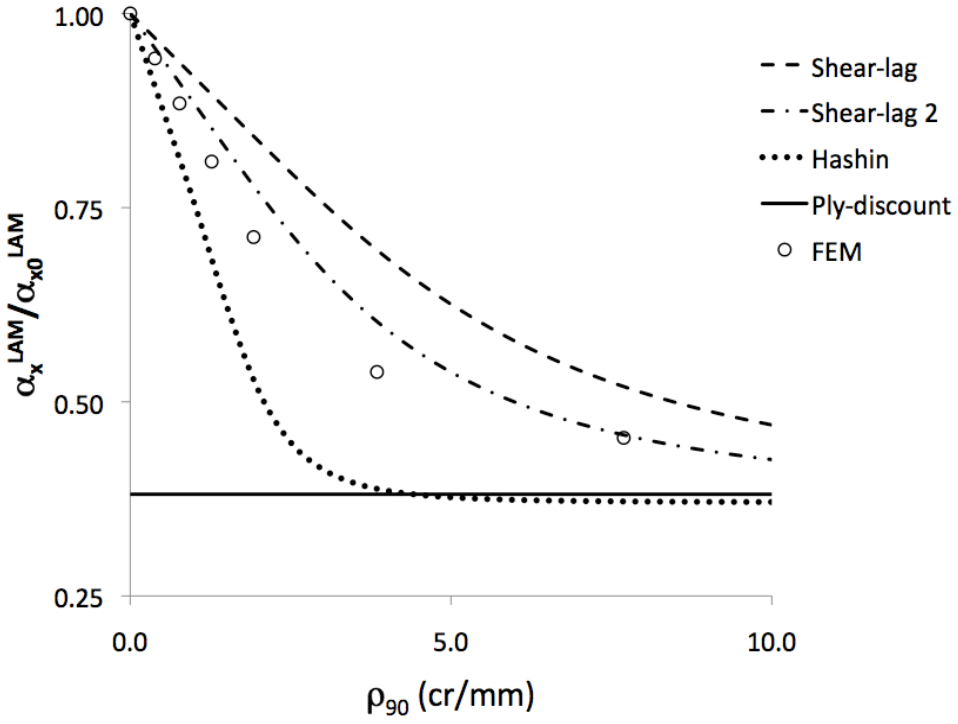

Figure 4.22. Simulations and FEM data showing the change in longitudinal coefficient of thermal expansion α_x^{LAM} of CF/EP [0/90]s laminate. "Shear-lag" corresponds to $d_0 = 0.0035\,\text{mm}$, "shear-lag 2" to $d_0 = 0.007\,\text{mm}$

Unfortunately, the value, which gives the best fit, will be different for different materials and lay-ups. In addition, this value of resin layer thickness in our case has no physical meaning because it is too large (more than one fiber diameter).

Application of the suggested calculation approach to quasi-isotropic laminates is demonstrated in Fig. 4.23 and Fig. 4.24. The material is GF/EP and the 90-layer thickness is the same as for cross-ply laminates analyzed in Fig. 4.17 to Fig. 4.19. The agreement of the shear lag model with FEM results is as good as in case of cross-ply laminates (using the same resin layer thickness). The Hashin's model even in this case strongly overestimates the rate of the reduction.

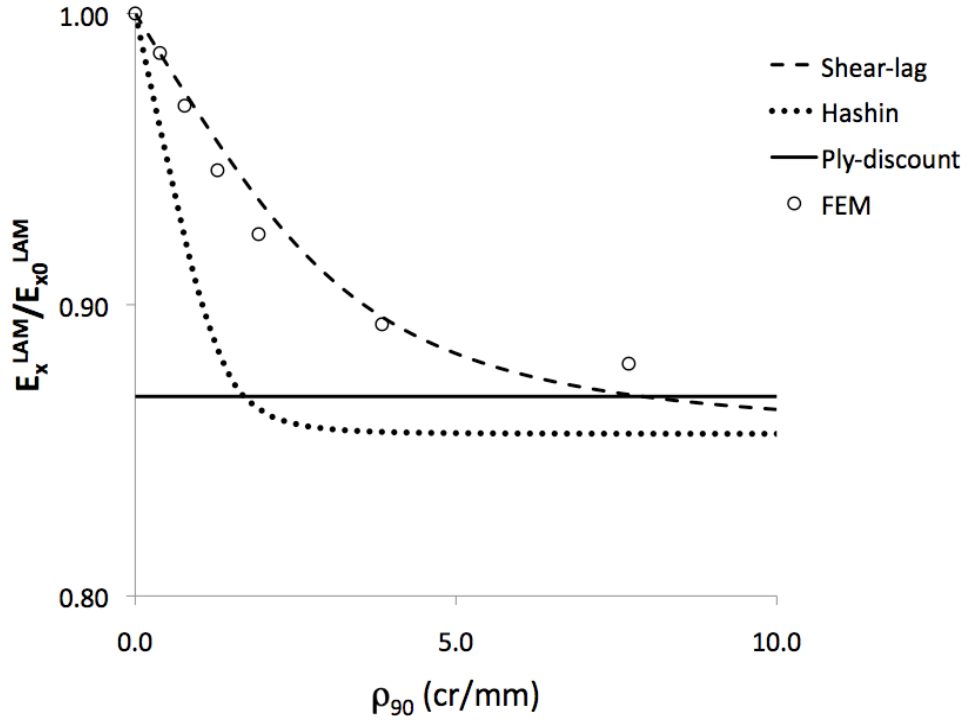

Figure 4.23. Simulations and FEM data showing the change in longitudinal modulus E_x^{LAM} of GF/EP [0/±45/90]s laminate

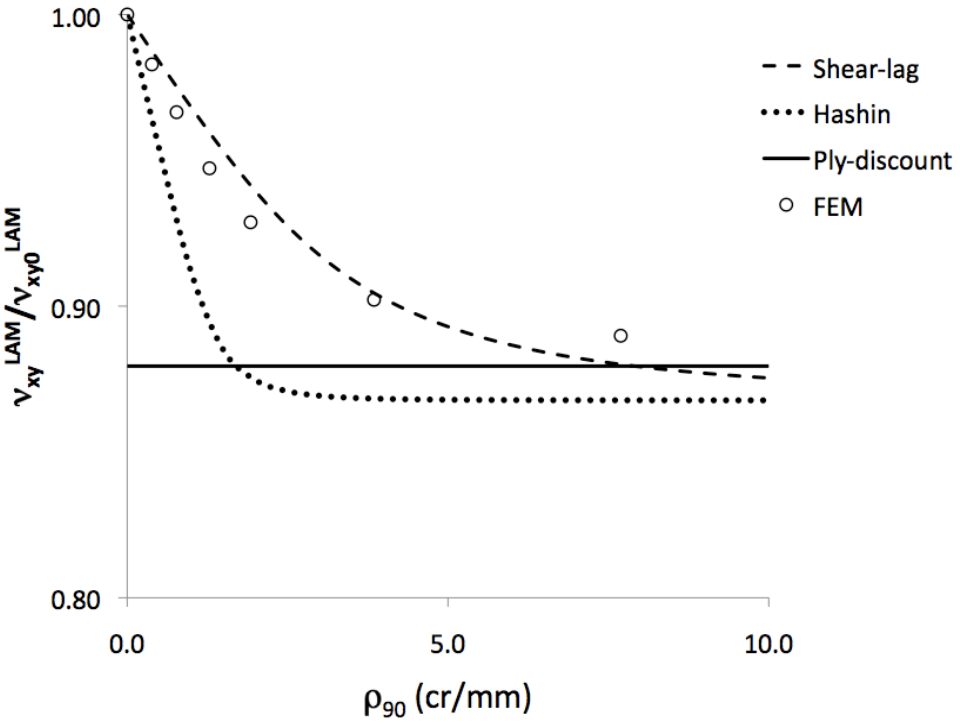

Figure 4.24. Simulations and FEM data showing the change in Poisson's ratio ν_{xy}^{LAM} of GF/EP [0/±45/90]s laminate

4.4.5 Ply-discount model and the asymptotic behavior of stiffness reduction

In this section we will address the observation from all presented figures that both models predict asymptotic values of thermo-elastic properties that are slightly lower than the ply-discount value calculated using CLT. It seems to be theoretically impossible. Nevertheless it is possible because in both analytical models the stress analysis is 2-dimensional, neglecting Poisson's interactions in layers and stress components in the specimen width direction. The used ply discount model was based on use of CLT which accounts for these interactions. In other words the comparison of asymptotic values in the way we did is inconsistent. The ply discount model used to compare asymptotic values should be based on the same assumptions as the stress analysis. In this particular case instead of CLT we should use rule of mixtures (ROM), for example, to calculate degraded laminate axial modulus with ply-discount.

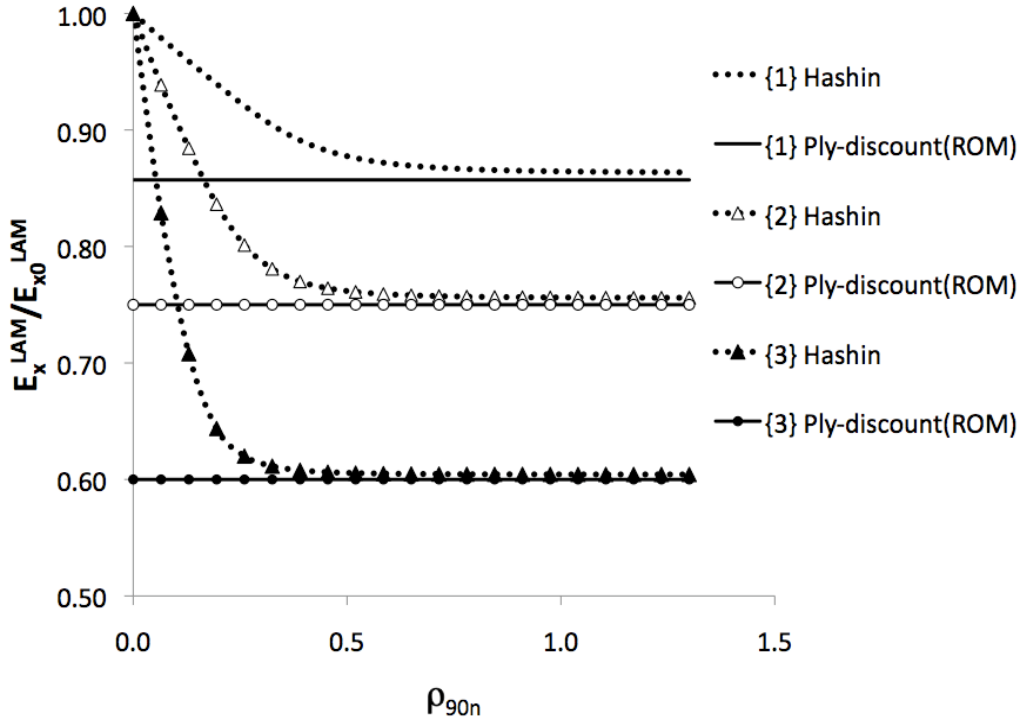

Figure 4.25. Simulation results showing change in the axial modulus of the laminate E_x^{LAM} for GF/EP

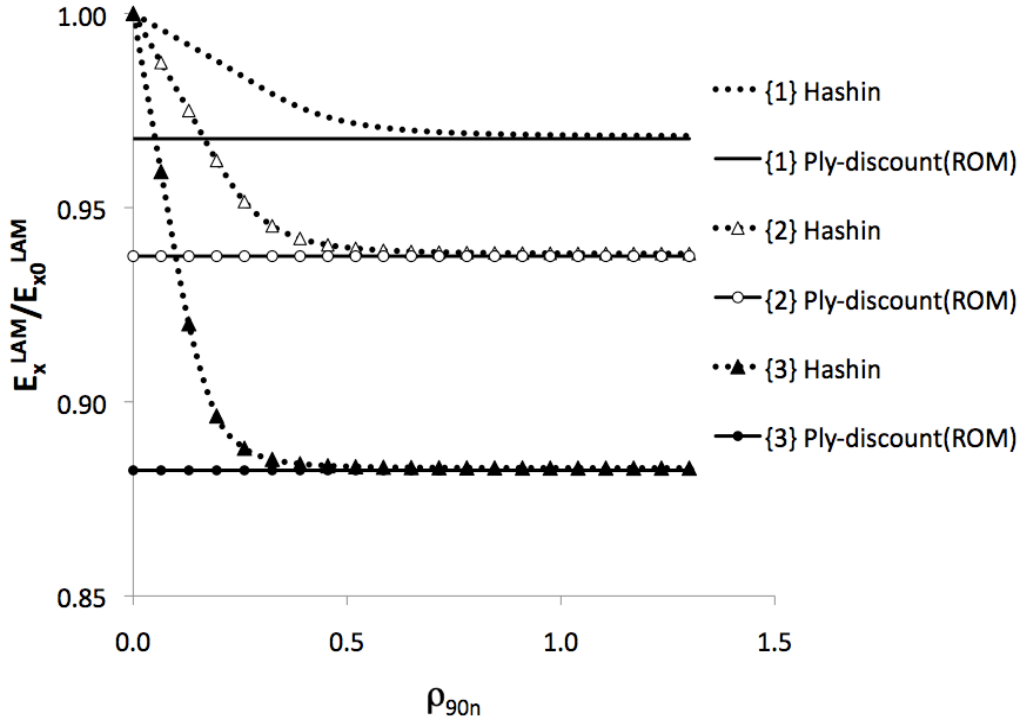

Figure 4.26. Simulation results showing change in the axial modulus of the laminate E_x^{LAM} for CF/EP

The results presented in Fig. 4.25 and Fig. 4.26 show that the asymptotic values coincide with the ply-discount values based on rule of mixture analysis (instead of CLT).

This result explains the observed discrepancies but it does not mean that the rule of mixtures based ply-discount value is more accurate than the CLT based.

4.5. Conclusions

Methodology has been developed for approximate evaluation of all thermo-elastic constants of general symmetric laminates with cracked 90-layers. It is based on use of stress solutions from shear lag and Hashin's models in a general framework where laminate macroscopic properties are expressed through average stress perturbation between two cracks. This methodology has been validated with FEM and experimental data.

As expected all predicted curves approach to the ply-discount model predictions which assume almost zero transverse and shear properties of the damaged layer.

The predictions of the Hashin's model are always conservative but may be close to experimental data if the layer is relatively thick and local delaminations occur.

Comparing the shear lag model with FEM the accuracy of axial modulus determination is the same as the accuracy of thermal expansion coefficients. The shape function of the elastic property reduction from shear lag model can give a good agreement to FEM results if the shear lag parameter (thickness of the resin layer in our case) is used as a fitting parameter. For given material and lay-up all properties can be fitted with the same value of the parameter. It applies even for quasi-isotropic laminates if the ply thickness is the same.

Chapter 5

Damage Characterization in Glass Fiber/Epoxy laminates using Electronic Speckle Pattern Interferometry

5.1. Introduction

Composite materials have found usage in many industrial applications and more recently they are increasingly being used in aerospace panels and airframes. The use of fiber composites in the aerospace industry is justified by their excellent specific modulus and strength (referred to the property divided by the density).

When cross-ply laminates are subjected to mechanical loading, different failure mechanisms are induced (see Fig. 1.4): transverse matrix cracking in 90° plies, delamination between 0° and 90° plies, and fiber fracture in 0° plies. In the case of uniaxial loading, the early stage of damage is transverse (intralaminar) matrix cracking in 90° plies. The transverse cracks develop in the fiber direction and extend across the laminates from the free edges of the specimen. The analysis of transverse cracking is important since cracking reduces the stiffness and strength of laminates. Transverse cracks induce local stress concentrations at crack tips and can initiate significant interlaminar delamination between 0° and 90° plies. Fiber fracture in 0° plies is induced only at high loads in the case of monotonic loading or for large cycle number in the case of fatigue loading.

The degradation of the elastic properties of composite laminates is caused by reduced average axial stress between two cracks in the damaged layer which is mainly due to two parameters: the crack face opening displacement (COD) and the crack face sliding displacement (CSD). Thus at fixed applied load the average axial stress in the layer with cracks is reduced and the remaining undamaged layers have to take an additional load,

leading to larger axial strain in these layers. Larger axial strain at the same macroscopic load means that the laminate modulus due to cracking is reduced. Similar reasoning explains the Poisson's ratio reduction of the damaged laminate: reduced average axial stress in the damaged layer leads to smaller amount of the Poisson's transverse strain which makes the transverse contraction strain of the whole laminate smaller.

Many theoretical analytical and numerical models have been developed to calculate the reduced stiffness [28,29,34,38]. All of them are based on idealized assumptions, for example, assuming linear elastic material behavior even in high stress concentration region at crack tip as well as linearity in shear loading and assuming idealized geometry of these cracks which would not change during the service life [40].

In a linear model these quantities are proportional to the applied load and, therefore, the COD and CSD should be normalized to be used in stiffness modeling. The effect of material properties on the normalized COD was studied experimentally using optical microscopy of loaded damaged specimens in [2,34]. It was shown that the measured COD profiles and average values are affected by the constraining layer orientation and stiffness.

To establish the link between the damaged laminate thermo-elastic constants and the microdamage parameters (COD and CSD) a theoretical framework was developed in [28,29]. It was shown that the details of the relative displacement profile along the crack surface are not important: only the average values of these quantities enter the stiffness expressions directly.

The effect of geometrical parameters and properties of the surrounding layers on the COD and CSD was studied using FEM in [28,29]. Analysis revealed that only two parameters are of importance for the normalized average COD and CSD: the modulus ratio of the cracked and the support layers in direction transverse to the crack and the

ratio of their thickness. Based on this analysis simple empirical relationships (power laws) were suggested.

The COD and CSD dependence on crack density was analyzed theoretically in [18] and studied using FEM in [38]. It was shown that if the crack density is high the stress perturbations of two neighboring cracks interact and the average stress between cracks at the given applied load is lower. It means that the COD and CSD of interacting cracks are smaller than for non-interactive cracks.

All these studies and analyses assume a linear elastic material with idealized geometry of cracks. The only correct way to validate these assumptions is through experiments. To study experimentally the COD and the CSD, the full-field measurement technique Electronic Speckle Pattern Interferometry (ESPI) [36,37] was used in this work.

The main objectives of the present study are to visualize the displacement field on the edge of a [0, $+70_4$, -70_4]s Glass Fiber/Epoxy (GF/EP) laminate specimen with multiple transverse cracks and to analyze the crack face displacement dependence on the applied mechanical load. Using the displacement map, it is possible to obtain the displacement profiles along the tensile-axis. The different profiles drawn along the specimen edge at several distances from the mid-plane correspond to the different plies. By studying the displacement discontinuities, we can measure the crack face displacements corresponding to the cracks in the measurement field. A comparison between the COD and the CSD (for the same crack) is given in this chapter.

5.2. Experimental technique and material

5.2.1 Experimental technique: ESPI

The principle of ESPI is based on the interference of two coherent laser beams: reference beam and observation beam. For in-plane measurement, the surface is illuminated by a coherent beam and the surface roughness causes multiple phase differences that create random interference. Hence, a Charge Coupled Device CCD

camera sensor collects a randomly distributed light intensity called speckle. Then, the first resulting speckle interferogram is transferred to a computer, and saved in memory. If a point of the surface is subjected to a displacement, the local speckle pattern undergoes the same displacement. The intensity of each speckle grain is also likely to vary because of the phase difference created by the displacement. Then the speckle interferogram is changed. This second interferogram is subtracted pixel by pixel from the first one. The result is rectified and displayed as a set of bright and dark fringes, known as correlation fringes, which constitute a contour map of the displacement of the object surface (see Fig. 5.1).

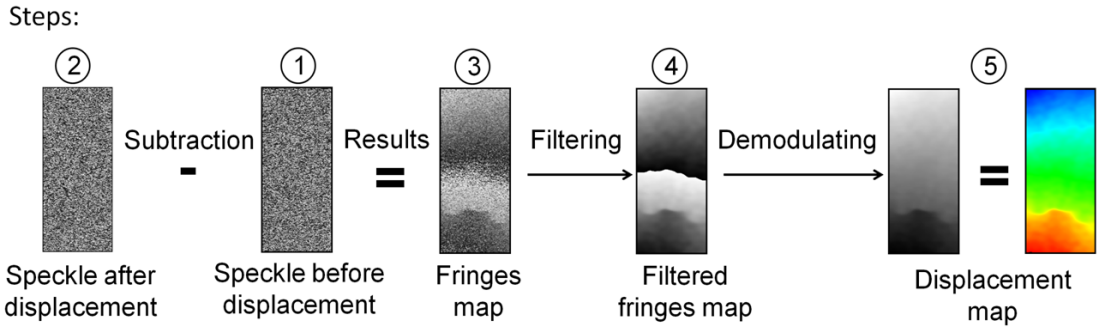

Figure 5.1. Necessary steps to measure the displacement using ESPI.

In our case, the surface is illuminated by two coherent beams that form the same angle θ with respect to the normal studied surface, so the corresponding speckle patterns also interfere. Fig. 5.2 shows a schematic setup for the in-plane deformation measurement by ESPI.

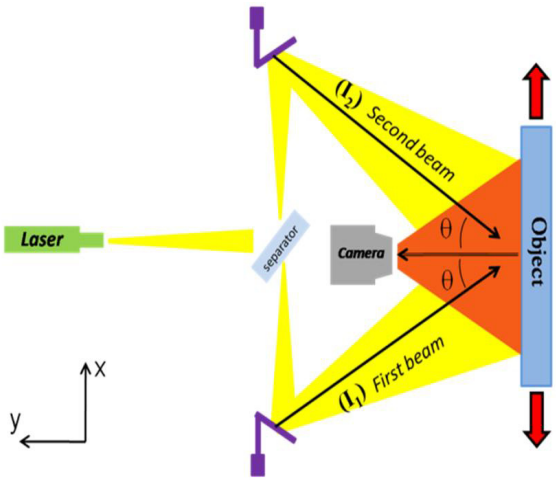

Figure 5.2. Schematic of ESPI setup

The resulting light intensity is given by [53]

$$I = I_0(x,z) + I_M(x,z)\cos\left(\phi(x,z)\right) \tag{5.1}$$

I_0, I_M and ϕ are respectively the background intensity, the modulation intensity and the phase, which is a random number directly linked to the speckle pattern of each beam.

In order to implement the phase-shifting technique [54,55], a piezoelectric device is used to introduce a $\pi/2$ phase shift in one of the two beams. The intensity images I_0, I_1, I_2, I_3 and I_4 corresponding to phase shifts of respectively $0, \pi/2, \pi, 3\pi/2$ and 2π are recorded so that the phase maps can be calculated using the following equation corresponding to the five-frame algorithm:

$$\phi = \tan^{-1}\left(\frac{2(I_3 - I_1)}{I_4 + I_0 - 2I_2}\right) \tag{5.2}$$

$U(x,z)$ is the relative displacement along the x-axis corresponding to a passage from an initial loading state to a final loading state. $U(x,z)$ is proportional to $\Delta\phi$ the phase difference between these two states:

$$\Delta\phi = \phi_{final} - \phi_{initial} = \frac{\left(4\pi \sin(\theta) U(x,z)\right)}{\lambda} \tag{5.3}$$

where θ is the incidence angle of the illumination beams, λ is the wavelength of the applied laser, in our case $\theta = 45°$ and the laser wavelength $\lambda = 638nm$.

The recordings of the phase maps for the initial and the final states lead to the relative displacement $U(x,z)$ at each point of the specimen surface. This displacement map corresponds to a $\Delta\sigma$ increase of the average stress applied to the specimen. The cracks naturally correspond to discontinuities of the phase difference at the crack locations [56] and lead to displacement jumps on displacement profiles.

ESPI can provide full-field deformation information of different materials with a very high-precision. However it has a very high sensitivity, which corresponds to a fraction of the laser wavelength, in our case we expected about 15 nm as sensitivity [36]. Hence, the results can be easily influenced by external factors such as noise and vibration. For that reason tests should be carried out in relatively quiet circumstances. Excessive displacement can be a source of de-correlation [54].

5.2.2 Material

The [0, 70_4,-70_4]s laminate (see the geometrical details in Fig. 5.3) was made of glass fiber/epoxy using vacuum bag technique. The thickness of the laminate is 2.75 mm.

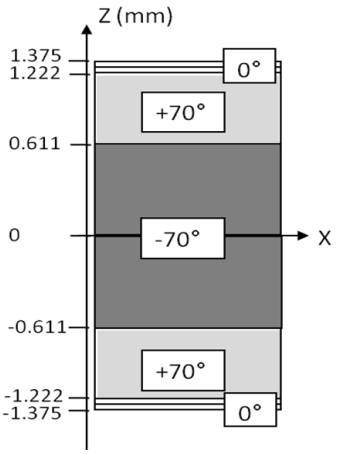

Figure 5.3. Schematic view of the [0,70_4,-70_4]s laminate lay-up. (Z-axis is in the thickness direction)

The elastic properties obtained in tests on unidirectional and angle-ply composite specimens are, see [2]:

Longitudinal modulus E_1(GPa) = 44.7

Transverse modulus E_2(GPa) = 12.7

Poisson's ratio ν_{12} = 0.297

In-plane shear modulus G_{12}(GPa) = 5.8

Thermal expansion coefficient $\alpha_T - \alpha_L = 10 \times 10^{-6} / °C$

Specimens of 20 mm width were reinforced with GF/EP end tabs in the gripping area.

A free length between tabs was 110 mm. The tensile loading to introduce damage in form of microcracks was applied using an INSTRON tensile testing machine with displacement rate of 3 mm/min. Cracks initiate first in the -70 layer, which is two times thicker than the +70 layer and propagate through the whole width of the specimen. At higher applied stresses, cracks appear in the +70 layer. The presence of these cracks (in +70 layer) affect the opening displacement of the large cracks in the -70 layer.

5.3. Results

5.3.1 Normalized relative displacement measurement

The specimen edge is illuminated by two beams which come from the same laser that has $\lambda = 0.638 \mu m$ as wavelength. These beams illuminate the object at equal but opposite angles $\pm\theta$ to the surface normal (see Fig. 5.4). Using this method of illumination, the measurement direction is in the x-axis direction which is the tensile-axis.

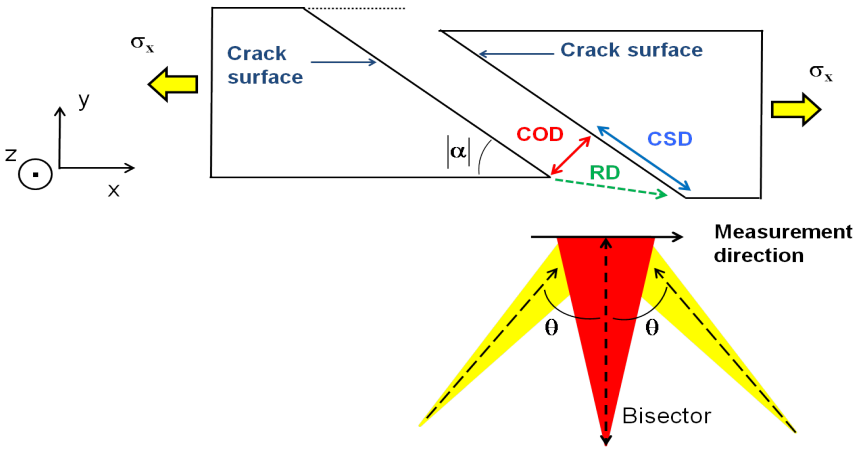

Figure 5.4. Symmetric illumination

The digitization of the $10mm \times 10mm$ image is performed at 512×512 pixels, thus the pixel size is $d = 19.5 \mu m$. To get the displacement map, the image corresponding to the phase difference was averaged using a $[11 \times 11]$ filter kernel.

Fig. 5.5 shows the X-displacement profile in the central ply (-70°) when the cracks were first initiated. The displacement discontinuities caused by the cracks are clearly visible.

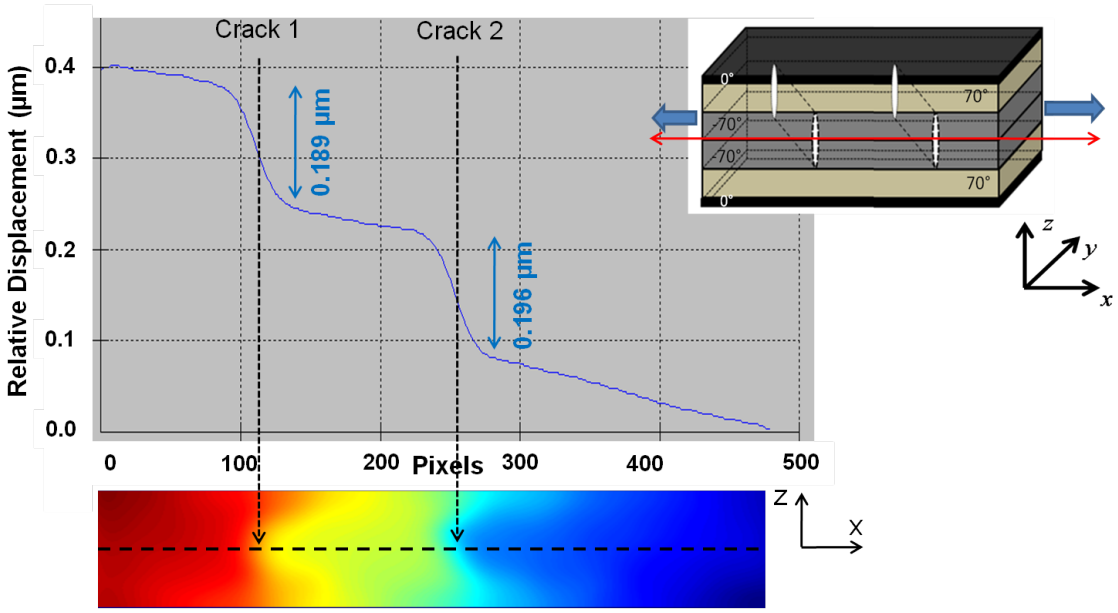

Figure 5.5. Profile of the relative displacement along the mid-plane (on the specimen edge) corresponding to a variation of the relative average stress $\Delta\sigma = 0.497 MPa$

These displacement jumps indicate the presence of two cracks in the region of study. The displacement slope (strain) is smaller in the area at the vicinity of the crack surfaces. It certainly results from the boundary condition with traction free crack surfaces. Just before and after a displacement jumps, we detected small regions where the displacement slope (strain) has a minimum. We have calculated the displacement jumps by evaluating the displacement difference between these regions of low strain.

Because of the 70° fiber orientation, the crack displacement discontinuity measured on the edge is not directly COD and neither the CSD. It is a projection of both these displacements on the specimen edge plane (Fig. 5.4). By definition, the crack opening displacement (COD) is transverse to the fiber direction and the sliding displacement (CSD) is in the fiber direction. The displacement jump is defined as a relative displacement (RD) which is related to the COD and the CSD by this relationship:

$$RD_x = COD \times \sin|\alpha| + CSD \times \cos|\alpha| \qquad (5.4)$$

where α is the fiber orientation of the damaged studied plies.

The displacement gap observed on the edge corresponds to a certain change in the applied average stress $\Delta\sigma$. In other words $\Delta\sigma$ is the increase of the average stress applied to the sample ($\Delta\sigma = \sigma_{final} - \sigma_{initial}$). Hence, the presented displacement data correspond to this load change.

In order to perform comparative analysis for several applied load levels the relative displacement (RD) has to be normalized with respect to the relative average stress $\Delta\sigma$. Thus, the results presented in the following for the normalized relative displacement (RD_n) correspond to 1 MPa of the applied stress to the laminate, where the lower index n is used to indicate the normalized values.

For an average stress increase from 27.01MPa to 27.51MPa a $0.189\mu m$ and $0.196\mu m$ relative crack face displacement was measured for the first and the second crack, respectively. It corresponds to $RD_{1n} = 0.380\mu m/MPa$ and $RD_{2n} = 0.394\mu m/MPa$ for the normalized relative displacement at the averaged applied stress $\sigma_{av} = \frac{27.01 + 27.51}{2} = 27.26MPa$.

It is also possible to estimate the displacement measurement resolution by evaluating the measurement noise. The physical quantity that is initially measured is the phase difference $\Delta\phi$.

The displacement is thereafter obtained using equation (5.3). We have calculated $\Delta\phi_{raw} - \phi_{f11}$: subtraction between the raw phase difference and the phase difference smoothed using a $[11\times11]$ pixels filtering kernel. This calculation was performed for 150 pixels randomly selected in the measurement field but far from the cracks. In these regions, the displacement jumps are outside the filtering kernel and the displacement variations are slow. The filtering being rather strong, it can then be considered that the subtraction corresponds essentially to the noise that affects $\Delta\phi_{raw}$.

For our 150 pixels sample, we have found that the standard deviation of the noise is: $S_{\Delta\phi raw} = 0.62 rad$. Using equation (5.3), it is then possible to estimate the standard deviation of the noise that affects the displacement measurement if no filtering is used: $S_U = 0.044 \mu m$. If the data is smoothed using a $[n \times n]$ filtering kernel, the standard deviation is divided by n [57]. For n = 11 pixels, we finally obtain $S_U^{11} = 0.004 \mu m$. A displacement jump is obtained by subtracting two displacement values corresponding to the two crack faces. The standard deviation of the error on the relative crack face displacement is then: $S_{RD} = \sqrt{2} \times 0.004 = 0.0057 \mu m$

Using the displacement map, the displacement profiles were drawn (not shown) along the tensile-axis at two different distances from the mid-plane (in the middle of +70° and 0° layers). Two cracks were detected on the edge of the +70° layer very close the cracks in the -70° layer. The normalized relative displacement of these cracks which run along fibers in the +70° layer was smaller than those in -70° layer and interface delamination between both crack systems was observed. It is not clear at present whether the delamination is only at the edge where the stress state due to intersection of two cracks and the edge is very complex, or it covers larger zone inside the material.

For 0° layer, the displacement profile does not show any displacement jumps, which means there are no cracks in this layer at this applied stress level.

The separation of the values of the COD and the CSD is explained in the following section.

5.3.2 Normalized crack opening displacement

The object is illuminated by two beams. To measure directly the COD, theses two beams have to illuminate the object at equal and opposite angles to the fiber direction axis, which means the bisector of the angle between the first and the second beam has to

be in the same direction as fibers of the studied layer (Fig. 5.6). In this case, the measurement direction is transverse to the fiber direction. Hence, using this method of illumination, we can measure directly the COD.

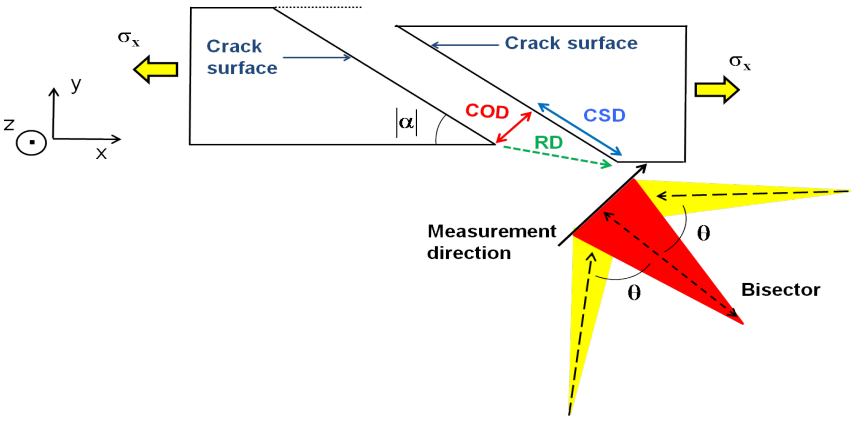

Figure 5.6. Non symmetric illumination

Fig. 5.7 shows the profile of the displacement transverse to the fibers in the central ply (-70°). For an average stress increase from 27.00 MPa to 27.53MPa a 0.160µm and 0.166µm crack face opening displacement was measured for the first and the second crack, respectively. It corresponds to $COD_n = 0.300\mu m / MPa$ and $COD_n = 0.311\mu m / MPa$.

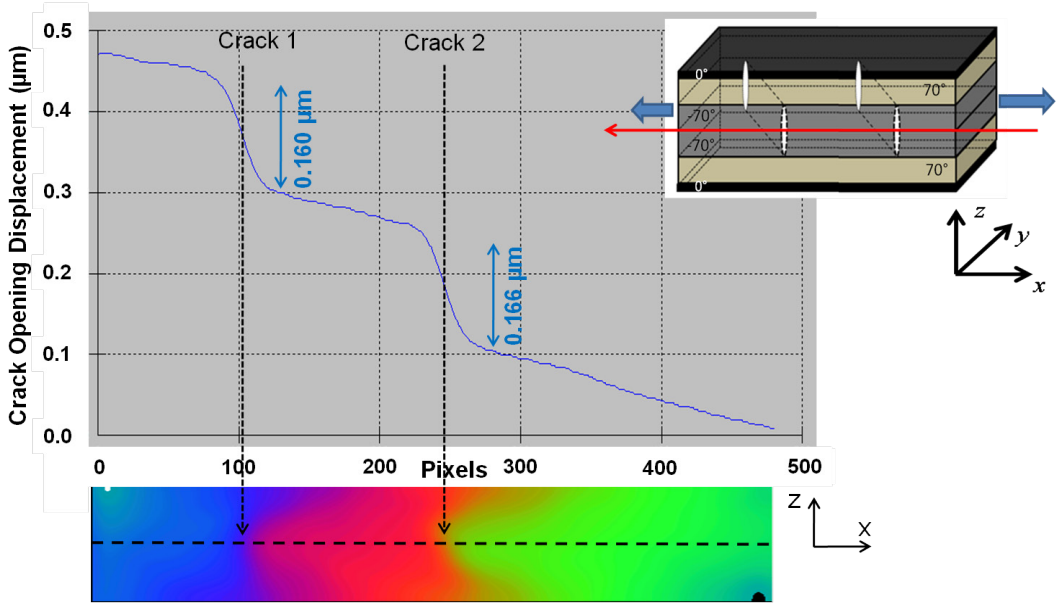

Figure 5.7. Profile of the displacement transverse to the fiber direction along the mid-plane (on the specimen edge) corresponding to a variation of the relative average stress $\Delta\sigma = 0.533MPa$

For the same crack, we measured the normalized relative displacement RD_n and the normalized crack opening displacement COD_n separately, and then we deduced the normalized crack sliding displacement CSD_n using equation (5.4).

All results are presented in this following table.

Table 5.1. A comparison between the COD and the CSD

	RD_n (μm/MPa)	COD_n (μm/MPa)	CSD_n (μm/MPa)	**COD/CSD**
Crack 1	0.380	0.300	0.286	**1.049**
Crack 2	0.394	0.311	0.297	**1.047**

For the analyzed GF/EP laminate, Table 5.1 shows that the COD is slightly larger than the CSD. The experimental data presented in Table 5.1 are valuable for evaluating adequacy of models for thermo-elastic properties degradation of multidirectional laminates with cracks [18,38]. In these models the COD and the CSD have been calculated assuming linear elastic material behavior even in the high stress concentration regions at crack tips where as well known the shear response could be very nonlinear and permanent strains could be introduced or interface delamination could take place. Idealized geometry of these cracks (straight cracks, perpendicular to the midplane, covering the whole layer thickness) is assumed which would not change during the service life. Real cracks are often “bridged” by fiber bundles oriented almost parallel to the crack plane. It is expected that their effect on COD is marginal whereas the crack face sliding could be affected more.

Using ESPI, we are performing measurements on the edge of the sample, for this reason the results can be affected by the edge effect. Even in an absence of damage the stress state at the specimen edge is 3-Dimensional [58]. Apart from the edge region the stress state follows the laminate theory and only in-plane stresses are active. In the specimen edge region out-of-plane stresses may be very high due to differences in thermal

expansion coefficients and Poisson's contraction. Therefore, the specimen edge region can be more and differently damaged than the interior part. Even if not (as checked in our study), the axial stresses in the edge region are slightly higher and crack face displacements may be larger. It has to be stressed that material models for damaged laminates are developed for the representative volume element and not for a specimen. Therefore, in this context all differences in behavior caused by edge effects should be considered as artifacts and their influence estimated and minimized. It is not clear whether the edge effect on COD and CSD is similar. Detailed numerical stress state analysis using finite element method is planed to decide how representative the edge measurements are.

In this investigation cracks are treated as non-interactive. The term non-interactive is used in the sense that the average normalized COD and CSD are not affected by the presence of other cracks in this layer. This may be true in our study with respect to other cracks in the same layer but it does not apply with respect to cracks in neighboring layer, where in the edge region cracks were very close to the cracks investigated in this chapter. Therefore in future a) care should be taken to minimize this interaction when significance of each individual crack is analyzed; b) the possible effects of interaction between different systems of cracks for most typical cases should be analyzed numerically.

5.4. Conclusions

The displacement field on the edge of a $[0/ +70_4/ -70_4]_s$ glass fiber/epoxy laminate specimens with two intralaminar cracks is studied and the crack face opening displacement (COD) and the crack face sliding displacement (CSD) change with the applied mechanical load is measured.

The presented results prove that Electronic Speckle Pattern Interferometry ESPI can be used to measure directly the crack opening displacement and deduce the crack sliding displacement. A comparison between these two parameters shows that the COD for this laminate is slightly bigger than the CSD.

The COD and the CSD depend on the materials properties and layer orientation and thickness which mean that the ratio (COD/CSD) varies dependent on laminate lay-up and therefore more studies on laminates with different lay-ups and material properties are required.

The measurement of COD and CSD at low and high crack density is planned to investigate the interaction effects at high crack density.

Chapter 6

Experimental and numerical analysis of the Crack Opening Displacement profile in damaged cross-ply laminates

6.1. Introduction

The final macroscopic failure of composite laminate is preceded by initiation and evolution of several microdamage modes. On the microscale, the failure can be in the matrix, at the fiber/matrix interface or fibers can fail. On the mesoscale, the first mode of damage is usually intralaminar cracking in layers with off-axis orientation regarding the main load component. These cracks run parallel to fibers in the layer with the crack plane being transverse to the laminate midplane. Intralaminar cracks do not usually cause the final failure of a laminate, but may significantly impair the effective properties of the laminate and serve as a source for other damage modes initiation, such as delamination and microcracking in the adjacent plies.

The degradation of the elastic properties of composite laminates is caused by overload on the undamaged layers resulting from reduced average axial stress between two cracks in the damaged layer. The reduction of the average stress is due to the crack face opening displacement (COD) and the crack face sliding displacement (CSD). In other words, the elastic modulus in the loading direction and the corresponding Poisson's ratio decrease.

The link between the damaged laminate thermo-elastic properties and the microdamage parameters (COD and CSD) was established theoretically in [28,29]. It was shown that

the details of the relative displacement profile along the crack surface are not important: only the average values of these quantities enter the stiffness expressions directly.

The effect of material properties on the normalized COD was studied experimentally using optical microscopy of loaded damaged specimens in [2,34]. It was shown that the measured COD profiles and average values are affected by the constraining layer orientation and stiffness. Experimental determination of the average COD and CSD needs the measurement of the displacement for all points of the crack surfaces, which justifies the use of full-field measurement technique Electronic Speckle Pattern Interferometry (ESPI). ESPI is an optical technique that provides the displacement for every point on a surface and offers the possibility to measure both, the in-plane and out-of-plane displacement without surface preparation [35].

This technique was used in [36,37] to measure the COD for cracks in internal layers on the specimen's edge. It was shown that the profile of the crack on the edge is very close to elliptical.

In a linear elastic model these quantities are proportional to the applied load and, therefore, the COD and CSD should be normalized to be used in stiffness modeling. Finite element method (FEM) studies were performed to understand which material and geometry parameters affect the COD and CSD in [18,28,29] and simple empirical relationships (power laws) were suggested. The effect of crack density (number of cracks per unit length) on the COD and CSD was analyzed in [18] and studied using FEM in [38,59]. It was shown that if the crack density is high the stress perturbations of two neighboring cracks interact and the average stress between cracks at the given applied load is lower. It means that the COD and CSD of interacting cracks are smaller than for non-interactive cracks.

The analytical and numerical models for laminate stiffness reduction [2,28,29,38,40] are based on idealized assumptions, for example, assuming linear elastic material behavior even in high stress concentration region at crack tip as well as linearity in shear loading and assuming idealized geometry of these cracks which would not change during the service life (delta cracks and small local delaminations at crack tip are neglected). The only correct way to validate these assumptions is through experiments.

The main objective of this chapter is to study intralaminar cracks in surface layers by measuring the COD variation along the crack path. For this reason the cross-ply laminate with surface cracks was selected.

In particular, the displacement field on the surface of a $[90/0]_s$ and $[90_3/0]_s$ carbon fiber/epoxy specimens with multiple intralaminar cracks in the surface layer is studied and the relative displacement dependence on the applied mechanical load is measured.

By looking to the displacement field the cracks appear as singularities and the corresponding displacement jumps are directly related to COD and CSD. In axially loaded cross-ply laminate the relative sliding displacement of the intralaminar crack faces is zero and the measured displacement discontinuity on the surface corresponds to COD.

To investigate the COD profile from surface to the crack tip, measurements were performed also on the edge of the specimen. To evaluate the significance of edge effects, the COD profile as dependent on the distance from specimen edge was measured. To explain the discrepancies between measured and calculated values the interaction in terms of COD between cracks in the same layer and cracks belonging to the other surface layer were analyzed. Theoretical studies for two extreme cases have been reported previously: a) nonuniform crack distribution but assuming that the damage is symmetric with respect to the midplane [40,60]; b) staggered crack

distribution in surface layers keeping periodicity [43]. In the present work FEM was used to simulate the real crack distribution in the specimen. The results are compared with experimental COD values obtained in this work and the significance of the unsymmetric damage distribution is analyzed.

6.2. Experimental technique and materials

6.2.1 ESPI measurements

The principle of ESPI is based on the interference of two coherent laser beams: reference beam and observation beam. For in-plane measurement, the surface is illuminated by a coherent beam and the surface roughness causes multiple phase differences that create random interference. Hence, a Charge Coupled Device CCD camera sensor collects a randomly distributed light intensity called speckle. Then, the first resulting speckle interferogram is transferred to a computer, and saved in memory. If a point of the surface is subjected to a displacement, the local speckle pattern undergoes the same displacement. The intensity of each speckle grain is also likely to vary because of the phase difference created by the displacement. Then the speckle interferogram is changed. This second interferogram is subtracted pixel by pixel from the first one. The result is rectified and displayed as a set of bright and dark fringes, known as correlation fringes, which constitute a contour map of the displacement of the object surface. In our case, the surface is illuminated by two coherent beams that form the same angle θ with respect to the normal studied surface, so the corresponding speckle patterns also interfere.

More details regarding the implementation of the phase-shifting technique and data reduction are given in [53-55]. In our case the incidence angle of the illumination beams $\theta = 45°$, the wavelength of the applied laser $\lambda = 638nm$.

The recordings of the phase maps for the initial and the final states lead to the relative displacement at each point on the specimen surface. This displacement map corresponds

to a $\Delta\sigma$ increase of the average stress applied to the specimen. The discontinuities of the phase difference naturally correspond to the crack locations and lead to displacement jumps on displacement profiles. ESPI can provide full-field deformation information of different materials with a very high-precision. However it has a very high sensitivity, which corresponds to a fraction of the laser wavelength, in our case we expected about 15 nm as sensitivity [35]. Hence, the results can be easily influenced by external factors such as noise and vibration. For that reason tests should be carried out in relatively quiet circumstances. Excessive displacement can be a source of de-correlation [54].

6.2.2 Materials

Carbon fiber/epoxy $[90/0]_s$ and $[90_3/0]_s$ laminates were used. The elastic properties of the unidirectional composite are the following: one prepreg ply thickness 0.3 mm, longitudinal modulus: E_1 (GPa) = 118, transverse modulus: E_2 (GPa) = 9, Poisson's ratio: $\nu_{12} = 0.3$, shear modulus: G_{12} (GPa) = 3.8.

6.3. Numerical parametric analysis of COD

6.3.1 Determination of COD

The average CSD and COD are defined as

$$u_{1a}^{90} = \frac{1}{2t_{90}} \int_0^{t_{90}} \Delta u_1^{90}(z)\, dz \qquad u_{2a}^{90} = \frac{1}{2t_{90}} \int_0^{t_{90}} \Delta u_2^{90}(z)\, dz \qquad (6.1)$$

Here Δu_i is the displacement gap between corresponding points at both crack faces. Index 1 denotes the displacement in fiber direction (sliding) and index 2 in the transverse direction (opening), z-is the coordinate in the laminate thickness direction with origin at the ply interface, t_{90} is thickness of the 90-layer.

In linear model the displacements u_2^{90} and u_1^{90} are linear functions of the applied average stress and the ply thickness. Therefore, they are normalized with respect to the

far field (CLT) shear stress σ_{xy0}^{90} and transverse stress σ_{x0}^{90} in the 90-layer (resulting from the macro-load $\{\sigma\}_0^{LAM}$ and temperature difference ΔT) and with respect to the thickness of the cracked layer t_{90}

$$u_{1n}^{90} = u_1^{90} \frac{G_{12}}{t_{90}\sigma_{xy0}^{90}} \qquad u_{2n}^{90} = u_2^{90} \frac{E_2}{t_{90}\sigma_{x0}^{90}} \tag{6.2}$$

Elastic constants E_2 and G_{12} of the UD composite are introduced in (6.2) to have dimensionless descriptors. The influence of each crack on thermo-elastic laminate constants is represented by u_{2n}^{90} and u_{1n}^{90}.

6.3.2 FEM analysis

In all calculations the commercial code ABAQUS was used and a 3-D model was created. All plies are considered to be transversely isotropic, and hence the thickness direction related properties are taken as $E_2 = E_3; G_{12} = G_{13}$ and $\nu_{12} = \nu_{13}$. We used $\nu_{23} = 0.4$ and $G_{23} = 3.2GPa$.

In order to mesh volumes, 3D continuum (C3D8) 8-node linear brick elements were used. A very fine mesh was used in each FE model. In the thickness (z) direction the 90° layer and the 0° layer were divided into 100 and 60 elements respectively with refined mesh near the crack surfaces. The number of elements in y-direction was 3 which as described below is more than sufficient for the used edge conditions. Constant displacement corresponding to 1% average strain was applied to the repeating unit in x-direction at x=L, see Fig. 6.1.

On the front edge (y=0) and the far-away edge (y=W) coupling conditions were applied for normal displacements (U_Y= unknown constant). In this way edge effects are eliminated and the solution does not depend on y-coordinate. It corresponds to solution for an infinite structure in the width direction. Obviously these conditions correspond to

generalized plane strain case and the size of the model in the y-direction could be reduced or 2D generalized plane strain elements used instead. For the "Specimen 90-n" model cracks were introduced in their real positions and $U_Z = 0$ was applied on the edge x=L. On the edge x=0, all displacements and rotations were equal to zero. These are clamped edge conditions approximately representing the real tensile test conditions with gripped ends of the specimen.

Modeling the damaged laminate as containing uniform distribution of cracks "Unit cell 90-n" model, with symmetry boundary conditions at x=0 and constant axial displacement applied at x=L was used.

The displacement in x-direction for the nodes at the crack surface was used to calculate the COD. Equation (6.2) was used to calculate (U_{2n}^{-}) the normalized displacement of the '-' face of the crack and (U_{2n}^{+}) the normalized displacement of the '+' face of the crack (see Fig. 6.1).

6.4. Results

6.4.1 [90/0]s CF/EP laminate

6.4.1.1 Positions of intralaminar cracks

A $[90/0]_s$ specimen of 17mm width and 1.2mm thickness was reinforced with glass fiber/epoxy end tabs in the gripping area. A free length between tabs measured 110mm. The sample was loaded in tension to 1% applied strain with displacement rate of 0.5 mm/min in order to introduce damage in form of intralaminar cracks in the 90-layer. With this load 3 cracks were created in the top layer and 4 cracks were created in the bottom layer. The positions of all cracks were given in Fig. 6.1(a). The studied crack is shown with dotted lines.

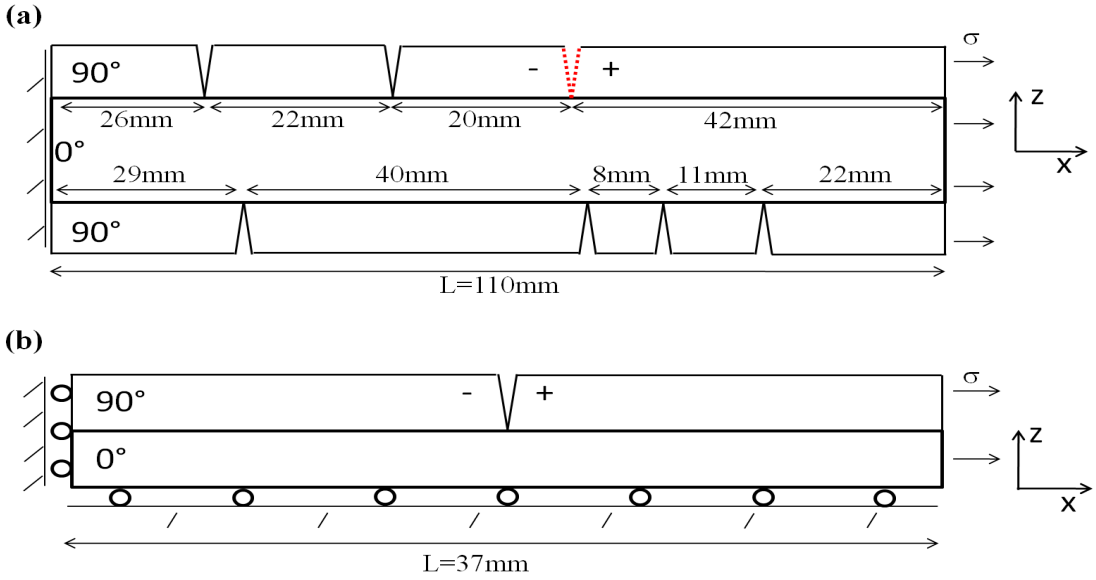

Figure 6.1. Positions of cracks in damaged [90/0]s CF/EP laminate. (a): "Specimen 90-1" model (The crack analyzed in detail is shown with dotted line), (b): "Unit cell 90-1" model used with uniform distribution of cracks

The cracks in the 90° layer were observed using optical microscopy. They appear in surface layers, hence the name "surface cracks". Observing specimen edges the shape of the studied crack was different from one edge to another. For this reason, the COD on each edge was measured separately.

6.4.1.2 COD measurement using ESPI

Fig. 6.2 shows the x-displacement profile in the top (90°) layer at the thickness coordinate $Z_n = 0.8$, ($Z_n = \frac{z}{t_{90}}$ where z is measured from the layer interface) obtained using the ESPI method described in Section 6.2.1. The displacement discontinuities caused by the cracks are clearly visible.

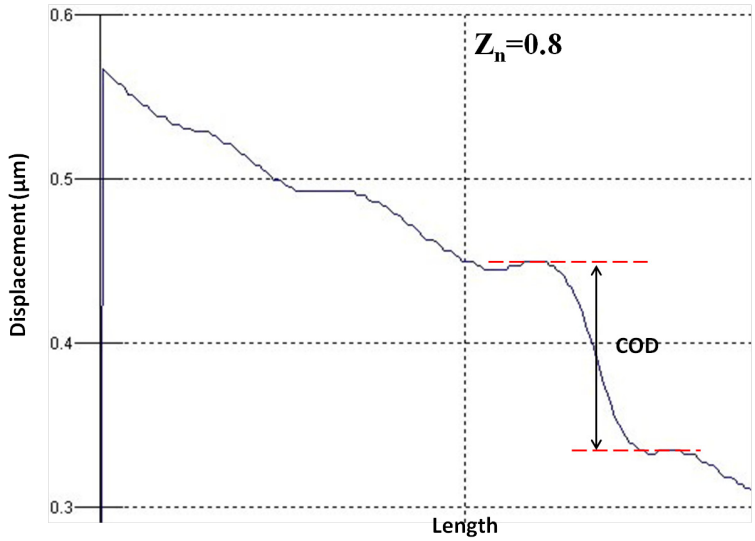

Figure 6.2. Profile of the x-displacement in the top 90° layer of [90/0]s CF/EP laminate on edge y=W at thickness coordinate Z_n=0.8 caused by variation of the relative average stress $\Delta\sigma = 4.65MPa$

In Fig. 6.2, just before and after a displacement jump, we detected small regions where the displacement slope (strain) has a minimum. It certainly results from the boundary condition with traction free crack surfaces. We have measured the displacement jumps by evaluating the displacement difference between these regions of low strain. Because of the 90° fiber orientation, the displacement discontinuity measured on the edge is directly COD (displacement gap between corresponding points on both crack faces).

The displacement gap corresponds to a certain change in the applied average stress $\Delta\sigma$ ($\Delta\sigma = \sigma_{final} - \sigma_{initial}$).In order to perform comparative analysis for several applied load levels the crack opening displacement (COD) has to be normalized using equation (6.2) with respect to the far field (CLT) transverse stress σ_{x0}^{90} in the layer (resulting from the change of the average stress $\Delta\sigma$) and with respect to the thickness of the cracked layer t_{90}.

To investigate the COD´s profile along the thickness coordinate of the damaged 90° layer, the COD of the studied crack was measured at different Z_n values. Fig. 6.3 shows

the x-displacement profile in the top (90°) layer at four different values (Z_n= 0, 0.2, 0.4and 0.6).

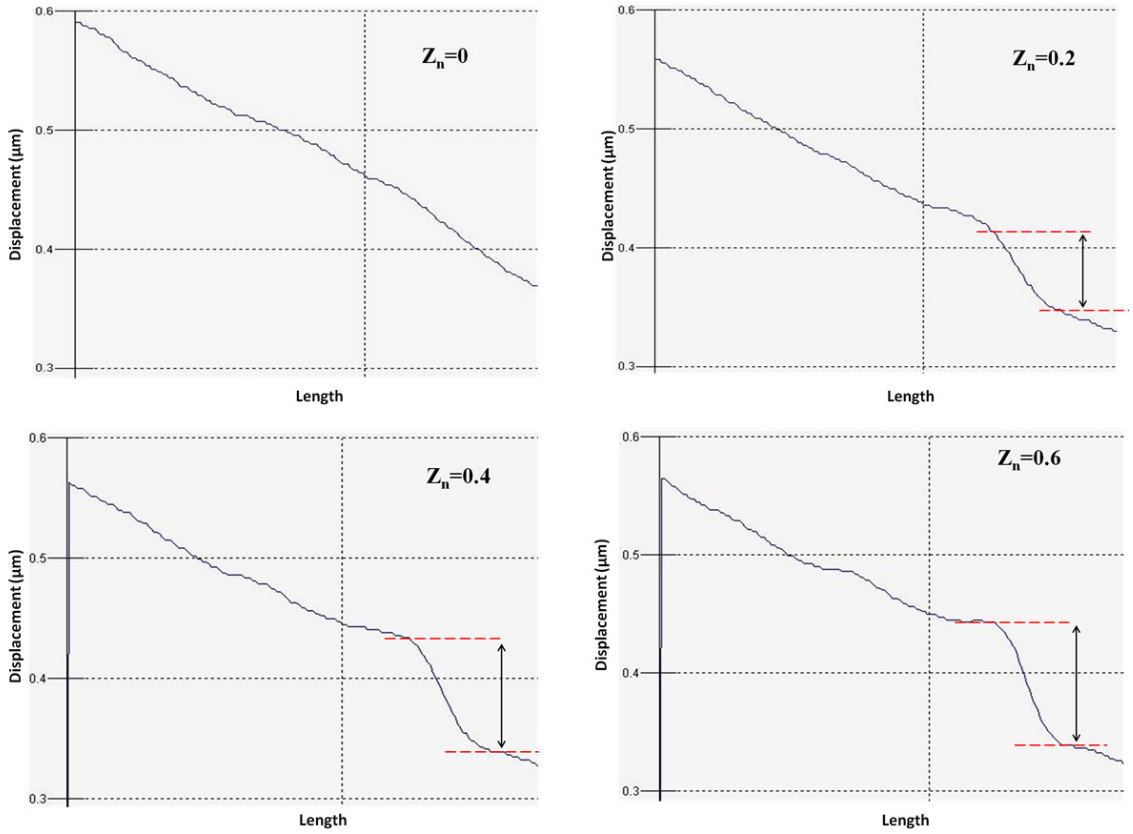

Figure 6.3. Profile of the x-displacement in the top 90° layer of [90/0]s CF/EP laminate at different Z_n on edge y=W. The average stress change $\Delta\sigma = 4.65MPa$

The measured COD is increasing with increase of the thickness coordinate. It varies from 0 (Z_n=0) to 0.0910µm (Z_n=0.6).

It is also possible to estimate the displacement measurement resolution by evaluating the measurement noise, see [36] for details. Calculation was performed for 100 pixels randomly selected in the measurement field but far from the cracks. In these regions, the displacement jumps are outside the filtering kernel and the displacement variations are slow. The standard deviation of the noise that affects the displacement measurement if no filtering is used was estimated: $S_U = 0.023\mu m$. If the data is smoothed using a $[n \times n]$ filtering kernel, the standard deviation is divided by n [57]. For n = 11 pixels, we finally obtain $S_U^{11} = 0.0021\mu m$. A displacement jump is obtained by subtracting two

displacement values corresponding to the two crack faces. The standard deviation of the error on the crack face displacement is then: $S_{COD} = \sqrt{2} \times 0.0021 = 0.0029 \mu m$

The measurement of this standard deviation was obtained for $\Delta\sigma = 4.65 MPa$. Equation (6.2) is used to normalize S_{COD} with respect to the far field (CLT) transverse stress σ_{x0}^{90} in the 90° layer and with respect to the thickness of the cracked layer t_{90}. The normalized standard deviation is $S_{COD}^{n} = 0.1278$.

6.4.1.3 Comparison with FEM for [90/0]s laminate

To compare the experimental results with the numerical results, the COD was calculated using FEM for the two different models described in Section 6.2.1. The "Specimen 90-1" model is shown in Fig. 6.1(a) where all cracks are presented at the real positions. The COD of the studied crack is calculated from this model. The "Unit cell 90-1" model is shown in Fig. 6.1(b) representing uniform crack distribution with the real crack density (3 cracks / 110 mm).

The profile of the normalized crack face displacement $2U_{2n}$ along the thickness coordinate Z_n is shown in Fig. 6.4. The $2U_{2n}$ is sum of the normalized displacement of the '-' face of the crack and the '+' face of the crack as shown in Fig. 6.1 ($2U_{2n} = U_{2n}^{+} + U_{2n}^{-}$).The normalized measured COD which is presented in Fig. 6.4 by squares is the displacement gap between corresponding points at both crack faces. Measurements at each position were repeated 2-3 times with unloading and loading again. There are some differences in measured values but there is no systematic trend regarding to repetition of the test. The agreement between experimental results and "Specimen 90-1" model is very good on both edges of the specimen. In contrary the agreement with the "Unit cell 90-1" model based on uniform crack distribution with average spacing is less good: the model underestimates the COD.

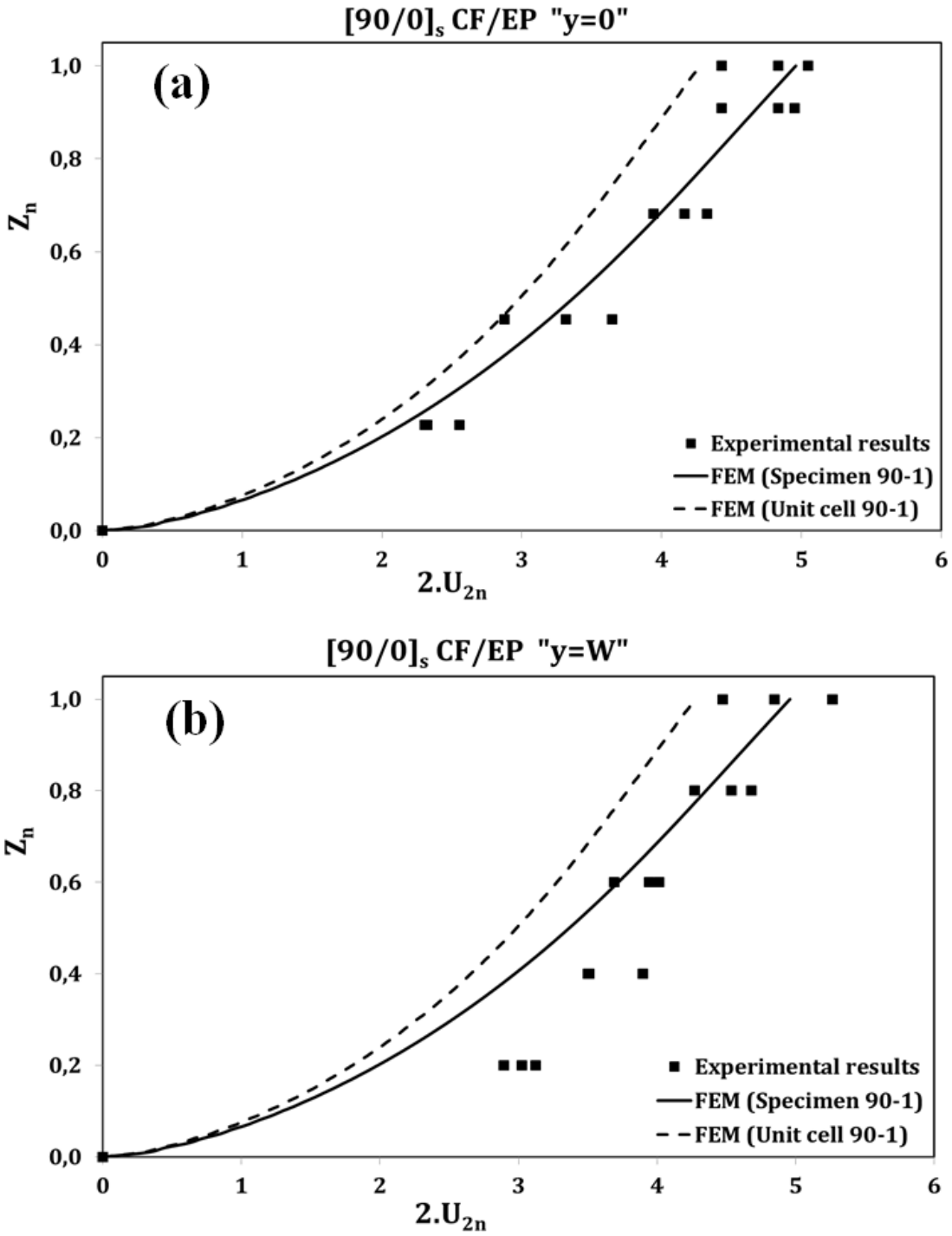

Figure 6.4. Crack opening displacement profiles along the thickness of 90° layer in [90/0]s CF/EP laminates ((a):COD measured on edge y=0 and (b): COD measured on edge y=W)

Fig. 6.5 shows the variation of normalized crack face displacement $2U_{2n}$ along the width coordinate Y_n. ($Y_n = \frac{y}{W/2}$) on the surface of the specimen. In Fig. 6.5 y varies from 0 to W/2.

There is no noticeable edge effect on the COD proving that the edge measurements are representative for the main domain too. FEM results using "Specimen 90-1" model (suppressing edge effects in the analysis) are in good agreement with measurements on the specimen surface. As in Fig. 6.4 the "Unit cell 90-1" model underestimates the COD. Reasons for that will be analyzed in Section 6.4.3.

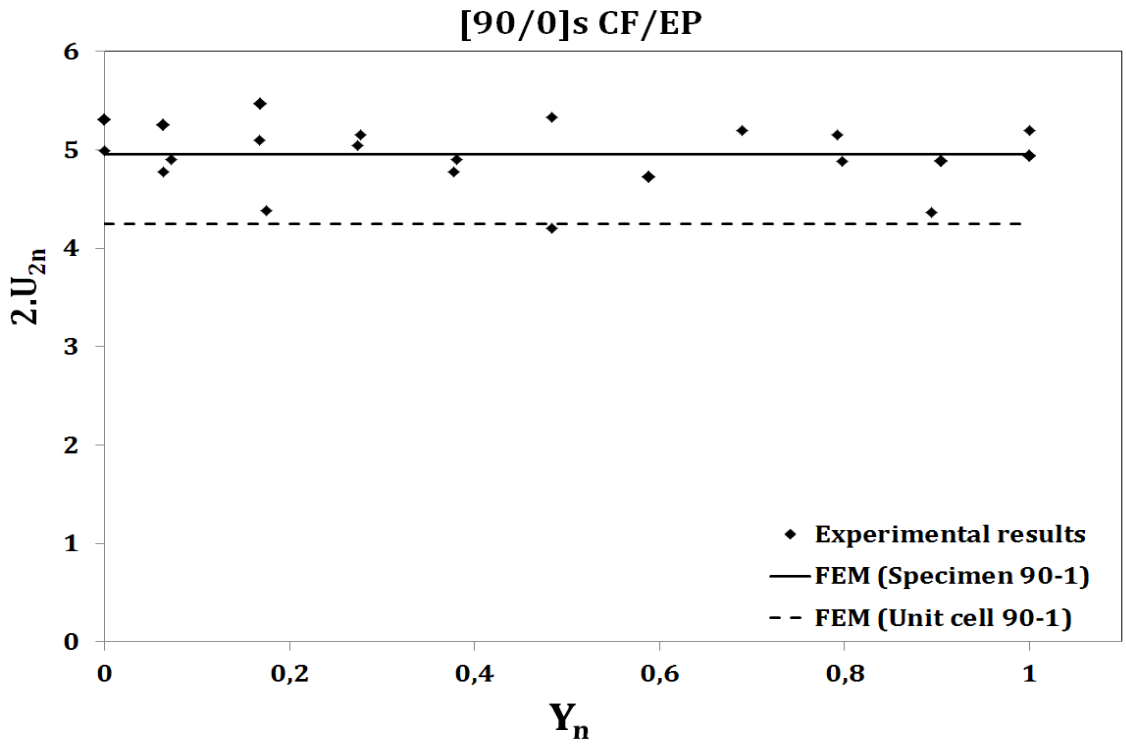

Figure 6.5. Crack opening displacement variation along the width of [90/0]s CF/EP laminates on the surface of the specimen

6.4.2 [90_3/0]s CF/EP laminate

6.4.2.1 Positions of cracks

The $[90_3/0]_s$ specimen of 20mm width and 2.4mm thickness reinforced with glass fiber/epoxy end tabs had 130mm free length between tabs. The sample was loaded in tension to 0.8% applied strain with displacement rate of 0.5 mm/min. With this load 2 cracks were created in the top layer and 2 cracks in the bottom layer. The positions of all cracks are given in Fig. 6.6(a). The studied crack is shown with dotted lines. The shape of the studied crack was different at the two edges of the specimen. For this reason, the COD was studied on each edge separately.

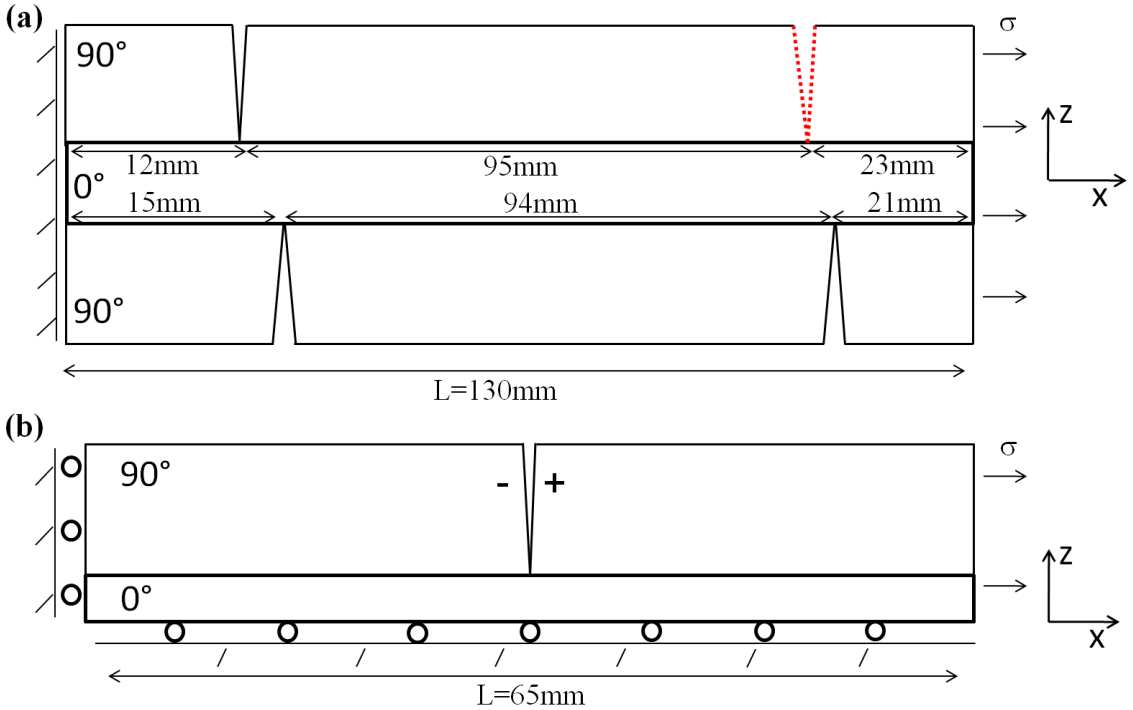

Figure 6.6. Positions of cracks in damaged [90_3/0]s CF/EP laminate. (a): "Specimen 90-3" model in FEM (the crack analyzed in detail is shown with dotted line), (b): "Unit cell 90-3" model used with uniform distribution of cracks

6.4.2.2 COD measurement using ESPI and FEM calculations

The COD measurement routine was described in detail in Sections 6.2.1 and section 6.4.1.2.

To compare the experimental results with the numerical results, the COD was calculated using two different models: "Specimen 90-3" shown in Fig. 6.6(a) and "Unit cell 90-3" shown in Fig. 6.6(b) (uniform crack distribution with the real crack density 2 cracks / 130 mm).

The normalized crack face displacement $2U_{2n}$ is a sum of the normalized displacement of the '-' face and the '+' face of the crack shown in Fig. 6.6 ($2U_{2n} = U_{2n}^{+} + U_{2n}^{-}$). The edge view of $2U_{2n}$ along the thickness coordinate is shown in Fig. 6.7.

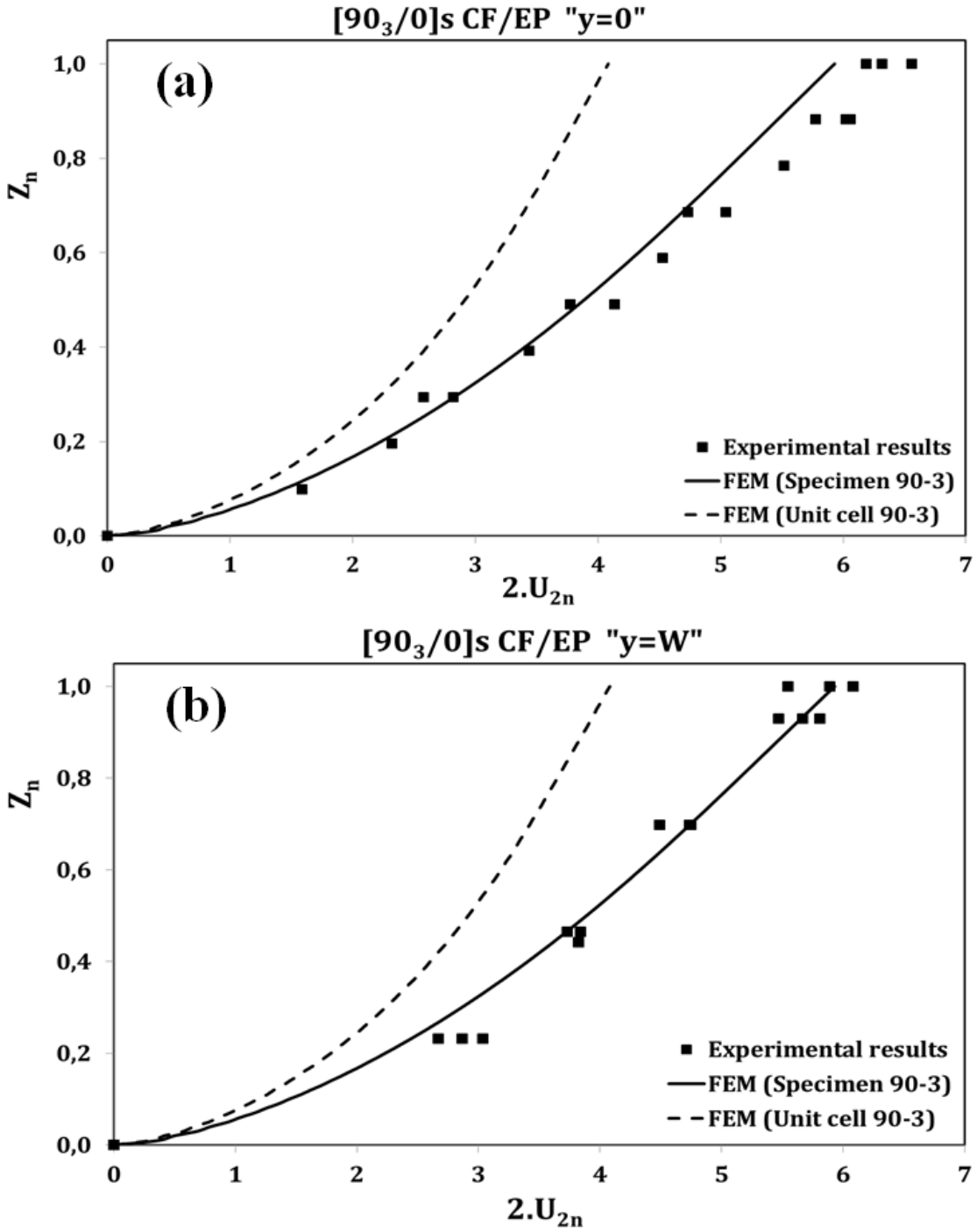

Figure 6.7. Crack opening displacement profiles along the thickness of 90° layer in [90_3/0]s CF/EP laminates ((a):COD measured on edge y=0 and (b): COD measured on edge y=W)

The conclusions are the same as in section 6.4.1.3: a) agreement between experimental results and "Specimen 90-3" model where cracks are in their real positions is very good; b) the "Unit cell 90-3" model significantly underestimates the COD.

Fig. 6.8 shows the profile of normalized crack face displacement $2U_{2n}$ along the width coordinate Y_n, ($Y_n = \frac{y}{W/2}$ where y varies from 0 to W/2). In this figure the COD is slightly larger closer to the edge (the left side) but it cannot be an edge effects. Edge effect (if any) is expected in a much smaller region at specimen edge. Even in this study the model with real crack positions gives much better agreement with measurements than the model based on uniform crack distribution with damage being symmetric with respect to the midplane.

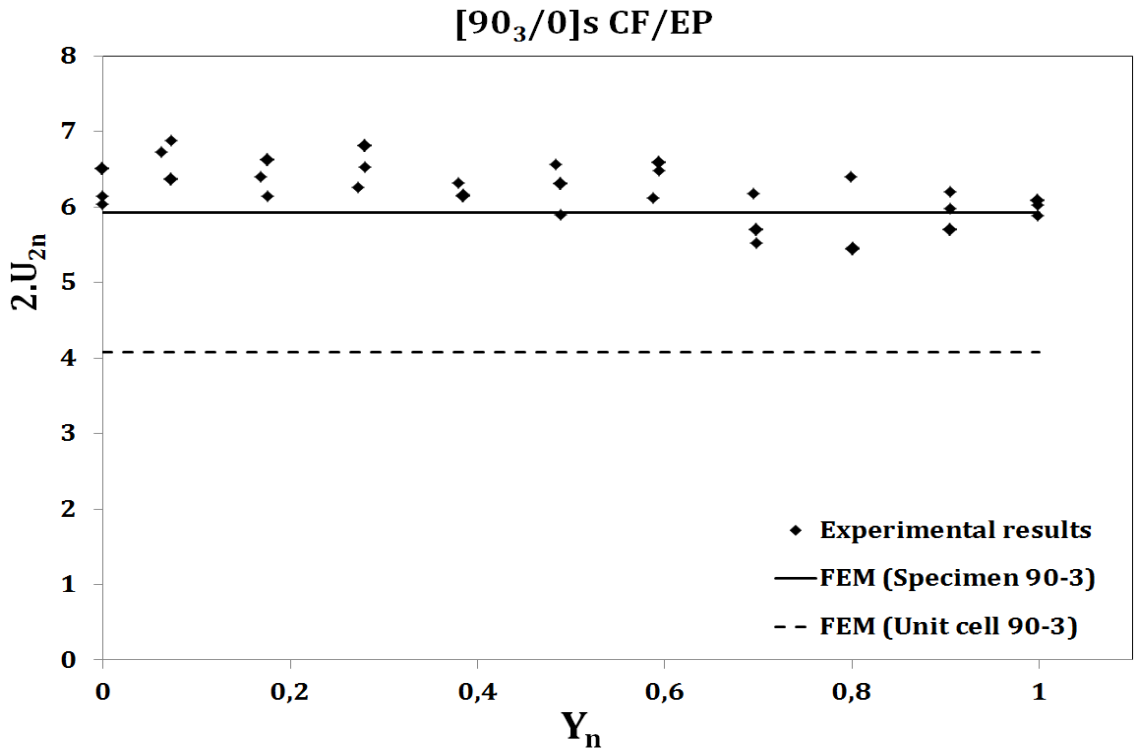

Figure 6.8. Crack opening displacement profiles along the width of [90_3/0]s CF/EP laminates

6.4.3 The effect of the unsymmetrical crack distribution on the axial modulus

Results presented above showed that the measured COD agreed well with COD calculated using models representing the real crack distribution in the specimen and the agreement was not so good comparing with models using uniform crack distribution. Since CODs are governing the elastic modulus reduction, similar effect of crack

distribution is expected on the specimen axial modulus. In this section the interaction effect on modulus is studied by analyzing cross-ply $[90_3/0_n]_s$ n=1,3 laminates made of materials with elastic constants given in Table 6.1. All results are presented for the same crack density (2 cracks/130 mm) in the surface 90-layer. The used four models are shown in Fig. 6.9.

Table 6.1. Materials properties used in simulations

Material	E_1 (GPa)	E_2 (GPa)	ν_{12}	ν_{23}	G_{12} (GPa)	G_{23} (GPa)
CF/EP	118	9	0.3	0.4	3.8	3.2
GF/EP	45	15	0.3	0.4	5	5.36

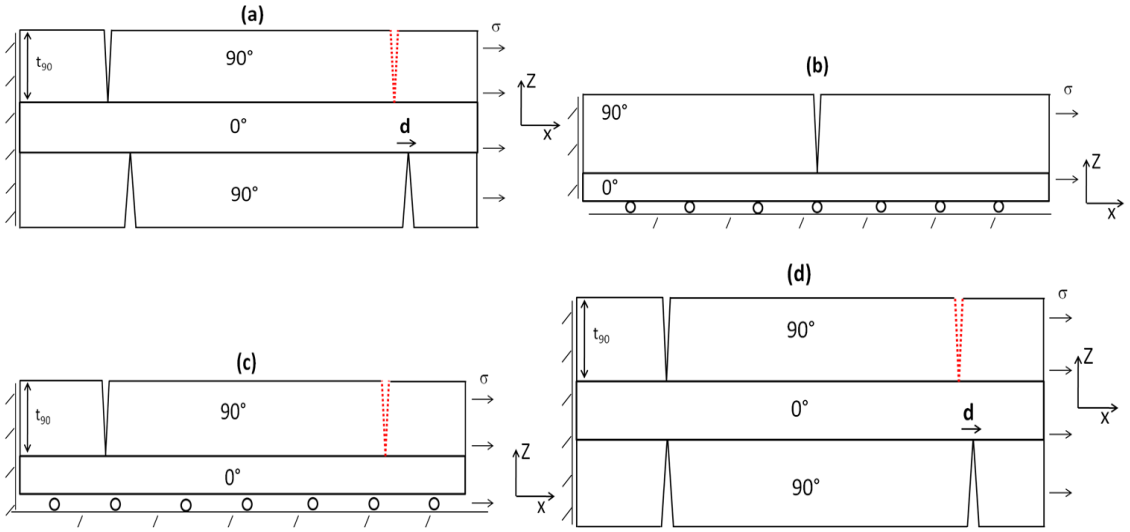

Figure 6.9. Models used to investigate the effect of interaction between cracks on the axial modulus ((a): Model A, (b): Model B, (c): Model C and (d): Model D).

In model A all cracks are in their real positions. Then the shift between the previously studied crack and its neighbor crack in the bottom 90° layer presented by d in Fig. 6.9 is used as a parameter in laminate Young's modulus calculations.

Model B is used to determine the axial modulus of a laminate with symmetric damage with respect to midplane and with uniform crack spacing. This is the most commonly used model.

In Model C, the cracks which are in the top 90° layer are in their real positions with symmetry boundary condition on z=0. This means that damage is symmetric with respect to midplane (no shifts between cracks in the top and bottom layers) but the spacing is not uniform. This model was used in [60] to analyze the effect of the nonuniformity of cracks in one layer.

Finally in model D, the cracks in the top layer are in their real positions. The left crack in the bottom layer is placed symmetrically to the crack in the top layer. The right crack in the bottom layer is shifted by distance d whereas the distance d varies from 0 to 5mm. When d approach to zero this model should give the same result as Model C.

In all cases the normalized axial modulus of the laminate is obtained calculating using FEM the average applied stress and using definition of modulus. The effect of the interaction between cracks on axial modulus of $[90_3/0]s$ and $[90_3/0_3]s$ laminates is shown in Fig. 6.10(a) for CF/EP and in Fig. 6.10(b) for GF/EP.

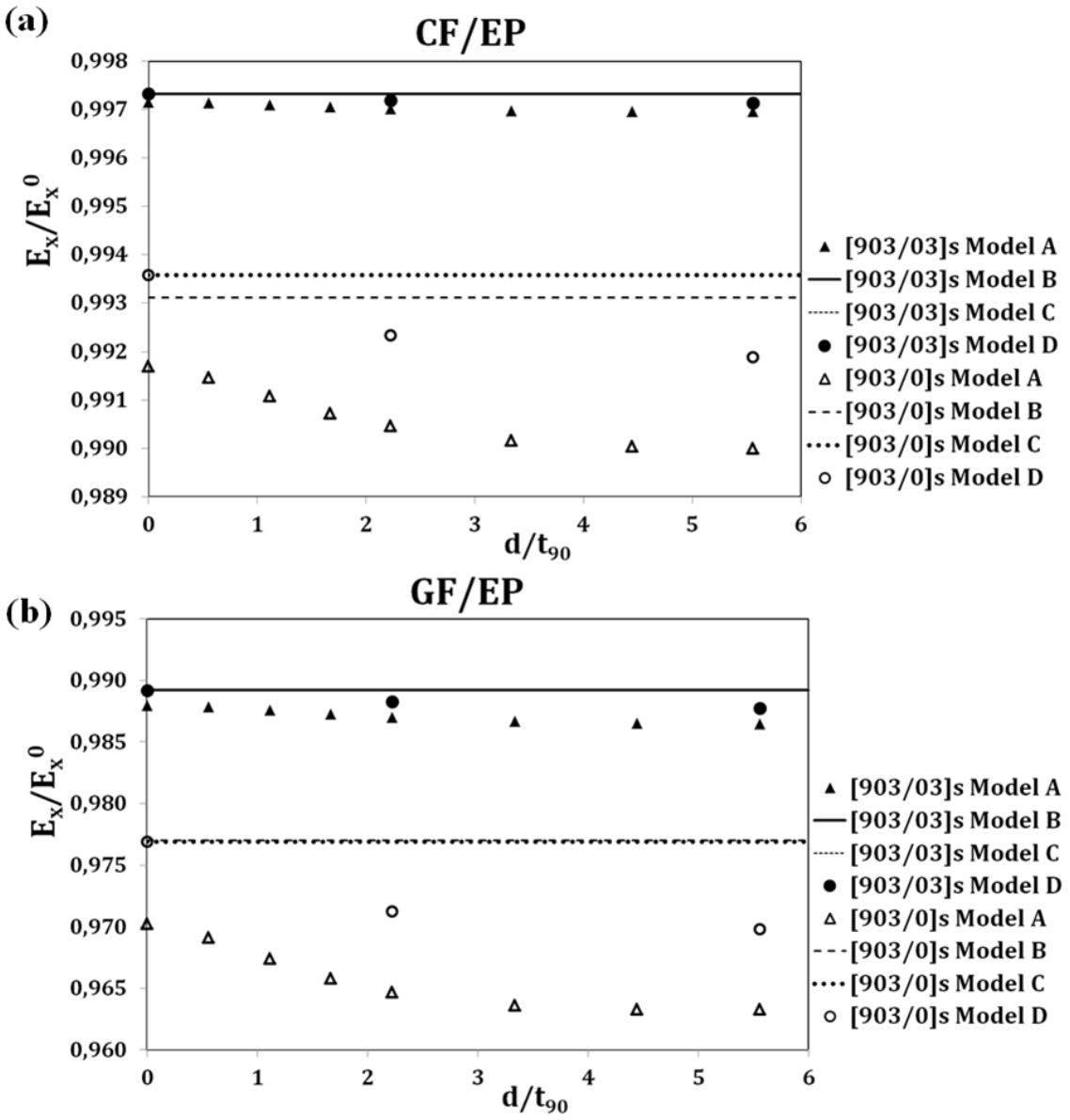

Figure 6.10. Effect of crack interaction on axial modulus of $[90_3/0]$s and $[90_3/0_3]$s laminates. (a): for CF/EP, (b): for GF/EP

Comparing models where the damage is assumed to be symmetric with respect to the specimen midplane (Model B and C) we conclude that assuming uniform crack spacing the modulus reduction is larger. This result agrees with conclusions in [60] where the effects of nonuniform spacing were analyzed. Since the crack density is low the effect of crack spacing nonuniformity in one layer is small. The next question is the effect on modulus of the shift between crack locations in the top and in the bottom layer. Predictions according to model D, where only one crack in the bottom layer is shifted,

show that with increasing shift d the decrease in the specimen modulus is much larger than due to non-uniform spacing in the top layer. Finally, Model A renders the lowest stiffness because the crack in the bottom layer on the left is already shifted and even at $d = 0$ for the crack on the right the specimen modulus is reduced. Further modulus reduction (similar to the one in Model D) is observed with increasing d .

6.5. Conclusions

The crack opening displacements (COD) and the crack density are the main parameters governing the reduction of laminate thermo-elastic properties. To validate the assumptions of linear elasticity and sharp crack geometry the COD of intralaminar cracks in surface 90-layers of cross-ply laminates with two different lay-ups was measured using Electronic Speckle Pattern Interferometry (ESPI) and analyzed using finite element method (FEM).

It was found that the COD measured from the displacement field on the specimen surface does not show any enhancement close to specimen edges proving that the measurements on edges are representative for the bulk of the laminate.

Crack opening profile measurement on specimen edges was performed and the obtained profile compared with calculations according to several FEM models. It was shown that the agreement of CODs is very good if in FEM the whole specimen is modeled with crack positions exactly as in the tested specimen. FEM calculations assuming uniform crack spacing in layers (the same spacing in the top and in the bottom damaged layer) underestimate the COD.

These results prove that linear elastic analysis and straight sharp crack assumption for this material is valid at least for cracks introduced below 1% applied strain.

Since COD is related to the laminate elastic modulus FEM parametric analysis was performed to find the nonuniformity parameters affecting most the modulus. It was

found that asymmetry in the damage with respect to the laminate midplane has larger effect on modulus than the nonuniform crack spacing in one layer. The shift in location between cracks in the top and bottom 90-layer is the dominating parameter.

Chapter 7

Conclusions and perspectives

Intralaminar cracks are the first mode of damage; they can trigger other damage modes and they change thermo-elastic properties of laminates. It has been shown that these phenomena are in a unique way related to transverse crack opening (COD) and sliding (CSD). The presented thesis is aimed to investigate these relationships and parameters affecting them.

The COD of an interactive crack is presented as a product of the COD of non-interactive crack and an interaction function which value is equal or smaller than one. The tanh() form of the interaction function for COD is introduced and parameters determined using data generated by FEM for large variety of geometrical and material parameters considering cracks in surface as well as inside layers. Comparison with direct FEM calculations show that the interaction function gives a very good axial modulus and Poisson's ratio prediction for all possible crack densities and cross-ply laminates. The interaction function derived for cross-ply laminates is adapted for more complex lay-ups and its accuracy is demonstrated for quasi-isotropic laminates.

The COD of non-interactive cracks is calculated directly from FEM. As perspective, a new expression of the COD "new power law" can be investigated for different materials and different lay-ups.

Earlier developed model for elastic properties of damaged symmetric laminates was generalized for case when the intralaminar crack distribution is non-uniform. This model was applied to cross-ply laminates with cracks in 90-layers located in the middle or on the surface. The dependence of the damaged cross-ply laminate axial modulus (it

depends on COD only) on the non-uniformity parameter in a repeating element containing two cracks was analyzed numerically. The non-uniformity parameter is defined as the ratio of the smallest and the average spacing between cracks. COD values needed as an input in the model were calculated using FEM in generalized plane strain formulation and stiffness calculations were performed for GF/EP as well as CF/EP laminates with low and also with high crack density.

An approximate "double-periodic" approach was proposed stating that the COD of a crack with different distances to the closest neighbors can be calculated as the average of two solutions for equidistant cracks. It was shown numerically for cross-ply laminates that in internal layers very accurate COD values for cracks with non-uniform spacing and elastic modulus values can be obtained using this approach. For cracks in surface layers this approach is accurate only for low crack densities. The applicability of the "double-periodic" approach to sliding displacement of non-uniformly distributed cracks has not been investigated.

As perspectives, the dependence of the COD on the non-uniformity parameter can be investigated for more complex lay-ups.

In chapter 4, methodology has been developed for approximate evaluation of all thermo-elastic constants of general symmetric laminates with cracked 90-layers. It is based on use of stress solutions from shear lag and Hashin's models in a general framework where laminate macroscopic properties are expressed through average stress perturbation between two cracks. This methodology has been validated with FEM and experimental data.

As expected all predicted curves approach to the ply-discount model predictions which assume almost zero transverse and shear properties of the damaged layer. The

predictions of the Hashin's model are always conservative but may be close to experimental data if the layer is relatively thick and local delaminations occur.

Comparing the shear lag model with FEM the accuracy of axial modulus determination is the same as the accuracy of thermal expansion coefficients. The shape function of the elastic property reduction from shear lag model can give a good agreement to FEM results if the shear lag parameter (thickness of the resin layer in our case) is used as a fitting parameter. For given material and lay-up all properties can be fitted with the same value of the parameter. It applies even for quasi-isotropic laminates if the ply thickness is the same.

In this part, only transverse cracks in 90-layers are studied. As perspectives, the effect of delamination on the COD and on the degradation of the elastic properties can be investigated using FEM and it can be compared with analytical models (shear lag and Hashin´s models).

In the last chapter of this thesis, the COD of intralaminar cracks in surface 90-layers of cross-ply laminates with two different lay-ups was measured using Electronic Speckle Pattern Interferometry (ESPI) and analyzed using finite element method (FEM).

It was found that the COD measured from the displacement field on the specimen surface does not show any enhancement close to specimen edges proving that the measurements on edges are representative for the bulk of the laminate.

Crack opening profile measurement on specimen edges was performed and the obtained profile compared with calculations according to several FEM models. It was shown that the agreement of CODs is very good if in FEM the whole specimen is modeled with crack positions exactly as in the tested specimen. FEM calculations assuming uniform crack spacing in layers (the same spacing in the top and in the bottom damaged layer)

underestimate the COD. These results prove that linear elastic analysis and straight sharp crack assumption for this material is valid at least for cracks introduced below 1% applied strain. Since COD is related to the laminate elastic modulus FEM parametric analysis was performed to find the nonuniformity parameters affecting most the modulus. It was found that asymmetry in the damage with respect to the laminate midplane has larger effect on modulus than the nonuniform crack spacing in one layer. The shift in location between cracks in the top and bottom 90-layer is the dominating parameter.

Using ESPI, the COD is measured for transverse cracks on the edge of the sample. As perspectives, the effect of delamination on the COD can be studied experimentally and some measurements using tomography can be done to investigate the COD inside the sample.

Appendix

Appendix 1. Homogenized stiffness of damaged laminate in global coordinates

Using divergence theorem it is easy to show [45] that for stress states that satisfy equilibrium equations the average stress applied to external boundary is equal to volume averaged stress. This statement is correct under assumption that stresses at internal boundaries (cracks) are zero. For laminated composites with applied average stress $\{\sigma_0\}^{LAM}$ this equality can be written as

$$\{\sigma_0\}^{LAM} = \{\overline{\sigma}\}^a = \sum_{k=1}^{N} \{\overline{\sigma}\}_k^a \frac{t_k}{h} \tag{A1.1}$$

In (A1.1) the volume average is calculated expressing the integral over the laminate volume as a sum of volume integrals over N layers. Upper index a is used to indicate volume averages. Using Hook's law and averaging it over a layer we have for averages the same form as for arbitrary point

$$\begin{Bmatrix} \sigma_x^a \\ \sigma_y^a \\ \sigma_{xy}^a \end{Bmatrix}_k = [\overline{Q}]_k \begin{Bmatrix} \varepsilon_x^a \\ \varepsilon_y^a \\ \gamma_{xy}^a \end{Bmatrix}_k \tag{A1.2}$$

Substituting (A1.2) in (A1.1) and using the relationship between volume averaged strain in a layer and the displacements applied to external and internal boundaries [45,46]

$$\begin{Bmatrix} \varepsilon_x^a \\ \varepsilon_y^a \\ \gamma_{xy}^a \end{Bmatrix}_k = \begin{Bmatrix} \varepsilon_x \\ \varepsilon_y \\ \gamma_{xy} \end{Bmatrix}^{LAM} + \begin{Bmatrix} \beta_x \\ \beta_y \\ 2\beta_{xy} \end{Bmatrix}_k \tag{A1.3}$$

we obtain

$$\begin{Bmatrix} \sigma_{x0} \\ \sigma_{y0} \\ \sigma_{xy0} \end{Bmatrix}^{LAM} = [Q]_0^{LAM} \begin{Bmatrix} \varepsilon_x \\ \varepsilon_y \\ \gamma_{xy} \end{Bmatrix}^{LAM} + \sum_{k=1}^{N} [\overline{Q}]_k \frac{t_k}{h} \begin{Bmatrix} \beta_x \\ \beta_y \\ 2\beta_{xy} \end{Bmatrix}_k \tag{A1.4}$$

In (A1.4) $\{\overline{\beta}\}$ is the Vakulenko-Kachanov tensor [46] written in Voigt notation. In Cartesian coordinates

$$\beta_{ij} = \frac{1}{V}\int_{S_c}\frac{1}{2}\left(u_i n_j + u_j n_i\right)dS \tag{A1.5}$$

Integration in (A1.5) involves the total crack surface S_c in the layer, u_i are displacements of the points on the crack surface, n_i is outer normal to the crack surface, V is the volume of the layer. Obviously (A1.5) represents the effect on stiffness of the crack face displacements (opening and sliding). Since β_{ij} and strain are tensors for both of them we have the same transformation expressions between local and global coordinates

$$\{\overline{\beta}\}_k = [T]_k^T \{\beta\}_k \tag{A1.6}$$

Expression for $\{\beta\}_k$ in local coordinates is given by (A2.9) in Appendix 2

The laminate theory stress $\{\sigma_0\}_k$ in the k-th layer in local coordinates can be expressed through the applied laminate stress as follows

$$\{\sigma_0\}_k = [T]_k \begin{Bmatrix}\sigma_{x0}\\ \sigma_{y0}\\ \sigma_{xy0}\end{Bmatrix}_k = [T]_k [\overline{Q}]_k \begin{Bmatrix}\varepsilon_{x0}\\ \varepsilon_{y0}\\ \gamma_{xy0}\end{Bmatrix}^{LAM} = [T]_k [\overline{Q}]_k [S]_0^{LAM} \begin{Bmatrix}\sigma_{x0}\\ \sigma_{y0}\\ \sigma_{xy0}\end{Bmatrix}^{LAM} \tag{A1.7}$$

Substituting (A2.9) with (A1.7) in (A1.6) and further in (A1.4) we obtain after arranging the result in form (3.5), the form of stiffness matrix of the damaged laminate given by (3.6).

Appendix 2 Incorporation of COD and CSD in Valulenko-Kachanov tensor in local coordinates

We consider a representative Volume Element (RVE) of a layer with M cracks. Schematic picture of a non-uniform crack distribution with varying spacing between cracks, l_m, m=0,1,2…M is shown in Fig. 1. Index denoting k-th layer is omitted to simplify explanation. The cracked layer is considered in its local coordinates with indexes 1, 2 and 3 corresponding to longitudinal, transverse and thickness directions. For transverse cracks the coordinates of the normal vector to the two faces of crack surface are

$$n_1 = n_3 = 0 \qquad n_2 = \pm 1 \qquad \text{(A2.1)}$$

If the crack density is high the stress perturbation zones of individual cracks overlap and the crack face displacements depend on the distance between cracks. Using the definition (A1.5) for β_{ij} we see that the matrix contains only two non-zero elements: β_{12} and β_{22}

$$\beta_{22} = \frac{1}{Lt}\sum_{m=1}^{M}\int_{-t/2}^{+t/2}\left[u_2^{m+}(z) - u_2^{m-}(z)\right]dz, \quad \beta_{12} = \frac{1}{Lt}\sum_{m=1}^{M}\int_{-t/2}^{+t/2}\frac{1}{2}\left[u_1^{m+}(z) - u_1^{m-}(z)\right]dz \qquad \text{(A2.2)}$$

In (A2.2) t is the cracked layer thickness, $u_1^m(z)$ and $u_2^m(z)$ are sliding and opening displacements of the m-th crack, symbol + or – denotes the particular crack face according to Fig. 1.

As in previous papers for uniform crack distribution [28,29] we introduce also here normalized opening and sliding displacements of crack faces (σ_{20} and σ_{120} are CLT stresses)

$$u_{1n} = u_1\frac{G_{12}}{t\sigma_{120}} \qquad u_{2n} = u_2\frac{E_2}{t\sigma_{20}} \qquad \text{(A2.3)}$$

Introducing average values of displacements of each crack surface over ply thickness

$$u_{1a}^{m+} = -\frac{1}{t}\int_{-t/2}^{+t/2} u_1^{m+}(z)dz\,, \qquad u_{1a}^{m-} = \frac{1}{t}\int_{-t/2}^{+t/2} u_1^{m-}(z)dz\,,$$

$$u_{2a}^{m+} = -\frac{1}{t}\int_{-t/2}^{+t/2} u_2^{m+}(z)dz\,, \qquad u_{2a}^{m-} = \frac{1}{t}\int_{-t/2}^{+t/2} u_2^{m-}(z)dz \qquad \text{(A2.4)}$$

The average value of average displacements on both surfaces is

$$u_{1a}^{m} = \frac{1}{2}\left(u_{1a}^{m+} + u_{1a}^{m-}\right) \qquad u_{2a}^{m} = \frac{1}{2}\left(u_{2a}^{m+} + u_{2a}^{m-}\right) \qquad \text{(A2.5)}$$

Using (A2.4) and (A2.5) the expressions for β_{12} and β_{22} are

$$\beta_{12} = -\frac{1}{L}\sum_{m=1}^{M} u_{1a}^{m}\left(l_{(m-1)n}, l_{mn}\right) \qquad \beta_{22} = -\frac{2}{L}\sum_{m=1}^{M} u_{2a}^{m}\left(l_{(m-1)n}, l_{mn}\right) \qquad \text{(A2.6)}$$

We indicate here that the displacements will be mostly affected by normalized distances to the two closest neighboring cracks. These expressions can be rewritten in terms of average crack density and average (over all cracks) displacements

$$\beta_{12} = -\rho u_{1a} \qquad \beta_{22} = -2\rho u_{2a} \qquad \text{(A2.7)}$$

$$u_{1a} = \frac{1}{M}\sum_{m=1}^{M} u_{1a}^{m}\left(l_{(m-1)n}, l_{mn}\right) \qquad u_{2a} = \frac{1}{M}\sum_{m=1}^{M} u_{2a}^{m}\left(l_{(m-1)n}, l_{mn}\right) \qquad \text{(A2.8)}$$

Normalization (A2.3) can be applied also to u_{1a}^{m} and u_{2a}^{m} using notation u_{1an}^{m}, u_{2an}^{m} for the result. Expressions for β_{ij} in (A2.8) in result of normalization are slightly modified. It is easy to check that they can be presented in the following matrix form

$$\{\beta\} = \begin{Bmatrix} 0 \\ \beta_{22} \\ 2\beta_{12} \end{Bmatrix} = -\frac{\rho_n}{E_2}[U]\begin{Bmatrix} \sigma_1 \\ \sigma_2 \\ \sigma_{12} \end{Bmatrix} \qquad [U] = 2\begin{bmatrix} 0 & 0 & 0 \\ 0 & u_{2an} & 0 \\ 0 & 0 & \dfrac{E_2}{G_{12}}u_{1an} \end{bmatrix} \qquad \text{(A2.9)}$$

In (A2.9) ρ_n is normalized crack density in the layer defined by (3.4).

References

1. Roeseler WG, Sarh B, Kismarton MU. Composite structures: the first 100 years. *16th International Conference on Composite Materials. ICCM 16*, July 2007, Japan.
2. Varna J, Joffe R, Akshantala NV, Talreja R. Damage in composite laminates with off-axis plies. *Composites Science and Technology* 1999; 59 (14): 2139-2147.
3. Nairn J, Hu S. Matrix microcracking, In: Pipes RB, Talreja R, editors. *Composites Materials*. Series, *Damage Mechanics of Composite Materials*, Amsterdam: Elsevier 1994; 9: 187-243.
4. Nairn J. Matrix microcracking in composites, In: Kelly A, Zweben C, Talreja R, Manson J-A, editors. *Composite Materials, Polymer Matrix Composites*, Amsterdam: Elsevier 2000; 2: 403-432.
5. Talreja R. Damage characterization by internal variables, In: Pipes R.B, Talreja R, editors. *Composites Materials*. Series, *Damage Mechanics of Composite Materials*, Amsterdam: Elsevier 1994; 9: 53-78.
6. Berthelot JM. Transverse cracking and delamination in cross-ply glass-fiber and carbon-fiber reinforced plastic laminates: static and fatigue loading. *Applied Mechanics Review* 2003; 56(1):111-147.
7. Smith PA, Wood JR. Poisson's ratio as a damage parameter in the static tensile loading of simple cross-ply laminates. *Composites Science and Technology* 1990; 38: 85-93.
8. Lim SG, Hong CS. Prediction of transverse cracking and stiffness reduction in cross-ply laminated composites. *Journal of composite Materials* 1989; 23: 695-713.

9. Henaff-Gardin C, Lafarie-Frenot MC, Gamby D. Doubly periodic matrix cracking in composite laminates Part 1: General in-plane loading. *Composite Structures* 1996; 36:113-130.
10. Zhang J, Fan J, Soutis C. Analysis of multiple matrix cracking in [±θm/90n]s composite laminates, Part I: In-plane stiffness properties, *Composites* 1992; 23(5): 291-298.
11. Hashin Z. Analysis of cracked laminates: A Variational Approach. *Mechanics of Materials*. North-Holland 1985; 4:121-136.
12. Hashin Z. Analysis of Orthogonally Cracked Laminates under Tension, *Journal of Applied Mechanics* 1987; 54: 872-879.
13. Varna J, Berglund LA. Multiple transverse cracking and stiffness reduction in cross-ply laminates. *Journal of Composites Technology and Research* 1991; 13(2): 97-106.
14. Varna J, Berglund LA. Thermo-Elastic properties of composite laminates with transverse cracks. *Journal of Composites Technology and Research* 1994; 16(1):77-87.
15. McCartney LN. Theory of stress transfer in 0-90-0 crossply laminate containing a parallel array of transverse cracks. *Journal of the Mechanics and Physics of Solids* 1992; 40: 27-68.
16. McCartney LN. A recursive method of calculating stress transfer in multiple- ply cross-ply laminates subject to biaxial loading 1995; NPL report DMMA(A): 150.
17. Schoeppner GA, Pagano N. Stress fields and energy release rates in cross-ply laminates. *International Journal of Solids and Structures* 1998; 35(11):1025-1055.

18. Joffe R, Krasnikovs A, Varna J. COD-based simulation of transverse cracking and stiffness reduction in [S/90n]s laminates. *Composites Science and Technology* 2001; 61: 637-656.
19. Fan J, Zhang J. In-situ damage evolution and micro/macro transition for laminated composites. *Composites Science and Technology* 1993; 47: 107-118.
20. Kashtalyan M, Soutis C. Stiffness degradation in cross-ply laminates damaged by transverse cracking and splitting. *Composites: Part A* 2000; 31: 335-351.
21. Kashtalyan M, Soutis C. Mechanisms of internal damage and their effect on the behavior and properties of cross-ply composite laminates. *International Applied Mechanics* 2002; 38(6): 641-657.
22. Kashtalyan M, Soutis C. Analysis of composite laminates with intra- and interlaminar damage. *Progress in Aerospace Sciences* 2005; 41:152-173.
23. Kashtalyan M, Soutis C. Stiffness and fracture analysis of laminated composites with off-axis ply matrix cracking. *Composites: Part A* 2007; 38: 1262-1269.
24. Barbero EJ, Cortes DH. A mechanical model for transverse damage initiation, evolution, and stiffness reduction in laminated composites. *Composites: Part B* 2010; 41:124-132.
25. Vinogradov V, Hashin Z. Variational analysis of angle-ply laminates. *Composites Science and Technology* 2010; 70: 638-646.
26. McCartney LN. Energy-based prediction of progressive ply cracking and strength of general symmetric laminates using a homogenization method. *Composites: Part A* 2005; 36:119-128.
27. Barbero EJ, Sgambitterra G, Adumitroaie A, Martinez X, A discrete constitutive model for transverse and shear damage of symmetric laminates with arbitrary stacking sequence. *Composite Structures* 2011; 93:1021-1030.

28. Lundmark P, Varna J. Constitutive relationships for laminates with ply cracks in in-plane loading. *International Journal of Damage Mechanics* 2005; 14(3): 235-261.

29. Lundmark P, Varna J. Crack face sliding effect on stiffness of laminates with ply cracks. *Composites Science and Technology* 2006; 66:1444-1454.

30. Zhang J, Herrmann KP. Stiffness degradation induced by multilayer matrix cracking in composite laminate. *Composites:Part A* 1999; 30 (5):683-706.

31. Talreja R. A synergistic damage mechanics approach to durability of composite material systems, In: Cardon A, Fukuda H, Reifsnider K, editors. *Progress in durability analysis of composite systems*. Rotterdam: A.A. Balkema 1996; 117-129.

32. Gudmundson P, Östlund S. First order analysis of stiffness reduction due to matrix cracking. *Journal of Composite Materials* 1992; 26:1009-1030.

33. Gudmundson P, Zang W. A universal model for thermoelastic properties of macro cracked composite laminates. *International Journal of Solids and Structures* 1993; 30:3211-3231.

34. Varna J, Berglund LA, Talreja R, Jakovics A. A study of the crack opening displacement of transverse cracks in cross ply laminates. *International Journal of Damage Mechanics* 1993; 2: 272–289.

35. Jacquot P. Speckle Interferometry: A review of the principal methods in use for experimental mechanics applications. *Strain 2008*; 44:57-69.

36. Farge L, Ayadi Z , Varna J. Optically measured full-field displacements on the edge of a cracked composite laminate. *Composite: Part A* 2008; 39:1245-1252.

37. Farge L, Varna J, Ayadi Z. Damage characterization of a cross-ply carbon fiber/epoxy laminate by an optical measurement of the displacement field. *Composites Science and Technology* 2010; 70: 94-101

38. Lundmark P, Varna J. Stiffness reduction in laminates at high intralaminar crack density: effect of crack interaction. *International Journal of Damage Mechanics* 2011; 20:279-297.

39. Varna J, Krasnikovs A. Transverse cracks in cross-ply laminates. Part 2, Stiffness Degradation. *Mechanics of Composite Materials* 1998; 34(2): 153-170.

40. McCartney LN, Schoeppner GA. Predicting the Effect of Non-uniform Ply Cracking on the Thermo-elastic Properties of Cross-ply Laminates. *Composites Science and Technology* 2000; 62: 1841-1856.

41. Silberschmidt VV. Matrix Cracking in Cross-ply Laminates: Effect of Randomness. *Composites: Part A* 2005; 36: 129-135.

42. Varna J, Krasnikovs A, Kumar R, Talreja R. A Synergistic Damage Mechanics Approach to Viscoelastic Response of Cracked Cross-ply Laminates. *International Journal of Damage Mechanics* 2004; 13: 301-334.

43. Nairn JA, Hu S. The Formation and Effect of Outer-ply Microcracks in Cross-ply Laminates: A Variational Approach. *Engineering Fracture Mechanics* 1992; 41(2): 203-221.

44. Loukil MS, Hussain W, Kirti A, Pupurs A, Varna J. Thermoelastic constants of symmetric laminates with cracks in 90-layer: application of simple models. *Plastics, Rubber and Composites*, in press. 2012.

45. Allen DH, Yoon C. Homogenization Techniques for Thermo-viscoelastic Solids Containing Cracks. *International Journal of Solids and Structures* 1998; 35: 4035-4053.

46. Vakulenko AA, Kachanov ML. Continuum Model of Medium with Cracks, Mekhanika Tverdogo Tela. *Mechanics of Solids* 1971; 4:159-166.

47. Highsmith AL, Reifsnider KL. Stiffness-reduction mechanisms in composite laminates. In: *Damage in composite materials*, ASTM STP 775. Philadelphia (PA): American Society for Testing and Materials 1982: 103-117.

48. Han YM, Hahn HT. Ply cracking and property degradation of symmetric balanced laminates under general in-plane loading. *Composites Science and Technology* 1989; 35:377-397.

49. Lim SG, Hong CS. Prediction of transverse cracking and stiffness reduction in cross-ply laminated composites. *Journal of Composite Materials* 1989; 23: 695-713.

50. Joffe R, Varna J. Analytical modeling of stiffness reduction in symmetric and balanced laminates due to cracks in 90° layers. *Composites Science and Technology* 1999; 59:1641-1652.

51. Krasnikovs A, Varna J. Transverse cracks in cross-ply laminates. Part 1, Stress Analysis. *Mechanics of Composite Materials* 1997; 33(6):565-582.

52. Varna J, Berglund LA. Two-Dimensional Transverse Cracking in [0m/90n]S Cross-Ply Laminates. *European Journal of Mechanics A/Solids No5* 1993; 12: 699-723.

53. Moore AJ, Tyrer JR. An electronic speckle pattern interferometer for complete in plane displacement measurement. *Measurement Science and Technology* 1990; 1:1024–1030.

54. Moore AJ, Tyrer JR. Two-dimensional strain measurement with ESPI. Optics and Lasers in Engineering 1996; 24:381-402.

55. Nakadate S, Saito H. Fringe scanning speckle interferometry. *Applied Optics* 1985; 24(14):2172–2180.

56. Avril S, Vautrin A, Surrel Y. Grid method: application to the characterization of cracks. *Experimental Mechanics* 2004; 44: 37–43.

57. Surrel Y. Some metrological issues in optical full field techniques, interferometry XI: techniques and analysis. In: Creath K, Schmidt J, editors. *Proceedings of SPIE* 2002; 4777.

58. Pipes RB, Pagano NJ. Interlaminar stresses in composite laminates under uniform axial extension. *Journal of Composite Materials* 1970; 4:538-548.

59. Loukil MS, Varna J, Ayadi Z. Engineering expressions for thermo-elastic constants of laminates with high density of transverse cracks, *Composite Part A*: Applied Science and Manufacturing 2013; 48(1): 37-46.

60. Loukil MS, Varna J, Ayadi Z. Applicability of solutions for periodic intralaminar crack distributions to non-uniformly damaged laminates. *Journal of Composite Materials* 2013; 47(3): 287-301.

Titre en français :

Étude expérimentale et numérique de la fissuration intralaminaire dans les composites à hautes performances

Résumé en français:

Le mécanisme d'endommagement le plus facilement observable lors d'un essai de traction est la micro-fissuration des plis. Ces fissures sont parallèles à la direction des fibres et s'étendent sur toute l'épaisseur du pli. L'apparition et la croissance du nombre de ces fissures engendrent une réduction progressive de la rigidité globale du composite. Lorsque le composite est sollicité mécaniquement, les concentrations de contraintes en pointe de fissures peuvent favoriser la création d'une zone où le pli fissuré et le pli adjacent sont décollés (phénomène de délamination). Il est évident que l'apparition de cette nouvelle forme d'endommagement modifiera la dépendance de l'ouverture et du glissement des lèvres des fissures avec le chargement appliqué. Il est donc nécessaire de trouver un moyen de mesure permettant l'estimation expérimentale des valeurs de l'ouverture moyenne et du glissement moyen des lèvres des fissures.

L'objectif principal de cette thèse est de caractériser l'endommagement des matériaux composites (Fibre de carbone/époxy et fibre de verre/époxy) utilisés dans le domaine aéronautique. En utilisant l'interférométrie de speckle (ESPI), des mesures de plein champs de déplacements aux bords des échantillons et dans différentes couches du stratifié ainsi que des études par élément finis ont été effectuées dans le but de calculer l'ouverture et le glissement des lèvres des fissures. L'effet des propriétés élastiques des matériaux sur l'endommagement aussi bien que l'effet d'interaction entre les fissures ont été déterminés. Une discussion essais/calculs est enfin réalisée afin de juger la validité des hypothèses retenues.

Mots-clefs en français :

Matériaux composites, endommagement, calculs par éléments finis, Fissures intralaminaires, Interférométries de Speckle

Titre en anglais :

Experimental and Numeriacal Studies of Intralaminar Cracking in High Performance Composites

Résumé en anglais:

The macroscopic failure of composite laminates subjected to tensile increasing load is preceded by initiation and evolution of several microdamage modes. The most common damage mode and the one examined in this thesis is intralaminar cracking in layers. Due to this kind of microdamage the laminate undergoes stiffness reduction when loaded in tension. The degradation of the elastic properties of these materials is caused by reduced stress in the damaged layer which is mainly due to two parameters: crack opening displacement (COD) and crack sliding displacement (CSD).

The first objective of this thesis is to investigate the effect of crack interaction on COD using FEM and to describe the identified dependence on crack density in a simple and accurate form by introducing an interaction function dependent on crack density. The application of this function to more complex laminate lay-ups is demonstrated. All these calculations are performed assuming that cracks are equidistant.

Using FEM, we assume linear elastic material with ideal crack geometry. Fiber bridging over the crack surface is possible which can affect COD and CSD. The only correct way to validate these assumptions is through experiments.

The second objective is to measure these parameters for different laminate lay-ups in this way providing models with valuable information for validation of used assumptions and for defining limits of their application. In particular, the displacement field on the edge of a $[90/0]_s$ and $[90_3/0]_s$ carbon fiber/epoxy laminates specimens with multiple intralaminar cracks in the surface layer is studied.

Mots-clefs en anglais:

Composite materials, Thermo-elastic properties, Transverse cracking, Finite element analysis, Speckle Interferometry